Frequency Recognition Algorithm for Multiple Exposures

Snapshot imaging using coded light

Dorozynska, Karolina

2020

Document Version:
Publisher's PDF, also known as Version of record

[Link to publication](#)

Total number of authors:
1

Frequency Recognition Algorithm for Multiple Exposures

Snapshot imaging using coded light

KAROLINA DOROZYNSKA
DIVISION OF COMBUSTION PHYSICS | DEPARTMENT OF PHYSICS | LUND UNIVERSITY

Faculty of Engineering
Department of Physics
Division of Combustion Physics

LUND
UNIVERSITY

9 789178 956463

Frequency Recognition Algorithm for Multiple Exposures

Frequency Recognition Algorithm for Multiple Exposures

Snapshot imaging using coded light

by Karolina Dorozynska

LUND
UNIVERSITY

Organization **LUND UNIVERSITY** Division of Combustion Physics Department of Physics Box 118, SE-221 00, Lund Sweden	Document name **DOCTORAL DISSERTATION**
	Date of disputation 2020-10-23
	Sponsoring organization
Author(s) Karolina Dorozynska	

Title and subtitle
Frequency **R**ecognition **A**lgorithm for **M**ultiple **E**xposures: Snapshot imaging using coded light

Abstract

The central challenge tackled in this thesis is the development of an optical imaging approach capable of multidimensional image capture of dynamic samples. Many conventional optical imaging approaches, which can obtain dimensional information such as spectral, polarisation, or volumetric, to name a few, about samples either employ sequential image capture or parallelised detector arrangements. Due to the motion of dynamic samples the use of such imaging approaches encounter difficulties. Multidimensional information therefore needs to be obtained in a single exposure in order to avoid inaccurate image reconstruction, poor image overlap and artefacts due to motion blur.

Snapshot techniques acquire multidimensional information in a single detector exposure and have been developed to meet the requirements for dynamic sample imaging. These approaches take many different forms, such as; the use of integrated camera sensor filter arrays, dispersive elements, lenslet arrays and coded light. In many of these cases there are constraints imposed, such as on the spectral resolution achievable or the number of unique images obtainable, by the manufacturing limits of the components required. In this thesis an alternative and novel snapshot imaging approach is presented which can intrinsically overcome some of the limitations of existing snapshot solutions available.

This thesis presents a snapshot imaging method called FRAME (Frequency Recognition Algorithm for Multiple Exposures). FRAME uses spatial modulation patterns to encode different dimensional information about samples so that multiple images can be captured in a single camera exposure. Using a Fourier filtering approach the different encoded images can be isolated and extracted from the multiplexed image. As a result the approach is compatible with dynamic sample imaging. The work presented demonstrates the use of FRAME for multispectral, polarisation, extended depth of focus, temporal, and volumetric imaging. Additionally, convincing results exemplifying FRAMEs more notable attributes, are presented. These include the ability to distinguish florescence emissions resulting from spectrally close (3nm) excitation sources, successful distinction of simultaneously acquired strongly spectrally overlapping florescence signals from four fluorophores, and also from as many as nine different fluorophores. These latter features can be of great benefit for applications involving fluorescence imaging.

Key words
Snapshot imaging, structured illumination, structured light, multispectral, fluorescence, frequency encoding, image multiplexing, lock-in detection

Classification system and/or index terms (if any)

Supplementary bibliographical information	Language English
ISSN and key title 1102-8718	ISBN 978-91-7895-646-3 (print) 978-91-7895-647-0 (pdf)

Recipient's notes	Number of pages 116	Price
	Security classification	

Signature _____   Date _____2020-9-14_____

Frequency Recognition Algorithm for Multiple Exposures

Snapshot imaging using coded light

by Karolina Dorozynska

LUND
UNIVERSITY

Cover illustration front: A photograph of the illumination part of the double modulated FRAME experimental setup. (Credits: Karolina Dorozynska).

There is still a lot to learn and there is always great stuff out there. Even mistakes can be wonderful.

Robin Williams

Till min mormor, Britta. Du är ständigt nyfiken och det finns ingen fråga du inte skulle ställa. Du är alltid tillgänglig för ett samtal när det behövs och ditt stöd för vad jag gör är oändligt. Tack för att du finns i mitt liv.

Contents

Abstract

The central challenge tackled in this thesis is the development of an optical imaging approach capable of multidimensional image capture of dynamic samples. Many conventional optical imaging approaches, which can obtain dimensional information such as spectral, polarisation, or volumetric, to name a few, about samples either employ sequential image capture or parallelised detector arrangements. Due to the motion of dynamic samples the use of such imaging approaches encounter difficulties. Multidimensional information therefore needs to be obtained in a single exposure in order to avoid inaccurate image reconstruction, poor image overlap and artefacts due to motion blur.

Snapshot techniques acquire multidimensional information in a single detector exposure and have been developed to meet the requirements for dynamic sample imaging. These approaches take many different forms, such as; the use of integrated camera sensor filter arrays, dispersive elements, lenslet arrays and coded light. In many of these cases there are constraints imposed, such as on the spectral resolution achievable or the number of unique images obtainable, by the manufacturing limits of the components required. In this thesis an alternative and novel snapshot imaging approach is presented which can intrinsically overcome some of the limitations of existing snapshot solutions available.

This thesis presents a snapshot imaging method called FRAME (Frequency Recognition Algorithm for Multiple Exposures). FRAME uses spatial modulation patterns to encode different dimensional information about samples so that multiple images can be captured in a single camera exposure. Using a Fourier filtering approach the different encoded images can be isolated and extracted from the multiplexed image. As a result the approach is compatible with dynamic sample imaging. The work presented demonstrates the use of FRAME for multispectral, polarisation, extended depth of focus, temporal, and volumetric imaging. Additionally, convincing results exemplifying FRAMEs more notable attributes, are presented. These include the ability to distinguish florescence emissions resulting from spectrally close (3nm) excitation sources, successful distinction of simultaneously acquired strongly spectrally overlapping florescence signals from four fluorophores, and also from as many as nine different fluorophores. These latter features can be of great benefit for applications involving fluorescence imaging.

Popular summary

We see the world in full colour, or at least that is how we perceive it. In reality, we have three different colour sensitive parts in our eyes which are able to capture the colours red, green and blue. What our visual system then does is to record how much, the light intensity, of each of these different colours reaches them and then interprets this mixture as a certain colour within the full rainbow of colours (fig. 1). Our brains therefore use only three actual colours and mix these to create a broader selection, a bit like when you mix different colours of paint to make another one, like yellow and blue to make green.

Figure 1: A multicoloured photograph of a lifeguard hut (far left) along with the three single colour images it is made up of. The black and white images show the light intensity for each of the three different colours, i.e. how much of that colour of light was captured.

When we think of everyday cameras we consider them as being able to capture multicoloured photographs. This has not always been the case, however, with the first photograph being in black and white. The reason why we can now take multicoloured photographs has to do with the development of the camera technology, which actually works in a very similar way to our own eyes. They record the light intensity in the same three colour channels by using a chequerboard pattern (fig. 2) of red, green and blue filters in front of the camera sensor, since the sensor on its own only records light intensity, not colour. The mixture of the different colour contributions are then mixed by the camera software to produce the multicoloured photograph.
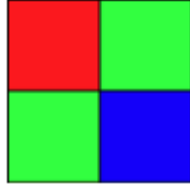
Figure 2: The chequerboard pattern of red, green and blue colour filters used in everyday cameras.

Multicoloured images are nice for recreational use, but they are also useful for learning about things in the world around us. Multicoloured images of cells, for example, are common in biology and medicine for learning about how they work, their structure and also for diagnosis of various illnesses. To be able to get all the information needed about these different things it is often not enough to only be able to capture the light intensity of the colours red, green and blue and mix them but to actually be able to capture each specific different colour, of all colours, on its own. To do this a black and white camera which only collects the light intensity from an object or scene can be used in conjunction with the colour filters needed. A filter can be placed in front of the camera, a picture taken and then repeated for all the different colours. In the end there will be a collection of different images which can be combined together into one which then has all the different coloured image contributions, to get a multicoloured picture. If there are lots of different coloured images needed this process can take some time. Additionally if the thing you want to take a picture of is moving, a dynamic sample, while all the images are being captured it will not be possible to combine them all into an accurate multicoloured picture. For this reason it is useful to be able to have a camera which can collect all the colours needed in a single instant so that it can be both fast and used for dynamic samples. The research in this thesis is on the development of an imaging method which can do exactly this.
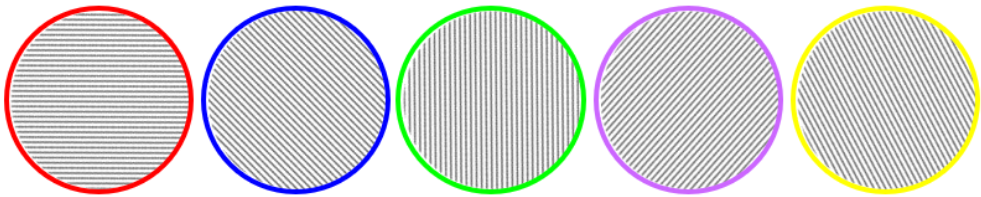
Figure 3: Striped patterns used to encode different colour information from samples.

The method developed uses a camera which collects only light intensity, i.e. black and white images. Unlike the approaches described above, it does not use colour filters to capture coloured images. Instead of using different coloured filters, a striped pattern in a certain direction (encoding) is used to identify each different colour (fig. 3) When the camera collects the light intensity corresponding to one of the colours in the sample, the image

collected is encoded, i.e. it contains the striped pattern which is the encoding belonging to a certain single colour. For each different colour, there is a unique encoding. The "multicoloured" image collected by the detector is then made up of lots of different encoded images, i.e. one for each of the different colours, where the striped patterns are all crossed over each other (fig. 4). A computer can then be used to select each encoding pattern and separate them to give each of the individual images, each corresponding to a different colour. In this way the method can use an encoding pattern for any colour needed, so it is not limited to a fixed selection of colours.
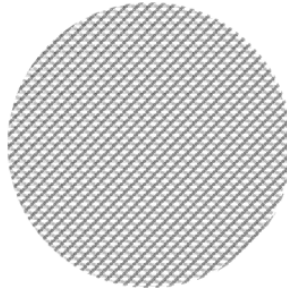
Figure 4: The striped patterns overlapped to illustrate what the "multicoloured" camera picture looks like before a computer has decoded the patterns.

In reality the encoding can even be used for different properties of the sample, not just colour imaging. The work presented in this thesis shows how you can encode, amongst other things, different "slices" inside the volume of a sample and then combine them to make a three dimensional representation of the sample. In general, the work demonstrates how you can encode different properties of a sample experimentally and explains how you can then decode the captured images.

Populärvetenskaplig sammanfattning

Vi ser världen i fullfärg, eller åtminstone så uppfattar vi den. I verkligheten har vi tre olika färgkänsliga delar i våra ögon som kan fånga färgerna rött, grönt och blått. Vad vårt synsystem sedan gör är att registrera ljusintensiteten för var och en av dessa olika färger och sedan tolkar denna blandning som en viss färg (fig. 5). Våra hjärnor använder därför bara tre färger och blandar dessa för att skapa ett bredare urval, lite som när du blandar olika målarfärger för att göra en annan, som gult och blått för att skapa grönt.

Figur 5: Ett mångfärgat fotografi av en strandvakt hydda (längst till vänster) tillsammans med de tre enfärgade bilderna som den består av. De svartvita bilderna visar ljusintensiteten för var och en de tre olika färgerna, dvs hur mycket av den ljusfärgen som fångats.

När vi tänker på vardagliga kameror anser vi att de kan ta flerfärgade fotografier. Detta har dock inte alltid varit fallet, till början var fotografier i svartvitt. Anledningen till att vi nu kan ta färgfotografier har att göra med utvecklingen av kameratekniken, som faktiskt fungerar på ett sätt mycket likt våra egna ögon. De spelar in ljusintensiteten i samma tre färgkanaler genom att använda ett schackbrädemönster (fig. 6) med röda, gröna och blåa filter framför kamerasensorn, som i sin tur bara registrerar ljusintensitet, inte färg. Blandningen av de olika färgbidragen blandas sedan av kameraprogrammet för att producera ett fotografi med många färger.
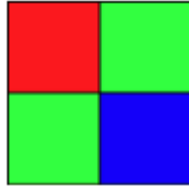
Figur 6: Schackbrädemönstret av det röda, gröna och blåa färgfilter som används i vardagliga kameror.

Färgfotografering tillhör vardagen för oss idag, men det har visat sig att också vara användbart för att lära sig om världen omkring oss. Mångfärgade bilder av celler är till exempel vanliga inom biologi och medicinsk forskning för att lära sig hur de fungerar, deras struktur och även för diagnos av olika sjukdomar. För att kunna få all information som behövs om dessa olika saker räcker det ofta inte bara att kunna fånga ljusintensiteten i färgerna rött, grönt och blått och blanda dem utan att faktiskt kunna fånga varje specifik färg som provet skickar ut. För att göra detta kan en svartvit kamera som bara samlar ljusintensiteten från ett objekt eller scen användas i kombination med lämpliga färgfilter. Vid fotograferingen placeras ett färgfilter främför kameran och bilden tas. Processen upprepas därefter med andra filter. I slutändan kommer det att finnas en samling bilder som kan kombineras ihop till en som har alla olika färgbidrag för att få en mångfärgad bild. Om det behövs många olika färgade bilder kan processen dock ta lite tid. Dessutom, om objektet rör sig, ett dynamiskt prov, under den tiden som alla färgbilderna tas är det inte möjligt att kombinera dem alla till en korrekt färgbild. Av denna anledning är det nödvändig att kunna ha en kamera som kan samla alla färger som behövs på ett ögonblick så att den kan vara både snabb och användas för dynamiska prov. Denna avhandling beskriver utvecklingen av en avbildningsmetod som kan göra just detta.
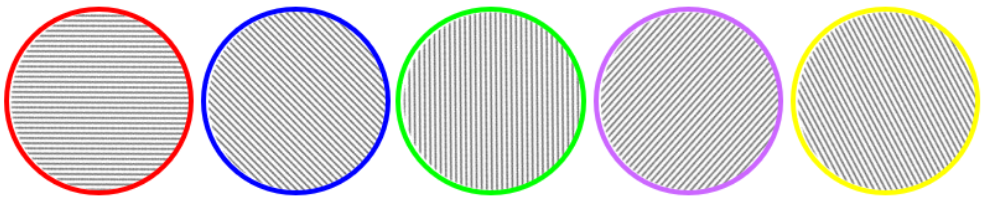
Figur 7: Randiga mönster som används för att koda olika färginformation från prover.

Den utvecklade metoden använder en kamera som endast samlar ljusintensitet, dvs svartvita bilder. Till skillnad från metoden som beskrivs ovan använder den inte färgfilter för att fånga färgbilder. Istället för att använda olika färgade filter används ett unikt randigt mönster (kodning) för att identifiera varje färg (fig. 7). När kameran fångar in ljuset för en av provets flera färger, blir denna information kodad, dvs den innehäller det randiga mönstret. För varje färg finns en unik kodning. Den "mångfärgadebilden som samlas

av detektorn består sedan av flera olika kodade bilder, dvs. en för var och en av de olika färgerna, där de randiga mönstren alla korsas över varandra (fig. 8). En dator kan sedan användas för att välja varje kodningsmönster och separera dem för att ge var och en av de enskilda bilderna, var och en motsvarande en annan färg. På detta sätt kan metoden använda ett kodningsmönster för vilken färg som helst, så det är inte begränsat till ett fast urval av färger.
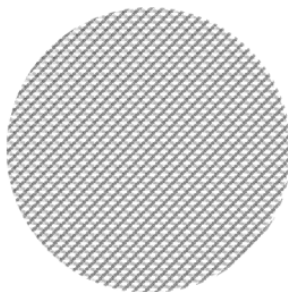
Figur 8: De överlappande randiga mönstren för att illustrera hur den "mångfärgade" kamerabilden ser ut innan en dator har avkodat mönstren.

Egentligen kan kodningen även användas för att koda olika egenskaper hos provet, inte bara det som är färgberoende. Arbetet som presenteras i denna avhandlingen visar hur man kan koda, bland annat, olika "skivor" inuti volymen på ett prov och sedan kombinera dem för att göra en tredimensionell representation av provet. Huvuddelen av arbetet visar hur man kan koda olika egenskaper för ett prov experimentellt och sedan förklarar hur man kan avkoda de tagna bilderna.

Acknowledgements

With you I have found someone who I can discuss politics and business with as well as be mocked for my inferior online gaming abilities. Isabel, we met while I was still at atomic physics and we continue to be friends today. You are surprisingly competitive in games, fiercely kind all the time but most importantly wildly fun to spend time with. Lisa and Niclas we have had so many adventures together already, both domestically and abroad, and I look forward to our next one. We can talk about anything, at any time of day or night and often over a few games and cheeky drinks.

I would also like to thank my family. Mormor du har alltid visat intresse i vad jag gör, även om du inte alltid har förstått allting det handlar om. To my parents, who have always strived to give me the best opportunities in life, without which I would not be where I am today. Last, but by no means least, to my partner Kenny, about whom I could write a thesis, if I had the energy for one more, of how much you mean to me. You are my companion, my best friend and my biggest supporter. You bring a calm into my life and humour me in all my ideas be they comedy, innovation or, in your eyes, pure madness.

List of publications

This thesis is based on the following publications, referred to by their Roman numerals:

I **Implementation of a multiplexed structured illumination method to achieve snapshot multispectral imaging**
K. Dorozynska, E. Kristensson
Optics Express, 2017, 25, 15, 17211-17226

II **A versatile, low-cost, snapshot multidimensional imaging approach based on structured light**
K. Dorozynska, V. Kornienko, M. Aldén, E. Kristensson
Optics Express, 2020, 7, 28, 9572-9586

III **Single-shot 3D imaging of hydroxyl radicals in the vicinity of a gliding arc discharge**
Y. Bao, **K. Dorozynska**, P. Stamatoglou, C. Kong, T. Hurtig, S. Pfaff, J. Zetterberg, M. Richter, E. Kristensson, A. Ehn
Manuscript in review. Submitted to Plasma Sources Science and Technology.

IV **Double modulated FRAME: Multiple fluorophore unmixing using a snapshot multiplexed structured illumination and detection setup**
K. Dorozynska, S. Ek, V. Kornienko, A. Andersson, E. Kristensson
Manuscript unpublished

All papers are reproduced with permission of their respective publishers.

Chapter 1

Introduction

Imaging is one of the ways in which we navigate the world around us. To do so we use the most accessible optical imaging system we have, our eyes. These allow us to observe and manoeuvre through the world around us in colour and three dimensions. Other creatures have optical sensitivities different to ours such as polarisation imaging, additional colour channels, higher spatial resolution or even wider fields of view. These different imaging characteristics have provided survival advantages and have inspired the development of technologies which can harness these properties. In the world of superheroes you even find the character, Superman, who possesses, colour, x-ray, heat, telescopic and macroscopic vision. It is clearly of interest and benefit to be able to capture visual information and the more types one can capture in a single instant, the more powerful.

Light has many different properties which, when interacting with objects, allows us to gain information about them. If we consider sunlight which illuminates the world around us, its interaction with different objects provides us with information about them. Light reflecting of deciduous leaves in the summertime reaches our eyes as green but in the autumn we see them as red, yellow, orange and brown. This inadvertently tells us about the chlorophyll content of the leaves, where it is present in the green ones but not in the others that have begun to die off for the year. Sunlight also reflects strongly off the surface of bodies of water, such as lakes, becoming linearly polarised. If we have polarised sunglasses on we can in fact block this light, or glare, and see below the surface of the water. This is due to the polarisation of the reflected sunlight due to its interacting with the waters surface. Sunlight is unpolarised and therefore contains all polarisation directions. When the light is incident on the water only horizontal linearly polarised light is reflected off the surface and reaches our eyes. Polarised sunglasses have vertical linear polarisation filters which block the surface reflected light, allowing us to see below the surface. These are very simple examples to illustrate how optical imaging can take advantage of the different light-matter

interactions. The reality of optical imaging applications are in fact far more powerful and wide ranging, from imaging microscopic cell structures to distant stars.

Using optical imaging it is possible, in a non-invasive way, to obtain structural, composition and functional information about different objects [1, 2] such as biological cell nuclei [3], collagen structure [4, 5] and molecules in combustion processes [6], to name a few. To achieve these outcomes numerous different optical dimensions need to be captured. An optical dimension can be defined as any of the following; the spatial coordinates, the wavelength, the polarization orientation and ellipticity angles, the propagation polar angles, and the emission time [7]. The more dimensions obtained from a sample, the more one can learn about it. This can be done by imaging the sample using a variety of different techniques. There are, however, disadvantages to this approach. Depending on the technique used, the sample may need to be specially prepared in such a way that it destroys the possibility of using certain other imaging methods afterwards. The sample itself may also deteriorate under certain imaging conditions. Additionally if the sample is dynamic, which is especially important when wanting to understand about interactions of or within the sample, it may not be possible to capture all the required information between sample movements. There is therefore a strong requirement for multidimensional imaging approaches with a specific focus on those with snapshot capabilities.

The focus of this thesis is on the development of a novel snapshot imaging approach dubbed "Frequency Recognition Algorithm for Multiple Exposures" (FRAME) [8, 9, 10, 11]. As the name suggests FRAME can capture multiple exposures, or images, with the ability to recognise them each due to a spatial frequency encoding. Structured light, illumination and/or detection, is used to encode dimensional information about the sample such that it can be multiplexed onto a detector and later computationally decoded to access each individual image. Different experimental implementations of the encoding result in different dimensional information about the sample being encoded. In each case, however, the computational post processing procedure follows the same structure, with only minor modifications or additions in places.

Chapter 2

Multidimensional Imaging

Classically, these days, when we consider images we picture colour photographs, be they printed or on our mobile phones or digital cameras. Images like these contain spectral information in two spatial dimensions and typically emulate the human eye capturing, red, green and blue intensity information. Light does, however, have many more properties, including a wider range of colours beyond simply red, green and blue, which we can capture depending on the imaging approach used. As a result it is possible to attain more powerful images if additional dimensions are captured. It has been proposed that there are in fact as many as nine different dimensions, namely; the spatial coordinates (x,y,z), the wavelength (λ), the polarization orientation and ellipticity angles (Ψ,χ), the propagation polar angles (θ, ϕ), and the emission time (t) [7]. By obtaining these different dimensions in optical imaging it is possible to visualise different properties about the sample imaged. This chapter focuses on some of the nine different dimensions, namely those which are relevant to the presented thesis work.

2.1 Spectral Imaging

Spectral information about samples can tell us a lot about their composition. If we consider sunlight dispersed by a prism we can see that white light is composed of the spectrum of visible wavelengths. When the world around us is illuminated by sunlight we see various objects as different colours depending on which wavelengths they reflect or absorb from the visible spectrum. When we look at the sky we see it as blue during the day and at sunset it can appear as variety of colours from red to purple, all as a result of how the particles in the atmosphere scatter the sunlight throughout the day. All of these spectral characteristics of light and the interaction with different objects and media around us, provides information

about them. Spectral imaging takes advantage of these and is used within a broad variety of different applications such as astrophysics [12], remote sensing [13], biomedical optics [14] and quality control in the food [15] and pharmaceutical [16] industries.

If a sample is illuminated with certain light source and the subsequent reflected, absorbed and transmitted light is measured, the images obtained will differ due to the varying interactions of the sample constituents with the incident light. In this way it is possible to learn about the different properties about a sample, such as its structure, composition and function, by capturing images in these different configurations. Simply capturing a colour image using a conventional RGB camera of a sample versus a monochromatic image, where only the light intensity is captured, can already tell us much more, as shown by fig. 2.1. Fig. 2.1 shows an X-rite Color Checker image, obtained using an RGB camera, which is a sample that contains a collection of coloured and monochromatic squares, normally used as a reference sample in spectral imaging systems to check light balance and colour capabilities. The fig. 2.1 shows a multispectral image, constructed of the combination of recorded light intensities captured in the red, green and blue colour channels. A greyscale version of the same image is also shown to illustrate monochromatic image capture, i.e. where only the light intensity is recorded with no spectral discrimination. It becomes clear when comparing the two images that in the monochromatic image some of the squares have a very similar appearance and would therefore be difficult to differentiate from each other based on their intensity responses alone. In the multispectral image, however, it becomes immediately clear that each square is uniquely coloured and therefore differentiation is straightforward. This increased sensitivity in discerning sample features based on different spectral responses, in fact forms the basis for spectral imaging.

Figure 2.1: Monochromatic and multispectral images of an X-Rite Color Checker. The greyscale image has numerous squares with similar light intensity values which therefore appear the same and their colour cannot be discerned. The colour image combines red, green and blue light intensity making it possible to discern the different colours in the sample.

2.1.1 Absorption & Fluorescence

$$E = h\nu = \frac{hc}{\lambda} \qquad (2.1)$$

Atoms and molecules have internal energies defined by discrete energy levels [17], fig. 2.2, which describe their possible energy transitions. The energy carried by light is packaged in discrete particles, called photons, whose energy can be described by eq.(2.1), where h is Planck's constant, ν is the frequency of the light, c is the speed of light in a vacuum, and λ is the wavelength of the light. If an atom or molecule absorbs a photon with energy equivalent to the gap between two of its energy levels, ΔE, an electron will be raised from the ground state to the excited state, in a process known as excitation. There are several possible outcomes for the electron raised to an excited state [2]. One possible outcome is that it may relax to the ground state by emission of a photon (a radiative process). If the emitted photon corresponds in energy to that of the excitation photon, the emission process is known as resonant fluorescence (fig. 2.2). An alternative relaxation of the electron can occur by emission of a photon with a lower energy than that of the excitation photon, known as Stoke's fluorescence (fig. 2.3). Stoke's fluorescence first involves the relaxation of the excited electron via vibrational relaxation, a non-radiative process, to a lower vibrational energy level in the excited state. Secondly, the electron relaxes to the ground state via the emission of a photon. Stoke's fluorescence is what is conventionally considered simply as fluorescence in many fluorescence measurements and resonant fluorescence is more generally referred to simply as emission.
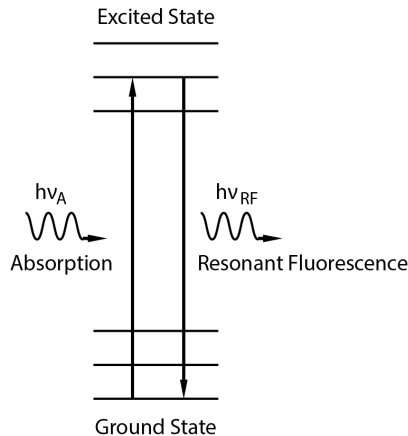
Figure 2.2: Jablonski energy diagram showing excitation followed by relaxation by resonant fluorescence. Each $h\nu$ denotes the photon energy, where the subscripts A and RF denote absorption and resonant fluorescence, respectively. Figure adapted from [2].

The atomic structure of different atoms and molecules are not the same, i.e. their pos-

sible energy levels transitions are different. Since the energy gap of the transitions correspond to a particular wavelength, the absorbed and emitted light for a specific energy gap will be of a characteristic wavelength. As such, optical probing using various illumination sources, as well as the detection of any resultant emission or fluorescence, can provide information about their composition, i.e. what element(s) are present and how much of each. Atomic and molecular spectroscopy is an approach which captures the characteristic spectral "fingerprints" of objects, i.e. which wavelengths of light they absorb and emit as a result of their energy level structure. In a lab environment one can record the emission spectra, for example, of various known elements to learn what their spectral "fingerprints" look like. On can then use emission spectroscopy to study the elemental composition of distant celestial bodies [18] by recording which spectral regions are emitted by them and comparing the captured spectra to the known elemental spectra, to determine their composition.
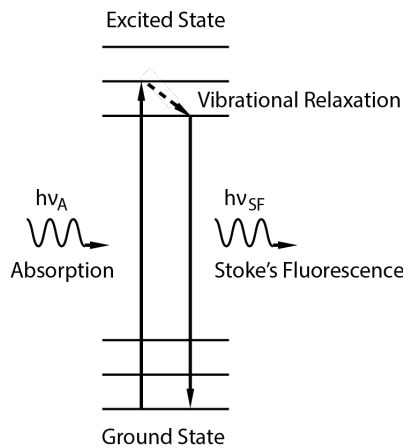
Figure 2.3: Jablonski energy diagram showing excitation followed by relaxation by Stoke's fluorescence. Each $h\nu$ denotes the photon energy, where the subscripts A and SF denote absorption and Stoke's fluorescence, respectively. Figure adapted from [2].

Due to the nature of fluorescence absorbing shorter wavelength light and re-emitting longer wavelength light it is useful for targeting specific features in samples, where the initial illumination wavelength can be spectrally filtered out during detection. Some samples have naturally occurring fluorescence called autofluorescence [19]. This can be advantageous when one is interested in the sample which auto-fluoresces, however, when the are other structures or molecules of interest within the sample, the autofluorescence can become an unwanted background signal. If the structures of interest in a sample do not auto-fluoresce then they can be labelled or "tagged" with fluorescent molecule known as a fluorophore [20]. This forms the main basis for fluorescence imaging whereby different structures are labelled and then illuminated with the appropriate excitation wavelength to induce a fluorescence response. The fluorescence emission can then be isolated, typically through the use of spectral filters which block the illumination wavelength and allow the fluorescence, only,

to be transmitted.

Fluorescence imaging is used in a variety of different applications from the investigations of combustion processes [21, 22] to subcellular structures in biology and medicine [23]. Flames are often optically probed with laser light to induce florescence within some of the molecules of interest within the combustion process. This technique is known as laser induced fluorescence (LIF). Since flames emit light, probing them with specific wavelengths to target certain molecules, and filter out the background light, makes it possible to isolate their distribution within the flame. Similarly, studying subcellular structures is useful for understating their structure and function in biological processes. Selecting appropriate fluorophores which attach to specific cellular structures makes it possible to optically image them using fluorescence. More powerful diagnostics is achieved when structures, such as different proteins of cell organelles [24], are each labelled uniquely such that it is possible to distinguish multiple structures in a single image. This way it is possible to obtain information about their functions within the cells.

When recording multiple different fluorescence signals there can be problems when trying to spectrally resolve the different, co-localized fluorophores due to their overlapping spectral emissions. Classically the different fluorescence emissions are separated through the use of band-pass filters. If there is a strong spectral overlap between the signals, however, such filters cannot be used to distinguish between them and, additionally, achieving a full spectral separation between the signals comes at the cost of greatly reducing the overall light collection. Of course one could select fluorophores which have distinct excitation wavelength ranges such that they could be sequentially imaged using different lasers and therefore eliminating spectral cross talk between them. In reality it is not always possible to select fluorophores which have either distinct excitation or emission and therefore it is necessary to be able to tackle the spectral separation even under such circumstances. There are numerous different solutions for multiple fluorophore imaging which have been proposed, from intensity modulated and phase shifted illumination sources [25], time of arrival approaches [26], and photo-activatable and photo-switchable fluorophores [27, 28]. The most classic approach, however, is linear unmixing [24, 29, 30] which can be used to spectrally separate co-localised fluorescent emissions.

Linear Unmixing

Linear unmixing [24, 29, 30] is a mathematical method used to determine the relative concentrations of different fluorophores present in a sample containing multiple fluorophores. The method is appropriate for both spatially separated and co-localised fluorophores, making it highly suitable for fluorescence imaging. Unlike some other post processing approaches, linear unmixing requires prior knowledge of the fluorophore spectral emission profiles, or reference spectra, in order to function. The reference spectra need to be de-

termined using pure samples of each of the different fluorophores using the same imaging system and conditions. As a result they will vary depending on the approach employed and as such calibration for each setup is needed.

Linear unmixing assumes that the signal intensity in each pixel of an image can be described by a linear combination of the fluorophores present. Eq.(2.2) describes such a relationship for a case with i number of different fluorophores (where λ denotes the spectral channel). Linear unmixing aims to determine the relative signal contributions, I_i, for the different fluorophores, $F_i(\lambda)$, for each pixel in an image. To determine the I_i terms the $F_i(\lambda)$ terms are required. These are known as the reference spectra and are the spectral profiles of the fluorophores, i.e. their different signal intensities for different wavelength values. Therefore if the detected signal, $S(\lambda)$, and the reference spectra are known then it is possible to solve the linear equations to determine their minimum solutions such that the minimum values for the I_i terms can be found. This is achieved by using an inverse least squares approach which minimises the difference between the measured and the calculated values.

$$S(\lambda) = \sum I_i F_i(\lambda) \tag{2.2}$$

It should be noted that the successful operation of linear unmixing to separate fluorophores signals is limited to the number of unique spectral channels (excitation or emission) used. Therefore if a setup can only detect three different spectral channels the images obtained can only successfully linear unmix up to three different fluorophores. If there are fewer channels than fluorophores, the equation system is underdetermined and a unique solution of the equations is therefore not possible. It should be noted that there are cases where the spectral characteristics of the fluorophores may heavily overlap making it difficult to linearly unmix the fluorophores even if there are a sufficient number of spectral channels.

2.2 Polarisation Imaging

Multispectral imaging can render certain sample features as "invisible" which can, using polarisation imaging, be visualised. Stress and strain in transparent objects [31], surface imperfections such as scratches [32], and subsurface imaging [33] are all properties which can be captured by utilising polarisation imaging. It has also found uses within medical diagnostics [34] such as; precancer detection, skin disease prediction and early cataracts detection.

In polarisation imaging there are different optical arrangements which can be used such as transmission imaging or reflection. In each case the light is normally polarised to a certain

linear state using a polariser, before interacting with a sample. The different properties of the sample, such as surface scratches or strain within a transparent object, can alter the polarisation state of the incident light. It is this change in the polarisation state which can then be detected in the transmitted or reflected light, by a polarisation sensitive imaging system.

2.3 Videography

Interactions, be they between atoms, molecules or cell organelles, are dynamic events and capturing them gives us key information about their behaviour and function. Videography, or temporal imaging, allows for the capture of dynamic events by obtaining images from different moments in time of the evolution of the event. Videography methods vary in their approaches and also in their temporal resolutions. In our everyday lives we have daily exposure to a few simple dynamic imaging methods such as the human visual system, which can process about 12 frames per second, and video cameras, which have a standard of about 30 frames per second. High speed cameras, which can capture 40500 frames per second, are available commercially [35] and are used in a variety of different research applications. Of course some events occur at much shorter time scales than these and therefore different methods have been developed to tackle this. Ultra fast cameras, with frame rates in the trillions per second [9, 36], have been developed within the last decade with the capability of imaging the propagation of a pulse of light. Ultra high speed videography is required for imaging molecules and electron dynamics whereby specialised methods are developed such as attosecond technology [37]. Pump-probe [38] is a widely used method to study repeatable events such as molecular dynamics and uses a pump light pulse to excite the sample followed by a probe pulse in order to probe the sample after a variable delay time. By repeating the pump and probe sequence with different delay times, different moments in the dynamic event are captured which eventually lead to a full video of the event. The sample imaged therefore needs to have a repeatable dynamic evolution and samples with erratic motion could not be imaged using this technique. The various videography methods available are temporally limited either by the properties of the illumination or the detection hardware used. Depending on the temporal resolution required and the nature of the sample being imaged, not all the videography methods will be applicable for any and all samples of interest.

2.4 Volumetric Imaging

When capturing images of things in order to learn about their structure and function it makes sense to do so in three dimensions, to obtain realistic representations. Volumetric

imaging tackles this three dimensional imaging requirement. There are numerous different approaches from magnetic resonance imaging (MRI) [39, 40] widely used in hospitals for anatomical and physiological processes imaging inside the human body, to confocal microscopy with applications in fields such as cell biology [41, 42]. Generally the different techniques work around the same basic principles of capturing images from different angles around the object, or "slices" at different depths within the object and then "stitching" these together computationally in post processing. Depending on the probing approach, different spatial resolutions, in both the, x and y, as well as the, z, dimensions, can be achieved. There are also three dimensional surface techniques, such as using structured illumination [43], which capture surface contours only and do not penetrate inside the sample.

Chapter 3

Techniques for Snapshot Imaging

Snapshot imaging has several application advantages [7]. Since the information is acquired in a single instant it is suitable for imaging dynamic samples, especially when interactions are of interest. Depending on the architecture of the method it can also yield better light collection efficiency. This is particularly important for passive light detection where there is no control over the illumination, and also for cases where increasing the light intensity leads to a saturation in the response or even damage to it. For fluorescence imaging specifically the latter is the case where an increase in the illumination intensity will reach a maximum when all the fluorophores have become excited and in some cases the samples are prone to photobleaching, especially under high intensity illumination. Over and above the light collection efficiency, snapshot imaging is advantageous here since it becomes possible to obtain all the information before the deterioration of the sample has occurred. Multidimensional snapshot approaches can be particularly powerful since they can capture many different aspects of a sample simultaneously.

Numerous different snapshot imaging techniques exist [7, 44, 45, 46, 47, 48, 49]; from a monochromatic detector capturing x and y dimensions, RGB detectors capturing (x, y) along with three spectral channels, to multidimensional approaches capturing (x, y), multispectral and polarisation information in a single exposure [50]. The techniques employ a variety of different solutions allowing them to obtain snapshot images including; optical filters, parallelised detectors, coded light, lens arrays and dispersive elements. In this chapter an exhaustive list of all the snapshot imaging techniques will not be provided, but instead simply a few notable ones. Additionally, since the work in this thesis obtains snapshot, multiplexed images using a single detector and in single exposure, parallelised detector methods will be excluded such that only the most relevant examples are covered.

3.1 Multispectral

In this subsection a few multispectral snapshot imaging approaches are presented. Each of the systems obtains (x, y, λ) information in various ways and subsequently they have different limitations, on properties such as their spectral image storage capacity.

Filter Stack
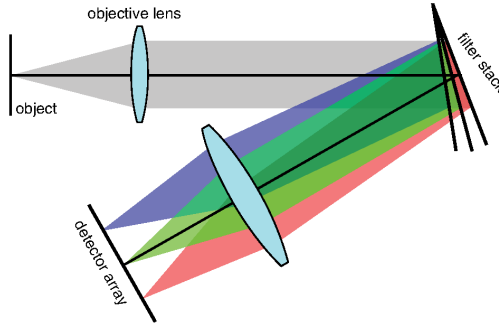
Figure 3.1: A schematic of the spectral filter stack imaging setup, courtesy of SPIE [44].

The use of a spectral filter stack [51], or spectral decomposition optical system, allows different wavelengths to be redirected onto a detector without the need to be split into different optical paths (fig. 3.1). The filters in the stack are each positioned at slightly different angles such that they reflect the different wavelengths onto different regions of the detector, thus providing spectral distinction. Since the filter angles need to be fairly low in order to maintain negligible optical path differences to the detector to ensure all the spectral images are in focus there is a limitation on how many spectral channels can be achieved. In a work by *Headland et al.* [52] a filter stack snapshot imager with 12 spectral channels was demonstrated.

Coded Aperture Snapshot Spectral Imager

The coded aperture snapshot spectral imager (CASSI) [53, 54, 55], applies a random binary pattern to the light emitted from a sample using an absorption mask. A prism is then used to spatially disperse the spectral elements before being imaged onto a detector (fig. 3.2). Full spatial separation of each spectral image is not achieved on the detector and therefore the coded pattern applied is used to identify the different spectral images in the captured multiplexed image in post processing. Due to the use of a dispersive element to separate the different spectral channels there is a limit imposed on the maximum spectral resolution

it can achieve. Additionally, CASSI has been found to experience saturation problems due to higher intensities from certain wavelength channels which lead to errors in neighbouring channels.
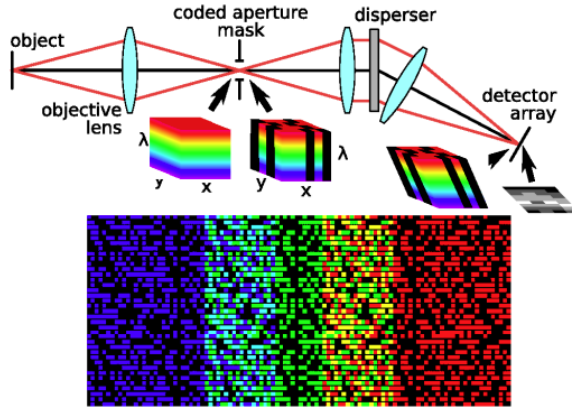
Figure 3.2: A schematic of the coded aperture snapshot spectral imager, courtesy of SPIE [44].

Image Replicating Imaging Spectrometry
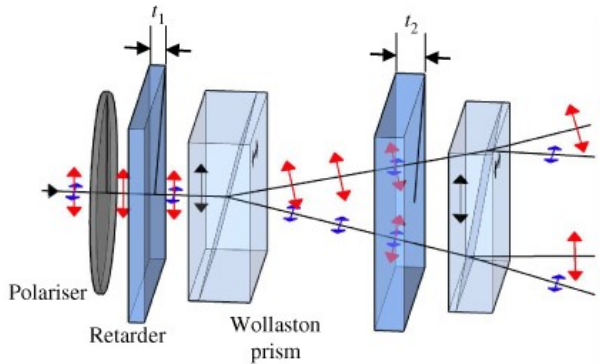
Figure 3.3: A schematic of the demultiplexing and filtering components of the image replicating imaging spectrometer, courtesy of OSA [56]

The image replicating imaging spectrometer (IRIS) [56, 57] uses a series of Wollaston polarisers to split the incident light into different spectral components. The polarisers split a single beam into two, such that there are then two spectral channels in parallel. By arranging multiple such polarisers it is then possible to split the light multiple times and direct different spectral images onto different regions of a detector (fig. 3.3). IRIS has been demonstrated with eight spectral channels [56] but may be limited to 16 channels [58] due

to the size limits of the Wollaston polarisers. In certain cases, e.g. narrowband and broadband, the spectral dispersion, intrinsic to the IRIS approach, may lead to the optical point spread function covering less than one detector pixel and more than 10 pixels, respectively. As a result, in such cases IRIS is sensitive to an overlap of the different spectral images which leads to a form of cross-talk. Additionally since the incident light needs to be polarised, when imaging unpolarised scenes the optical throughput will be reduced by half.

Integrated Spectral Filters
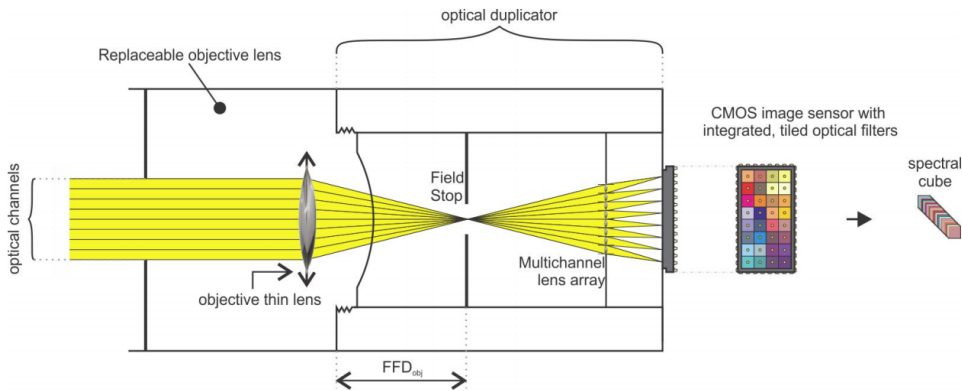
Figure 3.4: A schematic of the spectral imager which uses integrated detector chip tiled spectral filters, courtesy of SPIE [59]

Commercial products, such as from IMEC [59], exist which use spectral filters on top of their detector chips. The spectral filters are arranged in arrays which mean that different pixels on the detector chip therefore correspond to specific wavelengths (fig. 3.4). They therefore operate in much the same manner to a standard RGB camera, like we find in our mobile phones today, although with much greater spectral resolution with filter arrays giving up to 32 spectral bands. The drawback with such systems is that they have fixed spectral filters and therefore may not be suitable for all applications.

Lenslet Array Tunable Snapshot Imaging Spectrometer

The lenslet array tunable snapshot imaging spectrometer (LATIS) [60] uses a lenslet array to generate sub images, with void spaces in-between. These are then spectrally dispersed using a prism creating elongated images where the lengths are representative of their spectral constituents (fig. 3.5). These are then imaged onto a detector where the rotation of the lenslet array places the dispersed images into the void spaces, i.e. due to the spacing

between each lenslet. Since LATIS uses a dispersive element it has a non-linear spread of the point-spread-function of the shorter and longer wavelengths, resulting in a variation in the spectral resolution with respect to wavelength.
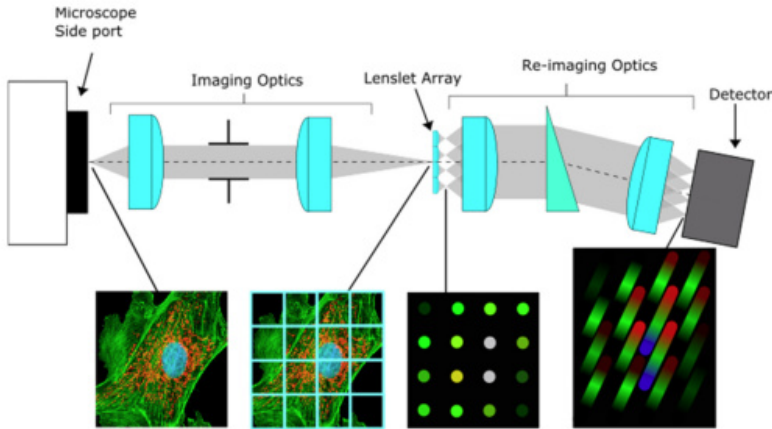
Figure 3.5: A schematic of the lenslet array tunable snapshot imaging spectrometer, courtesy of OSA [60]

3.2   Polarisation

Polarisation Filter Array
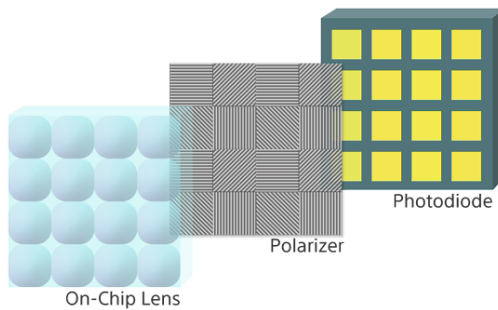
Figure 3.6: Polarsens on chip polarisation filter array, courtesy of SONY [61]

Polarsens [61] is a commercial polarisation camera from SONY. It uses a lens array followed by a polarisation filter array on its CMOS camera sensor, as illustrated in fig. 3.6. The polarisation array is constructed from a smaller array consisting four different polarisation direction linear polarisers. The pixels on the sensor therefore capture light corresponding to different degrees of polarisation. The Polarsens camera also comes in a multispectral

and polarisation compatible version where an RGB Bayer filter is overlaid over every 16 polarisers, i.e. each colour covers an array of four different direction linear polarisers. The spatial resolutions of the obtained polarisation and spectral images are therefore not the same. A Snapshot multispectral polarisation imager similar to Polarsens was also developed by *K. Shinoda et al.* [62]. In their demonstration four spectral filters with the wavelengths, 265nm, 280nm, 290nm and 305nm, were used and arranged with each colour over four different polarisation filters $(0°, 45°, 90°$ and $135°)$.

3.3 Volumetric

Distorted Phase Grating
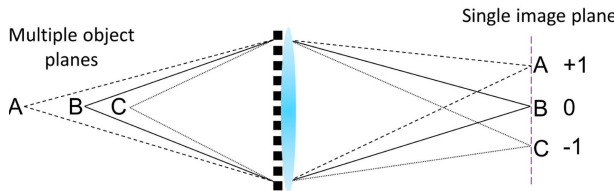
Figure 3.7: A distorted phase grating and lens combination used to image a scene with objects at different focal planes, into a single image plane with the depth information contained within different diffraction orders. Courtesy of Elsevier [7].

A distorted phase grating (DPG) [63] leads to different amounts of defocusing in the wavefront whereby each one occurs at a different diffraction order. When used in combination with a lens, each of the diffraction orders contains image information from a different focal plane, as illustrated in fig. 3.7. If the sample imaged is composed of objects located in different focal planes then the DPG, in combination with a lens, can be used to image these focal plane onto a single image plane. As a result each focal plane image is stored in a different diffraction order of the captured image. The depth images can then be assembled to construct a three dimensional representation of the scene.

3.4 Temporal

Frequency Recognition Algorithm for Multiple Exposures

The frequency recognition algorithm for multiple exposures (FRAME) technique, which is also the subject of this thesis, has been demonstrated for ultrafast temporal imaging [9]. In this experimental arrangement, illustrated in fig. 3.8, different pulses of light with different

arrival times on a dynamic sample are each encoded with a unique spatial modulation pattern. A multiplexed image containing the four images due to each light pulse are recorded in a single camera exposure. Each image is accessed by filtering the Fourier transformed image to decode each of the images and inverse Fourier transform them back into the spatial domain. The setup is therefore not temporally limited by the refresh rate of the detector used but instead by pulse separation time.
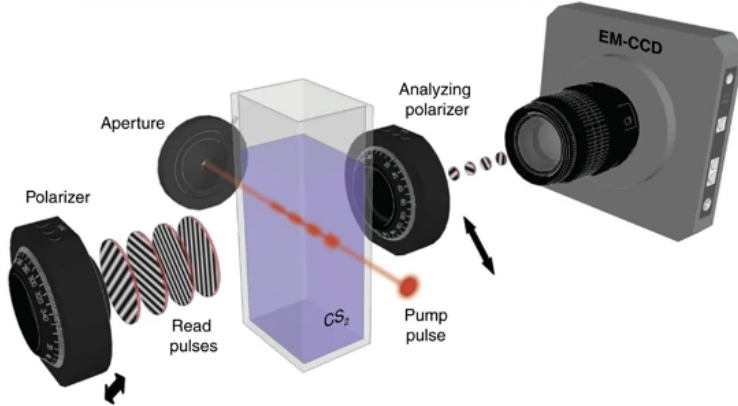
Figure 3.8: A schematic of the experimental arrangement for the FRAME videography demonstration, courtesy of Nature [9].

Sequentially Timed All-optical Mapping Photography

The sequentially timed all-optical mapping photography (STAMP) [64] method (fig. 3.9)stretches an ultra short optical pulse and then splits it into a series of discrete pulses each with different wavelengths. A dynamic sample is then illuminated by these coloured pulses, each arriving at the sample at different point in time. A spatial mapping unit then distributes the pulses onto different locations on a detector, based on their different wavelengths. Each pulse image corresponds to a different point in time in the evolution of the dynamic sample. In [64] the technique demonstrated an imaging speed of 4.4 trillion frames per second but for only up to six frames.
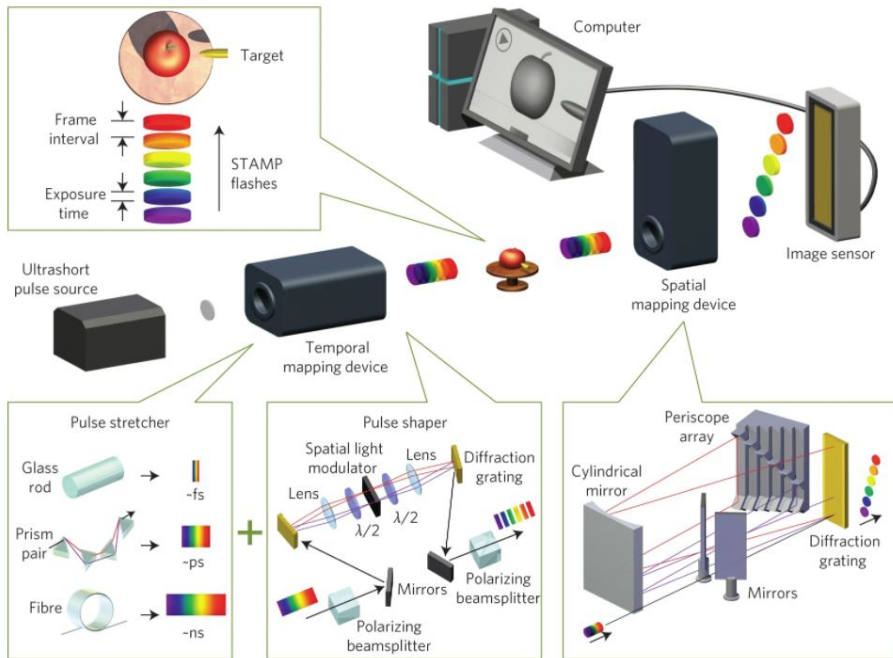
Figure 3.9: A schematic of the experimental arrangement for the sequentially timed all-optical mapping photography demonstration, courtesy of Nature [64].

Chapter 4

The Fourier Domain and Structured Light

In the advent of optical imaging techniques and the development of cameras which can capture digital images, there has been a growth in computational analysis techniques to process the information captured. With increasingly large image files obtained but a desire to share these globally there has been a need to compress the image files but to maintain the information within them [65, 66, 67]. Additionally the use of structured illumination in conjunction with computational analysis has allowed super-resolution imaging to be achieved [68, 69]. Both of these cases involve an understanding and manipulation of information in the frequency, or Fourier, domain. The work presented in this thesis is built upon the use of structured light along with making use of the unexploited frequency regions in digital images. This chapter therefore aims to give an overview of digital images, the Fourier domain and structured light to provide the reader with the foundation required for understanding the FRAME concept.

4.1 The Fourier Domain
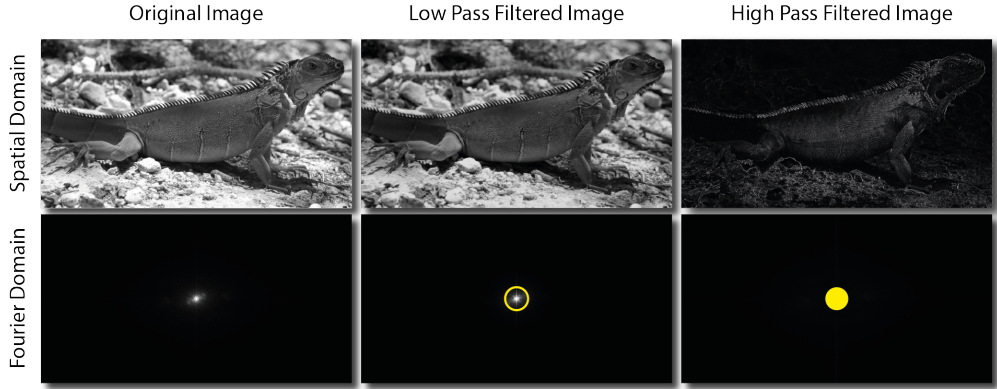
Figure 4.1: A digital image of an iguana shown in both the spatial and Fourier domains to illustrate the different frequencies an image is composed of. The image is high and low pass filtered as indicated by the yellow circle. The low pass image is constructed from only the frequencies inside the circle and conversely the high pass image from only the frequencies outside the circle.

The Fourier domain of an image is a mapping of the intensity distribution of different frequencies, i.e. it shows how much of each spatial frequency is present. The frequency distribution of a two dimensional Fourier domain goes from low to high frequencies from the centre outwards towards the edges. A digital image, which we more commonly view in the spatial domain, is in fact composed of different frequencies which we can see if we Fourier transform [70, 71] the spatial domain image into the Fourier domain (fig. 4.1). Moreover, most of the image information is in fact located at the centre of the Fourier domain [72] leaving much of the higher frequency region sparsely occupied. Fig. 4.1 shows the resulting images if one filters away certain frequencies in the Fourier domain. A low pass filter, allowing only the frequencies within the marked circle (fig. 4.1), actually contains most of the image information such that if the filtered Fourier domain is inverse Fourier transformed back to the spatial domain, the resulting image still appears much the same as the original unfiltered one. Finer structural details are described by higher frequencies and it is this information with is lost when low pass filtering is performed. Some lossy image compression methods, i.e. ones where the original image cannot be fully recovered, make use of such filtering. The high pass filtered image shown in fig. 4.1 removes all the frequencies within the marked circle and as a result only maintains the finer structural details, loosing most of the image information.

4.2 Structured Light

| Spatial Modulation | Rotated Spatial Modulation | Low Frequency Spatial Modulation | High Frequency Spatial Modulation |
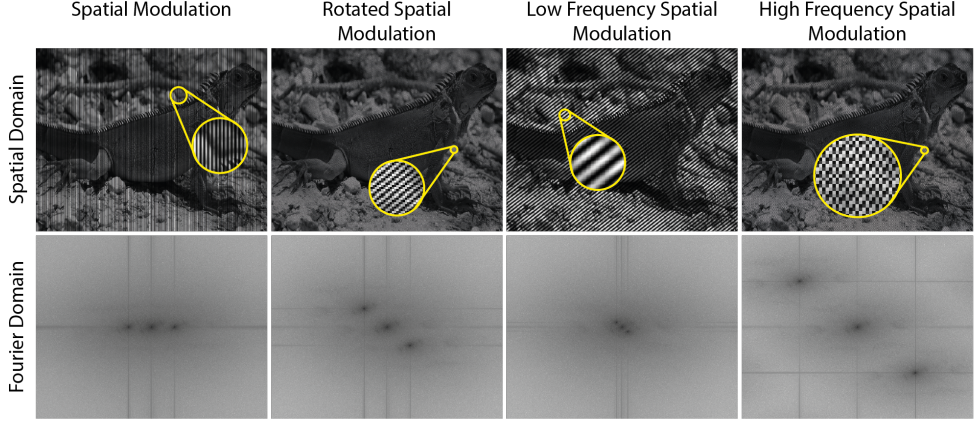
Figure 4.2: A digital image of an iguana shown after multiplication with a modulated intensity pattern to illustrate an image obtained using structured light (spatial domain), along with the accompanying image copies which are seen in the Fourier domain. The same image is also shown; with a rotated structured light pattern, showing how the image copies rotate in the Fourier domain, and with a higher and lower applied modulation frequency, to show how the image copies shift frequency location within the Fourier domain.

Classically we consider images obtained using what is called homogeneous, or uniform, illumination. Images obtained under this type of illumination have a frequency spread centred at the origin of the Fourier domain with the greatest intensity at the centre, decreasing radially. If one obtained images of samples either illuminated with structured illumination or where the emitted light is modulated using a structured mask (structured detection), the Fourier transform looks a little different. The original frequency spread of the sample centred at the origin of the Fourier domain remains but is accompanied by two additional clusters located symmetrically about the origin (fig. 4.2). The clusters in fact contain copies of the image information, found in the central one, but shifted to centre at the frequency $(+/-\nu)$ corresponding to the spatial modulation of the structured illumination or detection.

$$S_\phi(x, y) = 0.5 + m \cdot sin(2\pi x \nu + \phi) \tag{4.1}$$

The spatial modulation pattern used in structured light imaging can be described using eq. (4.1) [73], where m is the modulation depth, ν is the spatial frequency of the modulation pattern, x and y are the Cartesian coordinates and ϕ is the phase of the sine wave. When the modulation pattern interacts with the sample, be it structured illumination or structured detection, the image captured can then be expressed by eq. (4.2). The captured image now contains a non-modulated, $I_C(x, y)$, and modulated, $I_S(x, y) \cdot sin(2\pi x \nu + \phi)$ portion,

corresponding to the central and outer clusters respectively (illustrated by fig. 4.2 spatial modulation). The $I_S(x,y)$ term is the local amplitude information of the modulation and it is this component that one wishes to isolate, in computational post processing of the image, in order to access only the information in the modulated outer clusters. The centres of these clusters, expressed by $I_S(x,y) \cdot sin(2\pi x\nu + \phi)$, correspond to the frequency, ν, of the applied modulation pattern. The cluster locations in the Fourier domain can therefore be controlled by changing ν, where a smaller value shifts them towards the centre and a larger value shifts them away from the centre (fig. 4.2 low and high frequency modulation). Additionally, an angular rotation of the modulation pattern results in a corresponding rotation of the image clusters in the Fourier domain (fig. 4.2 rotated modulation). A vertical modulation pattern is given by clusters along the horizontal axis of the Fourier domain and a clockwise rotation of this pattern corresponds to a clockwise rotation of the cluster locations in the Fourier domain, of equal magnitude.

$$I_\phi(x,y) = I_C(x,y) + I_S(x,y) \cdot sin(2\pi x\nu + \phi) \qquad (4.2)$$

To make use of the modulated image information one needs to demodulate the clusters, $I_S(x,y) \cdot sin(2\pi x\nu + \phi)$, such that only $I_S(x,y)$ remains. Computationally filtering the clusters in the Fourier domain can be done in order to remove the $I_C(x,y)$ term and isolate only the outer clusters. They then need to be multiplied by reference matrices corresponding to the applied modulation in order to shift the $I_S(x,y)$ information to the centre of the Fourier domain, resulting in a demodulation of the cluster images. At this point the Fourier domain resembles that of a conventional homogenous image with the intensity mapping of the frequency spread, corresponding to the demodulated clusters, centred about the origin. The Fourier domain mapping can then be inverse Fourier transformed back into the spatial domain to obtain the sample image corresponding to the modulated cluster information only.

Depending on whether structured illumination or detection has been used in the imaging of a sample leads to a slight variation in the information which is stored in the image copy clusters. In conventional homogenous imaging all the light from a sample and its surroundings, such as any out of focus and background light present, are captured. If structured detection is used then all the same light, as in the conventional case, will be modulated before detection. As a result the central cluster and the outer image copy clusters will contain the same information, i.e. in and out of focus light. If, however, structured illumination is used then only the regions of the sample which interact with the modulated illumination will in turn become modulated. As a result, the captured image will contain the in focus and out of focus light in the central cluster but not in the modulated image copy clusters, which will contain the in focus sample information only. The outer clusters and the central one will therefore not contain exactly the same information in this case.

Structured Illumination Applications

Structured illumination probes a sample with an in focus modulation pattern at a particular plane, where the corresponding light emitted by the sample after interaction with the illumination maintains the modulated pattern. Other light emitted from the sample, either ambient background light or by stimulation or scattering from the out of focus image planes, i.e. in front of and behind the focal plane, will not be contained in the modulated components of the captured image. As a result, structured illumination provides optical sectioning, i.e. capturing image information from a particular focal plane only, and background light suppression. It is therefore possible to experimentally control the what sample information is modulated. There are consequentially numerous applications for structured illumination which take advantage of this such as volumetric imaging [74, 75] and overcoming multiple light scattering issues [76, 77, 78]. Additionally structured illumination has been used to achieve super resolution imaging [69], arguably the most familiar application to date, but also for surface structure imaging [43, 79] and ultra fast imaging [9].

Structured Detection Applications

Structured detection does not have the same optical sectioning and background light suppression qualities as structured illumination due to the modulation being applied to all the light emitted from a sample. This has not resulted in it being purposeless though. Structured detection has been used for image multiplexing where the sub-images stored are each identified according to a different applied spatial frequency [80, 81]. Structured detection has also been demonstrated for high-speed imaging [82, 83] and field of view extension [84].

Chapter 5

Frequency Recognition Algorithm for Multiple Exposures

FRAME can be seen as an imaging implementation of frequency or wavelength division multiplexing. Classically used in communications systems, frequency/wavelength division multiplexing [85] are techniques used to transmit multiple different signals along a single channel. As their names suggest they use different wave frequencies (radio region) or wavelengths (optical region) as signal carriers such that each of the carrier signals can be separated from each other at the end of the transmission. In the case of the FRAME approach a single detector is used, analogue to the one detection channel, and the use of 2D spatial frequency encoding on the light (incident or emitted from the sample) provides the signal differentiation. As a result FRAME captures multiple different spatially encoded signals in a multiplexed way which are then computationally separated in a post processing stage, leading to a new snapshot imaging regime.

In this chapter the principle of FRAME will be explained followed by the computational analysis stages and properties. The latter part of the chapter will present the different experimental implementations of FRAME created throughout the PhD studies, which have formed the bases of the content of the publications found at the end of this thesis.

5.1 Principle

FRAME imaging comprises of two parts, the experimental implementation of encoding light and the computational analysis. Experimentally, the encoding is applied in different ways, yielding different captured information (e.g. multispectral, volumetric, polarisation)

about the sample(s) imaged. The resulting images from the experimental encoding are in principle the same in that they all produce a multiplexed image, comprising of multiple encoded images, obtained in a single camera exposure. As a result, the computational analysis in order to extract the encoded images, operates using the same fundamental approach for the different experimental implementations.
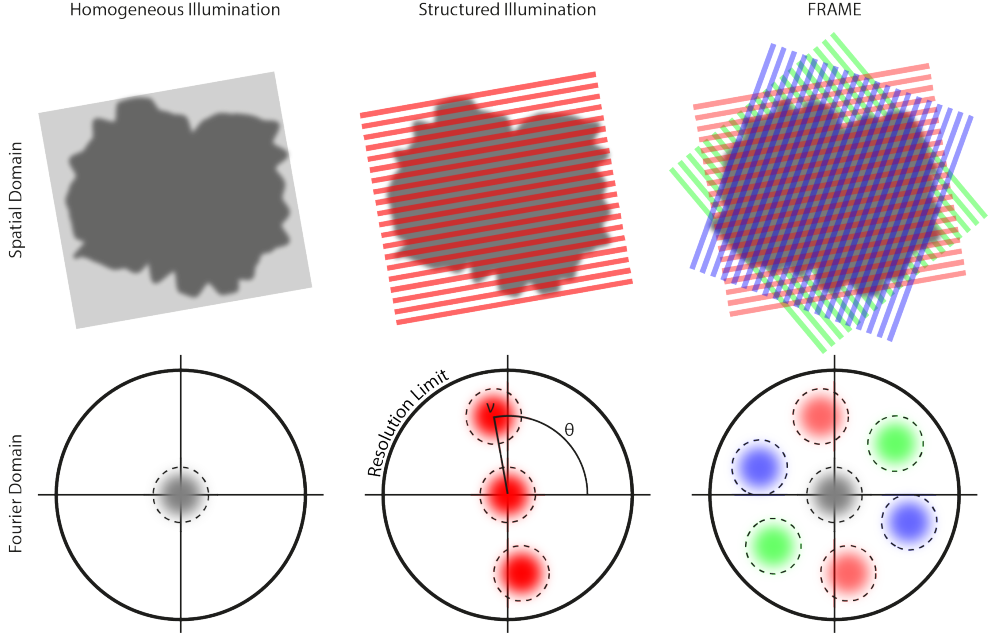
Figure 5.1: An illustration showing the spatial domain images and their corresponding Fourier domains for; homogeneous illumination, structured illumination and FRAME imaging.

When using structured illumination, or indeed structured detection, in an optical arrangement, the image captured contains the spatial modulation frequency information. Taking a Fourier transformation of the captured spatially modulated image yields three distinct data regions, or clusters, in the Fourier domain (fig. 5.1 (Homogenous Illumination)). The central cluster contains the image information as is classically obtained using homogenous illumination or detection (fig. 5.1 (a)). The pair of outer clusters (image copies) contain the same information, however, modulated. The positions of the outer clusters are determined by the applied spatial modulation frequency, ν, and rotation, θ, as illustrated in fig. 5.1 (Structured Illumination). As a result, depending on the ν and θ of the applied spatial modulation, the placement of the outer clusters can be chosen.

FRAME takes advantage of the fact that the spatially modulated images contain the same image information as non-modulated imaging, except located at selected regions of the Fourier domain. It does so by applying unique encoding, a spatial modulation pattern

with a specific ν and θ value, to each different image one would like to capture. As an example one may wish to capture the spectral response of a sample under illumination from three different wavelengths. In such a scenario one would apply a unique encoding to each illumination source such that when the light interacts with the sample information, the resulting response maintains the same encoding. When the sample responses are then captured by the detector in a single exposure, a multiplexed image is obtained (fig. 5.1 (FRAME)). This image can then be Fourier transformed to reveal the modulated image copies, which are located in the cluster pairs found at the corresponding ν and θ of the applied encoding. If the cluster pairs are then demodulated and filtered, it is possible to retrieve each individual image pertaining to each of the different spectral responses.

5.2 Computational Analysis

An illustration of the encoded image extraction, or demultiplexing, procedure is found in fig. 5.2. The encoded images are accessed by demodulation and subsequent filtering, in the Fourier domain. The effectiveness of the image demultiplexing procedure is dependent on several different factors which include; the sample imaged, the encoding frequencies applied, the shape and size of the computational filter, distortions in the encoding and the signal to noise ratio. The following sections present the demultiplexing procedure, along with the impact of the different factors, on its effectiveness.
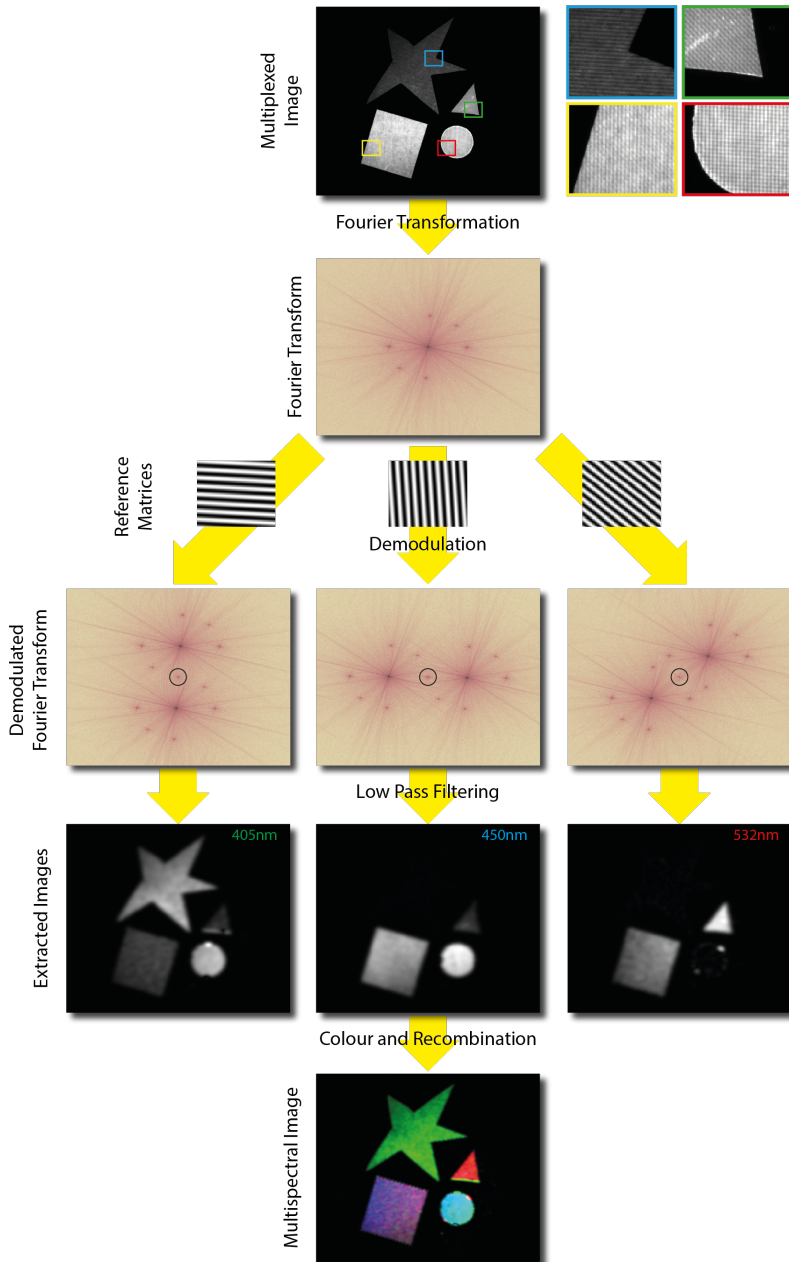
5.2.1 Image Demultiplexing

Figure 5.2: A schematic flow diagram of the demultiplexing method used in the extraction of the encoded images from the multiplexed image captured using FRAME imaging.

Fig. 5.2 illustrates the demodulation process of a raw detector image, comprised of three uniquely encoded images, into its constituent images. To obtain the detected image, experimentally the intensity profile of the light (illumination or emission) is modulated with a sinusoidal pattern with frequency, ν, and phase, ρ. If it is the illumination being modulated, the sample structures, A, become superimposed multiplicatively with the light when they interact, i.e. the modulation pattern is maintained in the sample response. Alternatively, if it is the light emitted from the sample which is encoded, it is at the point where the light interacts with the diffractive element, that the sample information becomes superimposed multiplicatively with the spatial frequency of the element. Eq. (5.1) gives the mathematical description of a multiplexed image where three different spatial modulations have been applied (e.g. multiplexed image in fig. 5.2). B_{DC} represents the DC component, which contains the unmodulated sample structures as well as any out of focus background signal, which is not present in the modulated regions if they were generated using structured illumination. For simplicity, the remainder of the mathematical description will consider only one of the modulated components, with ν_y set to zero (eq. (5.2)), which can be described by eq. (5.3).

$$
\begin{aligned}
I_{mod} = B_{DC} &+ A_1 sin(2\pi\nu_{x1}x + 2\pi\nu_{y1}y + \rho_1(x,y)) \\
&+ A_2 sin(2\pi\nu_{x2}x + 2\pi\nu_{y2}y + \rho_2(x,y)) \\
&+ A_3 sin(2\pi\nu_{x3}x + 2\pi\nu_{y3}y + \rho_3(x,y))
\end{aligned} \tag{5.1}
$$

$$
I_{mod} = B_{DC} + A_1 sin(2\pi\nu_x x + 2\pi\nu_y y + \rho_1(x,y)) \quad set\ y = 0 \tag{5.2}
$$

$$
I_{mod} = \overbrace{0.5(A}^{DC} + \overbrace{Asin(2\pi\nu_x x + \rho_x)}^{Modulated\ Image}) \tag{5.3}
$$

The detected image needs to be demodulated in order to extract the sample information (A). To achieve this a demultiplexing procedure based on the lock-in detection principle [86, 87], is used. Since we know that we applied a sinusoidal modulation we can therefore construct two reference matrices, R_1, R_2 (eqs. (5.4), (5.5)), with a phase shift of $\pi/2$ between them and the same frequency as the applied encoding. I_{mod} is multiplied by the reference matrices. We also assume the phase, ρ_x to be constant in this analysis. The demodulation by reference matrix multiplication can be seen in fig. 5.2, where the image copy clusters, corresponding to each encoded image, have become shifted to the centre of the Fourier domain.

$$
R_1 = sin(2\pi\nu_x x + \rho) \tag{5.4}
$$

$$
R_2 = sin(2\pi\nu_x x + \rho + \pi/2) \tag{5.5}
$$

$$R_1 I_{mod} = 0.5A sin(2\pi\nu_x x) + \rho) + 0.5A sin(2\pi\nu_x x + \rho_x) sin(2\pi\nu_x x + \rho) \tag{5.6}$$

$$R_2 I_{mod} = 0.5A sin(2\pi\nu_x x) + \rho + \pi/2) + 0.5A sin(2\pi\nu_x x + \rho_x) sin(2\pi\nu_x x + \rho + \pi/2) \tag{5.7}$$

$$\begin{aligned} R_1 I_{mod} = 0.5A(sin(2\pi\nu_x x + \rho) \\ + 0.5(cos(\rho_x - \rho - \pi/2) - cos(4\pi\nu_x x + \rho_x + \rho + \pi/2))) \end{aligned} \tag{5.8}$$

$$\begin{aligned} R_2 I_{mod} = 0.5A(sin(2\pi\nu_x x + \rho + \pi/2) \\ + sin(2\pi\nu_x x + \rho_x) sin(2\pi\nu_x x + \rho + \pi/2)) \end{aligned} \tag{5.9}$$

$$\begin{aligned} R_1 I_{mod} = 0.5A(sin(2\pi\nu_x x + \rho) \\ + 0.5(cos(\rho_x - \rho) - cos(4\pi\nu_x x + \rho_x + \rho))) \end{aligned} \tag{5.10}$$

$$\begin{aligned} R_2 I_{mod} = 0.5A(sin(2\pi\nu_x x + \rho + \pi/2) \\ + 0.5(cos(\rho_x - \rho - \pi/2) - (4\pi\nu_x x + \rho_x + \rho + \pi/2))) \end{aligned} \tag{5.11}$$

To select the shifted, demodulated component only, we apply a low pass filter (illustrated by the black circle in the demodulated Fourier transform in fig. 5.2) with a cut off at ν_x. The filtering yields the expressions given by eqs. (5.12), (5.13)), where the tilde assignment indicates the frequency filtering. The final image information is determined by calculating eq. (5.14), to obtain $\widetilde{A}$, which is equivalent to the amplitude of the modulated image component desired. Only the central, demodulated region is retained after filtering, which can then be inverse Fourier transformed to return to the spatial domain (extracted images in fig. 5.2). The resulting image(s) are now the demultiplexed images from the raw data. These can be viewed individually or could be false coloured and recombined in order to visualise the sample details in a single image (multispectral image in fig. 5.2).

$$R_1 I_{mod} = 0.5^2 \widetilde{A} cos(\rho_x - \rho) \tag{5.12}$$

$$R_2 I_{mod} = 0.5^2 \widetilde{A} sin(\rho_x - \rho) \tag{5.13}$$

$$0.5\widetilde{A} = \sqrt{R_1 I_{mod}^2 + R_2 I_{mod}^2} \tag{5.14}$$

5.2.2 Fourier Filtering

When the encoded images are accessed in the Fourier domain and filtered in order to select the information pertaining to each individual image (as illustrated in fig. 5.2), the shape and size of the filter used impacts the resulting image obtained. Throughout the work presented in this thesis, Gaussian filters have been used, although other filter shapes could be chosen, such as the non-uniform band-pass filters found in [88]. The size, or radius, of the filters used, however, has not been constant across the work. This is because different imaging conditions, such as the frequency of the applied modulation used or the sample being imaged, lead to different image copy cluster placement and frequency spread, respectively, in the Fourier domain. Therefore, the filter size one chooses to analyse the data with is dependent on the outcome desired in terms of; the spatial resolution of the extracted images, the specificity required, the degree of cross talk which is acceptable and the total number of image copies acquired in an exposure.

Cross Talk

Since image information is predominantly composed of low frequencies [72], the FRAME approach takes advantage of the sparsely occupied higher frequency region of the Fourier domain. This is not to say that it is devoid of any information, however, and the finer the structural details of a sample imaged are, the more higher frequency information there will be. As a result there is a degree of cross talk intrinsic to the FRAME image multiplexing approach, although this can be extremely low, with R^2 values of 0.99 demonstrated when comparing the extracted images and their corresponding ground truths. The degree of cross talk in the resulting images is dependent on how much unwanted information is found within the encoded image regions that are demodulated and extracted. This can originate from the non-modulated sample information captured, neighbouring encoded sample information, and of course background signals and noise.

The Sample and Image Storage Capacity

An image of a sample is constructed from a variety of different spatial frequencies. If the sample has a high degree of structural details then it will contain a broad spread of frequencies (high and low), which can be seen in the Fourier domain as a large data cluster. Conversely, if the sample has a low degree of structural details it will contain only low frequency information which, in the Fourier domain, is represented by a much narrower data cluster. Fig. 5.3 shows two images and their corresponding Fourier transforms where it can be seen that the spread of frequencies is broader for the higher resolution image of the iguana which has a high degree of structural details, compared with the low frequency

rocket trail image. As a result, when sample information becomes experimentally encoded, the properties of the sample captured will remain in the image copy clusters used in the FRAME approach. If the sample imaged has a high degree of structural details then the encoded images will have a large spread in the Fourier domain. In order for these images to be successfully extracted from the multiplexed image, the image copy clusters need to be well separated from the central and neighbouring clusters. This can be achieved by carefully choosing what encoding to apply experimentally to "place" the encoded image information in distinct regions of the Fourier domain. Strongly overlapping data clusters can lead to a high degree of cross-talk in the resulting, demodulated images, since the encoded images will occupy the same space in the Fourier domain.
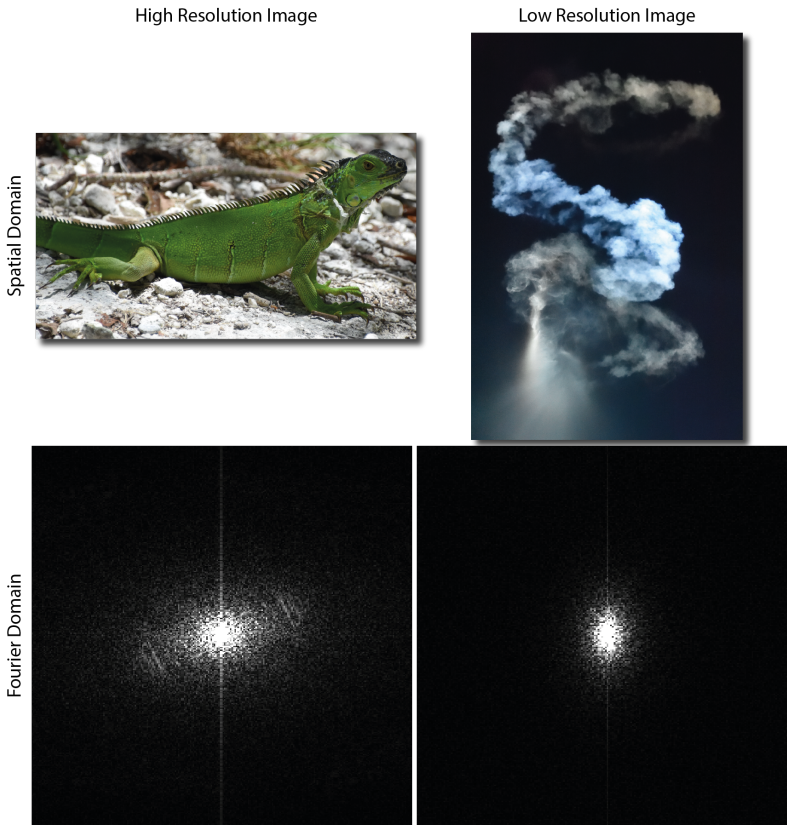
Figure 5.3: A high and low resolution image illustrating how the frequency spread in the Fourier domain differs depending on the level of detail contained within the sample imaged.

The greater the image storage capacity desired, the more densely packed the images will be in the Fourier domain. As a result there will be a limit to how many images can be stored and successfully demultiplexed for a given detector (the resolution limit, as indicated

in fig. 5.1, is set by the detector). The image storage limit will, however, to some degree be set by the sample and its frequency spread. Samples with a lower degree of structural details will be more suitable for dense image storage due to their low frequency spread in the Fourier domain.

Specificity vs. Spatial Resolution
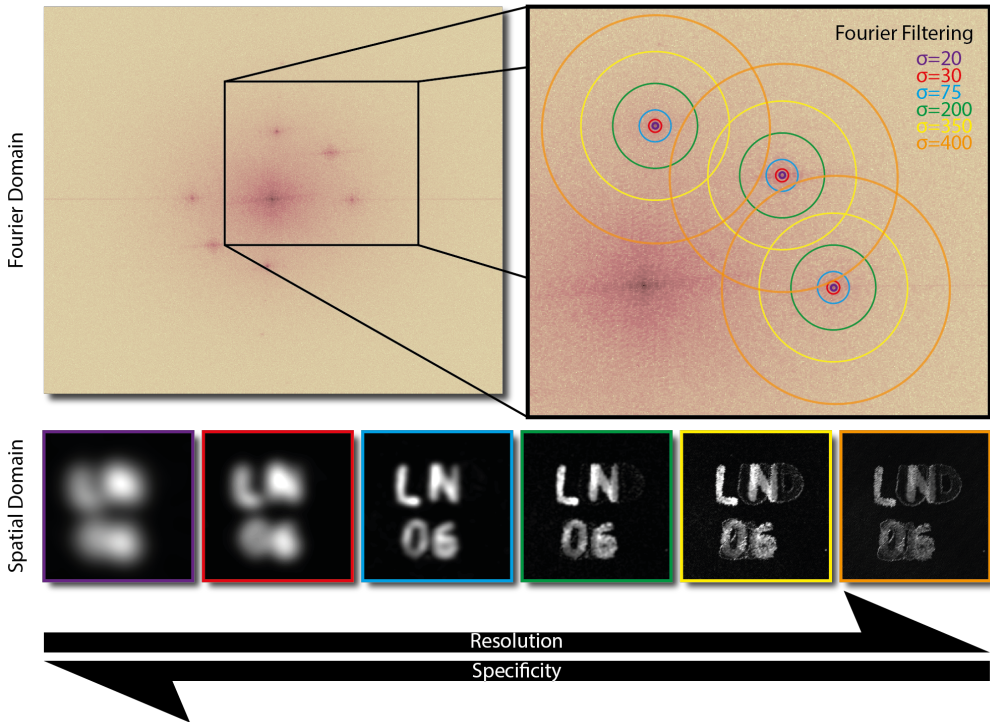
Figure 5.4: Resolution versus Specificity: An illustration of the trade off that exists between specificity and spatial resolution when varying the filter size in the Fourier domain.

The size of the filter used to select the information within each data cluster leads to a trade-off between the resulting specificity and spatial resolution of the image, as shown in fig. 5.4. A small filter size selects the information with a high degree of specificity, which can either reduce or remove cross-talk from any neighbouring clusters. The small filter size does, however, only select the data at the centre of the cluster, which corresponds to the low spatial frequencies that the sample image is comprised of. As a result the extracted image will contain a low degree of spatial details. If a large filter size is instead chosen there is a risk that it will "capture" some of the data from neighbouring clusters leading to cross-talk in the extracted image. This is illustrated in fig. 5.4 for the filter sizes $\sigma = 200, 350, 400,$

where the outlines of U, D, 2 and 1, originating from neighbouring clusters, can be seen in the extracted images. The degree of cross-talk will of course be dependent on how much additional, unwanted data is included within the filter size used. The advantage of the larger filter size is that more of the data points pertaining to the image cluster of interest are included, which correspond to high frequencies. As a result the extracted image will contain more structural details.

5.2.3 Phase

In structured illumination imaging techniques, such as structured illumination microscopy [89] and fringe projection profilometry [90, 91], it is of critical importance that the full characteristics, i.e. spatial frequency, angle and phase, of the illumination pattern, are known. To date, FRAME analysis has only considered the spatial frequency and orientation of the encoding pattern when extracting different exposures in the Fourier domain. By assuming the phase to be constant FRAME may suffer from inaccuracies in the image reconstruction. Therefore, if a more accurate estimation of the encoding pattern is used, more robust image extraction could potentially be achieved.
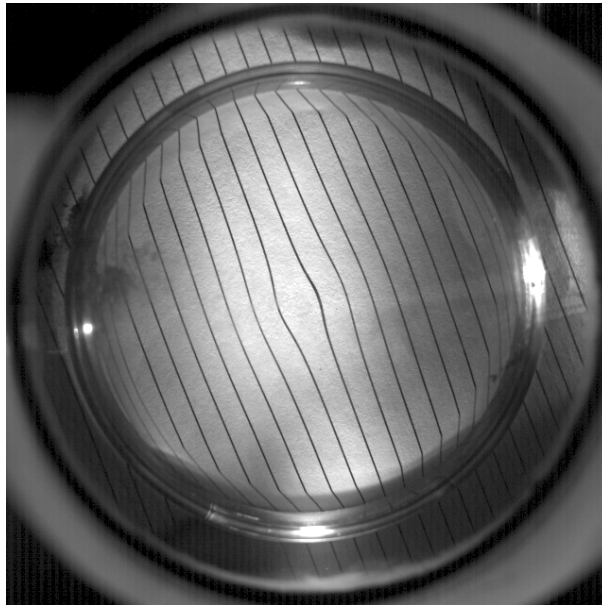

Figure 5.5: Distorted parallel black lines as seen through a quartz piston used for optical access in combustion diagnostics, in combustion engines.

Optical imaging is widely used in research and industry where there are scenarios where the optical access to the sample can be limited and distortions in the obtained images can

occur. FRAME uses a modulated line pattern and if this is distorted the ability to efficiently demodulate the images obtained may lead it to be unsuitable for such difficult imaging cases. Combustion processes are a good example of such candidates. Snapshot imaging of multiple species simultaneously is of interest in combustion diagnostics [92], however, such measurements are often performed in optically difficult conditions, such as within combustion engines with distorting, transparent pistons (see Fig. 5.5). Other examples of imaging scenarios which can suffer from modulation distortions include, but are not limited to, optical fibres, such as in biomedical optics, and lens distortion [93]. It is therefore of interest to investigate the robustness of the FRAME decoding technique on images with extreme distortions in the phase intensity profile.
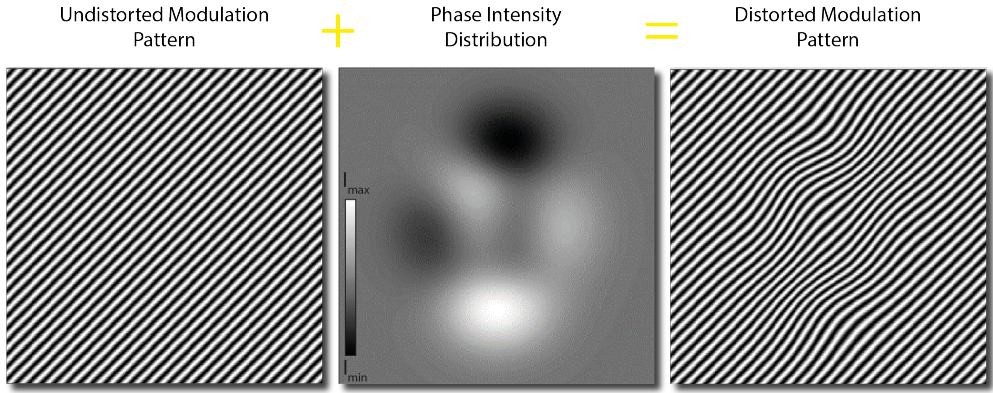
Figure 5.6: **Distorted modulation pattern:** An illustration of a non-uniform phase intensity distribution across a uniform modulation pattern, leading to a distorted modulation pattern.

To investigate the impact of distortions in the spatial frequency pattern, on the ability to extract the encoded images, simulations were performed in MatLab. An undistorted line pattern was distorted using an arbitrary phase intensity distribution, as illustrated in fig. 5.6. The distorted pattern was then used to encode a stock MatLab image (of grains of rice) to simulate how an image, where the captured encoding pattern had a non-constant phase, would appear. A second stock MatLab image (of the cameraman) was also encoded with a different distorted modulation pattern which was then multiplexed with the first, along with a third image (of trees) to simulate a background, non-modulated signal. The multiplexed image, shown in fig. 5.7, was then demultiplexed in both the conventional way described in **Section 5.2.1**, using two reference matrices and setting the phase to zero, and also using the input, distorted modulation patterns where the non-constant phase component was included. In the latter case one does not use two reference matrices for each image extraction but instead uses the distorted line pattern as a single reference matrix. Fig. 5.7 shows the original images along with the multiplexed image and the two sets of demultiplexed images. Despite ignoring the phase, the conventional FRAME approach manages

to extract the two different input images although artefacts, due to the extreme modulation distortion of the encoding pattern, seen most noticeably as dark regions, are visible. Incorporating the non-constant phase, and therefore using a more accurate spatial frequency pattern for the decoding, clearly yields better results when there are extreme modulation distortions. These extracted images also lack the artefacts due to the distortions. The simulated case shown in fig. 5.7 illustrates extreme modulation distortions, probably more than would be experienced in the "real world" scenarios given above. The same simulation was therefore also performed using slightly reduced phase intensity distributions, of a more comparable nature to "real world" cases, yielding more moderate modulation distortions. The extracted images using the conventional FRAME approach in this case had minimal artefacts. To provide a measure of the performances of the two demultiplexing approaches, using constant or non-constant phase assumptions, R^2 values comparing the original input images with the extracted images in each case, were calculated. The results can be seen in tables 5.1 and 5.1 for the cameraman and rice images, respectively. The R^2 between the extracted images, using the two different approaches, are also included to give a measure of how different they are from each other. Since the extracted images using constant and non-constant phase, for moderate distortions, are comparable and all have R^2 values over 0.94 compared to the original images, one can conclude that the FRAME approach is robust in the image extraction even when the encoding is distorted. Of course, the use of the phase leads to better results, especially under extreme distortions, and would therefore be beneficial to include where possible.

Table 5.1: R^2 **Cameraman Images:** The R^2 values when comparing the input cameraman image with the extracted images using constant and non-constant phase, as well as the comparison between the two extracted images. Under extreme modulation distortion the conventional FRAME demultiplexing, which assumes a constant phase for the reference matrices, performs more poorly than when the distorted modulation pattern is used as a reference matrix. Under moderate distortion, however, the extracted images, using the two different approaches, are comparable to each other.

	Original vs Non-constant phase	Original vs Constant phase	Non-constant phase vs Constant phase
Extreme distortion	0.8389	0.9660	0.8717
Moderate distortion	0.9572	0.9660	0.9917

Since FRAME currently uses two parameters, modulation frequency and angle, to uniquely encode different images, incorporating the phase could add another encoding parameter. Additionally it was found that using a more accurate estimation of the encoding pattern in the demultiplexing makes image extraction more robust, particularly under modulation distortion conditions. In April 2020, *C.Hu et al.* [94] demonstrated using the phase as part of the encoding to double the image storage capacity. By choosing a phase shift of $\pi/2$ between encoding patterns, it is possible to encode images with exactly the same spatial frequency and orientation. Fig. 5.8 shows the simulated results of two input images en-

Table 5.2: R^2 **Rice Images:** The R^2 values when comparing the input rice image with the extracted images using constant and non-constant phase, as well as the comparison between the two extracted images. Under extreme modulation distortion the conventional FRAME demultiplexing, which assumes a constant phase for the reference matrices, performs more poorly than when the distorted modulation pattern is used as a reference matrix. Under moderate distortion, however, the extracted images, using the two different approaches, are comparable to each other.

	Original vs Non-constant phase	Original vs Constant phase	Non-constant phase vs Constant phase
Extreme distortion	0.5081	0.9631	0.5202
Moderate distortion	0.9417	0.9631	0.9964

coded with $\pi/2$ phase shifted encoding patterns, which are multiplexed with a background signal image. The extracted images are obtained using one reference matrix for each image, where the same phase component corresponding to each input encoding pattern, is included. Fig. 5.8 illustrates that this precise knowledge of the encoding patterns, despite the heavy overlap of the image copy clusters, successfully extracts the two input images from the multiplexed image. Initial tests did find that deviations from the $\pi/2$ phase shift showed deteriorations in the extraction ability and therefore that precision in encoding and decoding is required. The results are nevertheless encouraging as a method of doubling the image storage capacity.

The findings when incorporating the true encoding phase versus assuming it to be a an arbitrary constant can be summarised as follows:

- Constant and non-constant phase assumptions yield comparable results when distortions are moderate.

- More accurate image extraction using non-constant input phase when modulation distortion is extreme.

- 50% faster computational processing time when non-constant phase included, as only one reference signal is needed in the demodulation instead of two.

- Image storage capacity can be doubled using $\pi/2$ phase shifted encoding patterns.
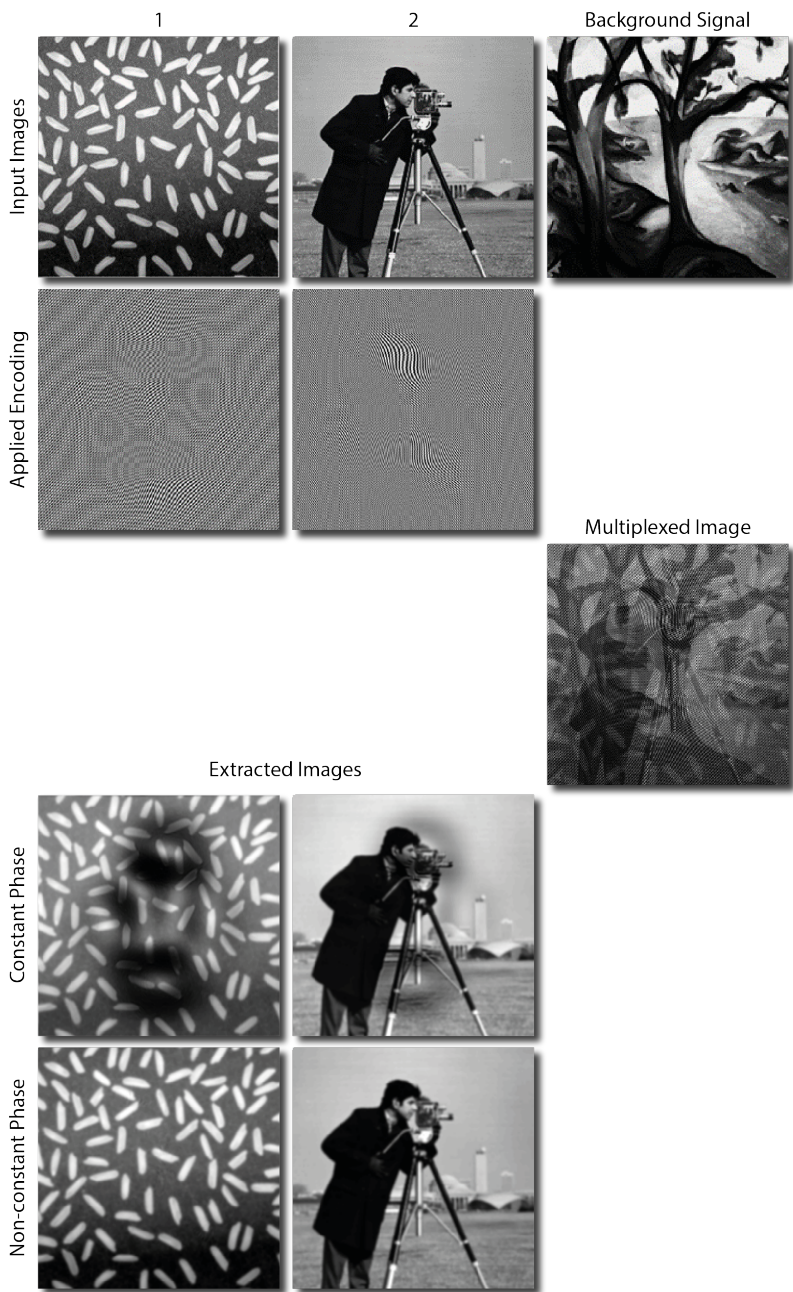
Figure 5.7: Constant vs non-constant phase: An example illustrating the demultiplexing of two encoded images. The multiplexed image, including a non-modulated background signal, is demodulated where the phase is assumed constant, and then when the non-constant, input phase is used.

Figure 5.8: Doubling image storage capacity: A multiplexed image composed of two images encoded with modulation patterns which have the same ν and θ values but a phase difference of $\pi/2$, along with an unmodulated background signal, is successfully demodulated using the fully described encoding modulation patterns.

5.3 Experimental Encoding

FRAME can experimentally be implemented in a number of different ways as is demonstrated by work presented in the papers found at the end of this thesis. The different implementations involve either structured illumination, structured detection or both. Depending on the experimental implementation of the encoding, the resulting type of imaging achieved varies. This section will focus on the different experimental setups that were built and what types of imaging they are applicable for.

5.3.1 Experimental Considerations

There are some more general experimental considerations which are applicable across the different FRAME setups which are perhaps better addressed here in order to give a brief overview of more minor considerations to have in mind. Intrinsic properties of the encoding as well as certain experimental choices are addressed in this section.
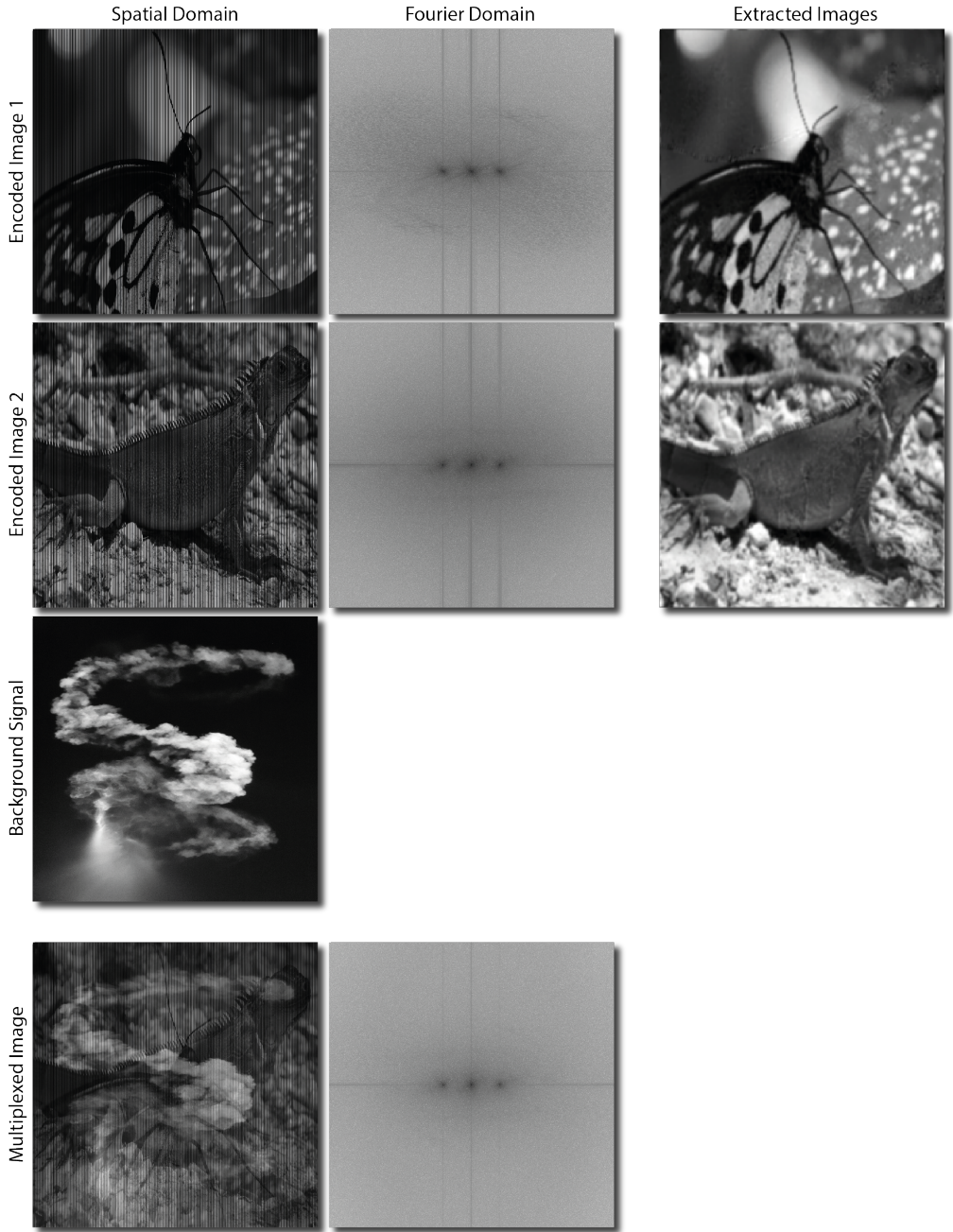
Modulation

A "good" spatial modulation is key to obtaining the best possible results using the FRAME setup. There are different things which impact the modulation and therefore determining the optimal result for a specific setup is required. Since using a line encoding leads to a reduction in the spatial resolution one wants to choose the highest frequency resolvable for the optical arrange and detector resolution. The modulation depth should also be optimised. A poor SNR, for example, will lead to a poor modulation depth. Adjusting the illumination intensity, the detector exposure time, or the aperture size can be done to aid in improving this.

Encoding Element

The encoding is applied through the use of line gratings or diffractive optical elements (DOE). When using the line gratings in the illumination encoding schemes, all the diffraction orders, except ± 1, are blocked. This results in a doubling of the spatial frequency on the sample relative to the grating and also an extended depth of focus of the modulation pattern. There is, however, a loss of light intensity as a result which may be disadvantageous depending on the sample being imaged and the maximum output of the sources being used. The DOEs are a good way to preserve light as they do not produce a zeroth order in the Fourier plane so only the higher orders (greater the 1), of lower intensity are blocked. In certain cases DOEs are required due to the wavelength range used as the standard line

gratings are not suitable. Diffraction gratings have the advantage, where they can be used, to be more easily interchangeable than DOEs, which are custom components designed for specific wavelengths only.

Optical Sectioning

The FRAME approach uses either structured illumination, structured detection or both. Where the encoding is applied affects the content of the images and thus the type of imaging achievable. The multiplexed images obtained, however, are mathematically described in the same way and can therefore be demodulated in the same way regardless of where the encoding occurred. The practical outcome of the two schemes do, however, differ slightly. When structured illumination is employed one gains the benefit of optical sectioning. As a result, background signals can be removed from the resulting demultiplexed images by only selecting the modulated image data clusters. In the case of the emission encoding, all the light from the sample is modulated and therefore optical sectioning due to the spatial modulation is no longer present. There are of course other practical reasons for choosing one encoding scheme over the other and therefore one needs to select the most appropriate one taking such considerations as sectioning, into account.

Fig. 5.9 illustrates the z-sectioning achieved using the multispectral illumination FRAME setup when using an aperture of $f\#5.6$ was used. In this example the depth of focus was measured to be about $7mm$ for a field of view of $59x50mm$.
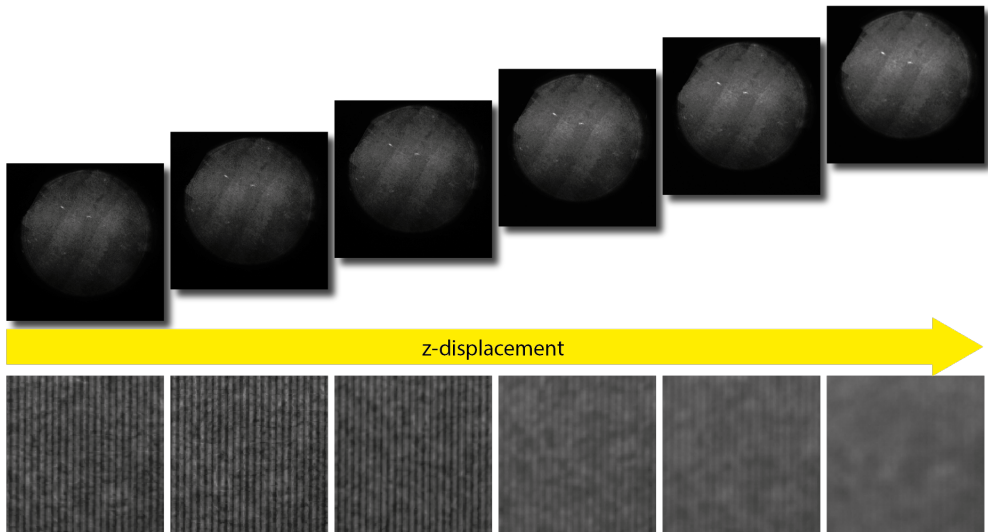

Figure 5.9: **Optical sectioning:** Raw images (top) are shown along with zoomed regions (bottom) showing the fading modulation pattern as the sample is moved out of the focal plane of the structured illumination.

Experimentally, adjusting the detector aperture size also affects the sectioning. A small aperture size yields a long depth of field and vice versa, a large aperture size yields a short depth of field. As a result, when imaging over an extended depth the aperture size needs to be carefully chosen in order to capture all the information, in focus.

5.3.2 Multispectral Illumination Encoding

Microscope
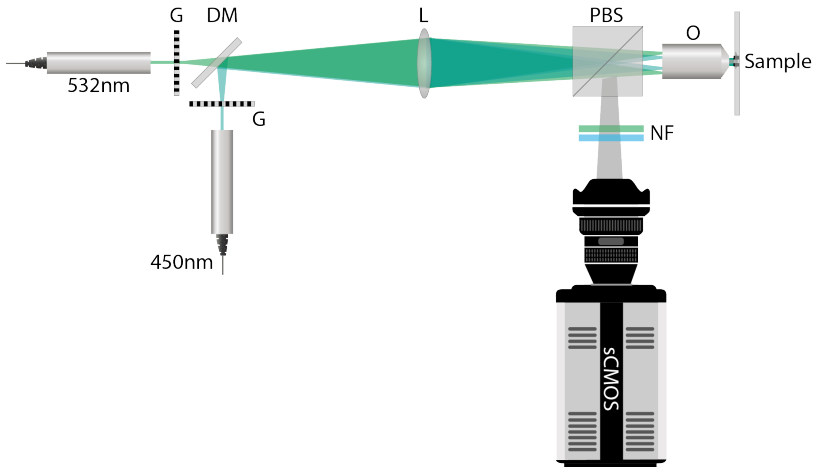
Figure 5.10: A schematic of the microscope setup. G=line grating, L=lens, M=mirror, NF=notch filter, PBS=polarisation beam splitter, O= microscope objective.

Fig. 5.10 shows the microscope FRAME setup using two encoded lasers to illuminate a sample. The light from each laser ($450nm$ and $532nm$) is initially expanded and collimated before being encoded using a sinusoidal diffraction grating. The two uniquely encoded beams are then spatially overlapped using a dichroic mirror and focussed onto the back of the microscope objective. The modulated patterns are then imaged onto the sample. In this case two different samples were imaged, paper and lens tissue, stained with two fluorescent dyes. The fluorescence from the sample was then directed to the detector using a polarising beam splitter (PBS).
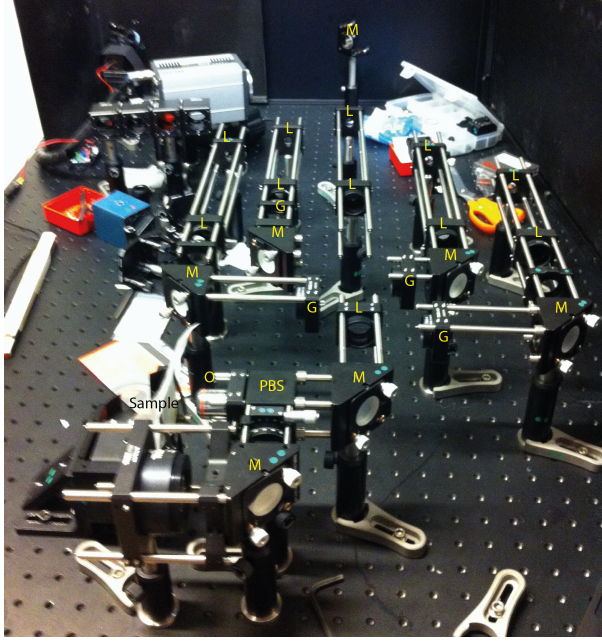
Figure 5.11: A photograph of the microscope setup under construction. G=line grating, L=lens, M=mirror, PBS=polarisation beam splitter, O= microscope objective.

Alignment of the beams onto the focal plane of the microscope objective was not straight-forward. The focal plane was located 19mm inside the objective (fig. 5.12) and therefore fine tuning of the position of the Fourier plane of the focussed beams onto the correct point of the objective, by eye, was not possible. The position of the back of the objective within the setup was therefore noted and then the objective was removed. The Fourier plane of the focussed beams was then adjusted to fall a further 19mm ahead of the marked position objective position, hence where the back focal plane of the objective should be. When the free space alignment of the beam was complete the objective could be replaced. The fine tuning of the modulation pattern and sample position were then done by observing the detector view in live mode, where a continuously updating image is displayed.

Fig. 5.13 shows the raw images captured along with the corresponding Fourier transforms and extracted, demodulated images. A magnification of the lens tissue is shown were it is possible to discern a modulation pattern. Since two different lasers were encoded the setup obtains multiplexed images containing two different images of the samples. These can be seen in the Fourier domain where two pairs of data clusters are visible. Each of these pairs are demodulated and then false coloured and recombined to produce the multispectral images seen under the extracted frames. To verify that the results obtained are accurate they were compared to ground truth images. These were obtained using the same microscope setup but illuminating the samples sequentially, capturing two spectral images. The same

setup was used in order to ensure the best comparison of the images with regards to optical sectioning and spatial resolution consistency. Since the use of structured illumination here provides optical sectioning and a reduction in the spatial resolution, if the FRAME images had been compared with homogeneously illuminated ground truth images one would expect these to have a higher spatial resolution as well as the presence of out of focus and background light. A comparison of the FRAME images and their corresponding ground truths confirms that the snapshot multispectral method provides accurate results.

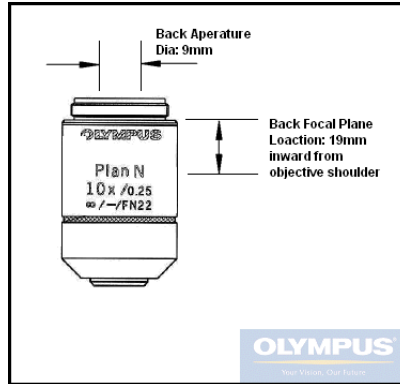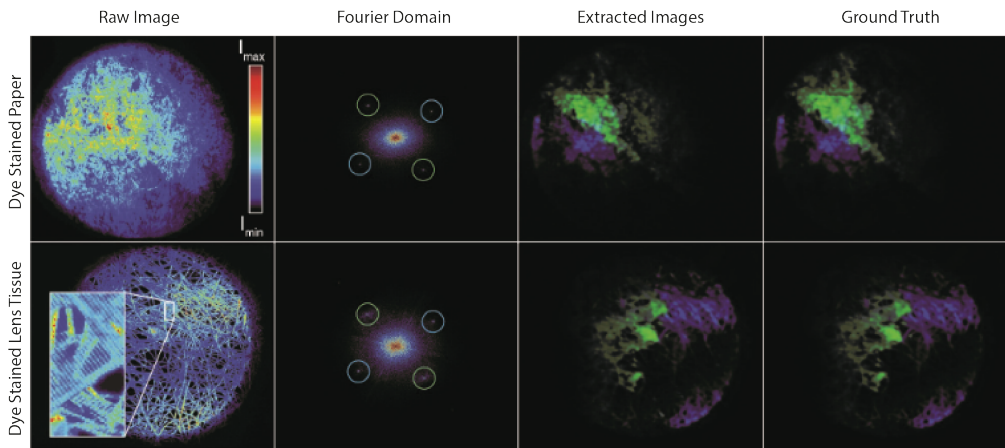Figure 5.12: A sketch of the microscope objective, with courtesy of Thorlabs.

Figure 5.13: Results from the two beam FRAME microscope setup of paper and optical lens tissue, stained with two different fluorescent dyes.

Macroscopic Setup

Fig. 5.14 shows the macroscopic multispectral FRAME experimental setup based on structured illumination. This setup used three different diode lasers ($405nm$, $450nm$ and $532nm$),

each with neutral density (ND) filters (filter wheels) at their outputs. The optical intensity outputs of the lasers differed and additionally, when performing florescence imaging the responses of the different fluorophores to each excitation source often varies in intensity. Using neutral density filters at the exit of each laser source allows the intensity of the lasers to be adjusted so that it becomes possible to balance the signal intensities recorded by the detector. In this way different fluorescence responses can be compensated for in cases where one signal due to excitation from one laser may be very low relative to another signal due to a different excitation source. Similarly, if the exposure time of the detector is suitable for one or more of the detected fluorescence signals but there is saturation from others due to a particular laser, then the high intensity signal can be reduced by using a more attenuating ND filter to ensure there is no saturation on the detector.
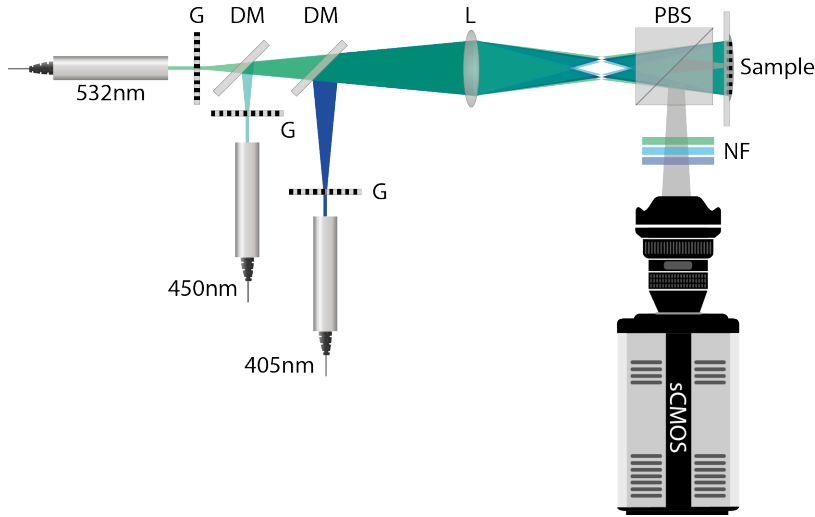
Figure 5.14: A schematic of the macroscopic multispectral illumination encoding FRAME setup. DM=dichroic mirror, G=line grating, L=lens, M=mirror, NF=notch filter, PBS=polarisation beam splitter.

Each laser is expanded and collimated and then encoded using a line grating. The encoded beams are then spatially overlapped using a series of dichroic mirrors. A lens is then used to image the encoded beams onto the sample. In the Fourier plane the beams are partially blocked using an iris, to block diffraction orders over 1, and a metal needle, to block the zeroth order. As a result, only the ± 1 orders are maintained and subsequently interfere to create a line pattern on the sample of double the modulation frequency of the grating used. Additionally, keeping only these orders leads to an extended depth of focus of the modulation pattern. The structured illumination causes excitation of the fluorophores in the sample where the subsequent emission maintains the spatial modulation pattern. A PBS is used to direct half of the resultant fluorescence emission towards the detector, where notch filters are placed in front of the detector to block any stray laser light from reaching it.
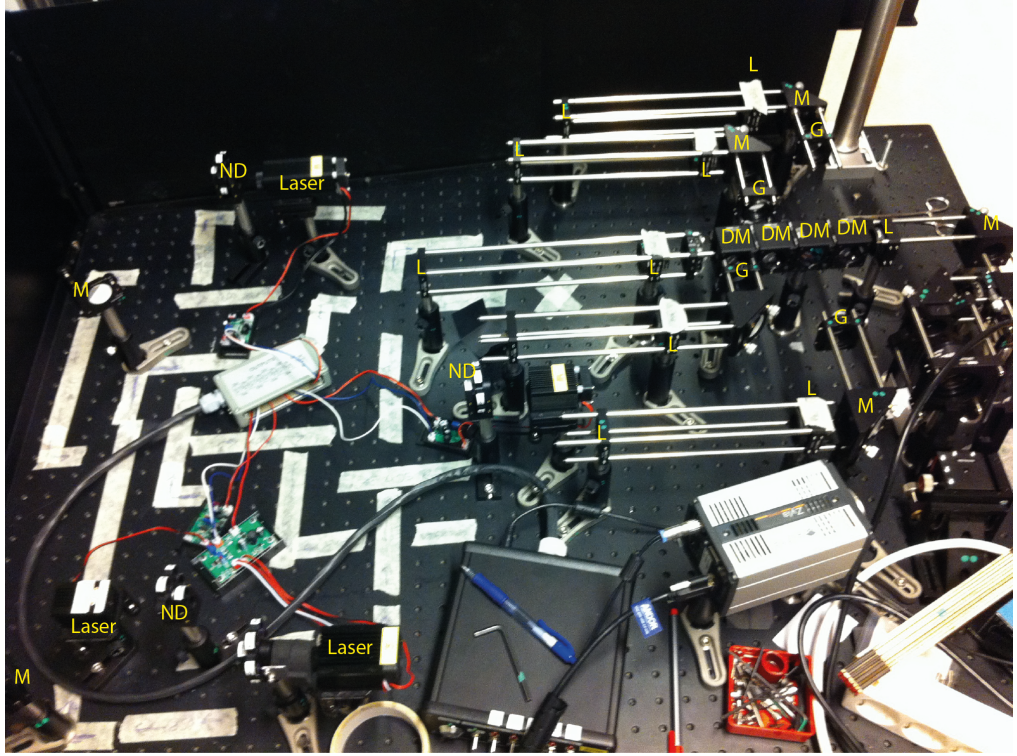
Figure 5.15: A photograph of the macroscopic setup under construction. DM=dichrois mirror, G=line grating, L=lens, ND=neutral density filters.

The macroscopic setup was a proof on concept multispectral FRAME setup used to acquire images of both stationary and dynamic samples. To test the extent of the separability of the multiplexed images obtained, stationary samples were prepared where the fluorophores were spatially separated and also co-localised. For both of these cases ground truth images were taken for comparison to verify the successfulness of the image demultiplexing. The stationary samples were used to assess if the different images due to the different excitation sources could be accurately demultiplexed. Additionally the optimal computational analysis parameters were determined using these images, the findings of which can be found described in **Section 5.2**. It was important to determine, for example, the largest filter size that would ensure the best spatial resolution while not incorporating cross-talk. This was key in order to be confident that the results, using the same setup and coupled computational analysis, were reliable and therefore implementable for dynamic sample imaging, for which it is not possible to obtain ground truths to be able to compare with. Dynamic samples were then imaged using two of the structured laser beams ($450nm$ and $532nm$) and analysed using the determined optimal parameters for this setup. **Paper I** provides a collection of different stationary and dynamic results obtained.

Figure 5.16: An illustration of the two illumination beams overlap across the sample when performing the spectrally close wavelength measurements.

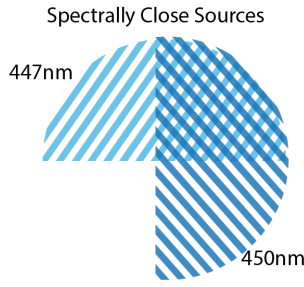Since it was established from the three beam setup that the extracted images had a good correspondence with their ground truths it was postulated that perhaps the wavelength did not play a role in the ability to separate the multiplexed images but in fact it was only the encoding that impacted this. As a result images due to *any* wavelengths which are differently encoded should be equally well separable. To test this theory a modified version of the setup shown in fig. 5.14 was constructed where a $477nm$ laser was added and used in conjunction with the $450nm$ laser only. The other alteration made in this modified setup was that each of the two beams were 50% blocked as illustrated by fig. 5.16. In fluorescence imaging setups which rely on spectral filters the ability to distinguish between very spectrally close excitations and emissions relies on the manufacturing limits of the filters. These do not generally have a spectral resolution of $3nm$ or less while still allowing for a good signal intensity to be transmitted. If it is possible, instead, to obtain accurate distinction between the emissions based on decoding the encoded images then the spectral resolution limit is no longer set by the filters but instead by the applied encoding and demultiplexing procedure.

Fig. 5.17 shows one of the results obtained using the modified setup, where a sample consisting of fluorescent dyes stamped on card in the shapes of letters, L,T and H. Since the laser beams were blocked in the manner illustrated in fig. 5.16, one quarter of the sample was not illuminated at all, while the opposite quarter was illuminated by both lasers. The top left and bottom right quarters were illuminated by only one of the two lasers, the $450nm$ and $447nm$, respectively. To compare the emissions of the fluorophores, two different line-cuts of the demodulated images were taken and the intensity profiles were plotted. Comparing the shapes of the intensity profiles to their corresponding ground truths yielded R^2 values of 0.993 or greater. These results confirm that the encoding and subsequent decoding of the multiplexed images produce highly reliable results independent of the similarity of the signals recorded from the sample.
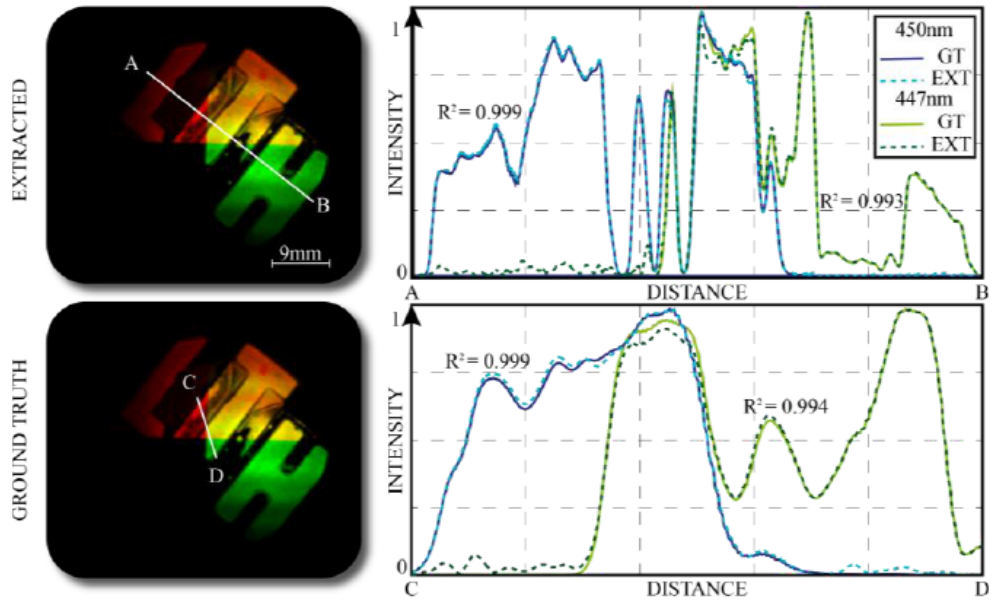
Figure 5.17: False coloured and combined extracted images from the close wavelength setup along with the corresponding ground truth image. The intensity along two different line cuts for each of the laser induced fluorescence emissions are shown in the graphs. The R^2 values from comparing the extracted and ground truth images show that a reliable extraction of the encoded images is achievable. Courtesy of OSA.

5.3.3 Volumetric Imaging using Structured Light Sheets
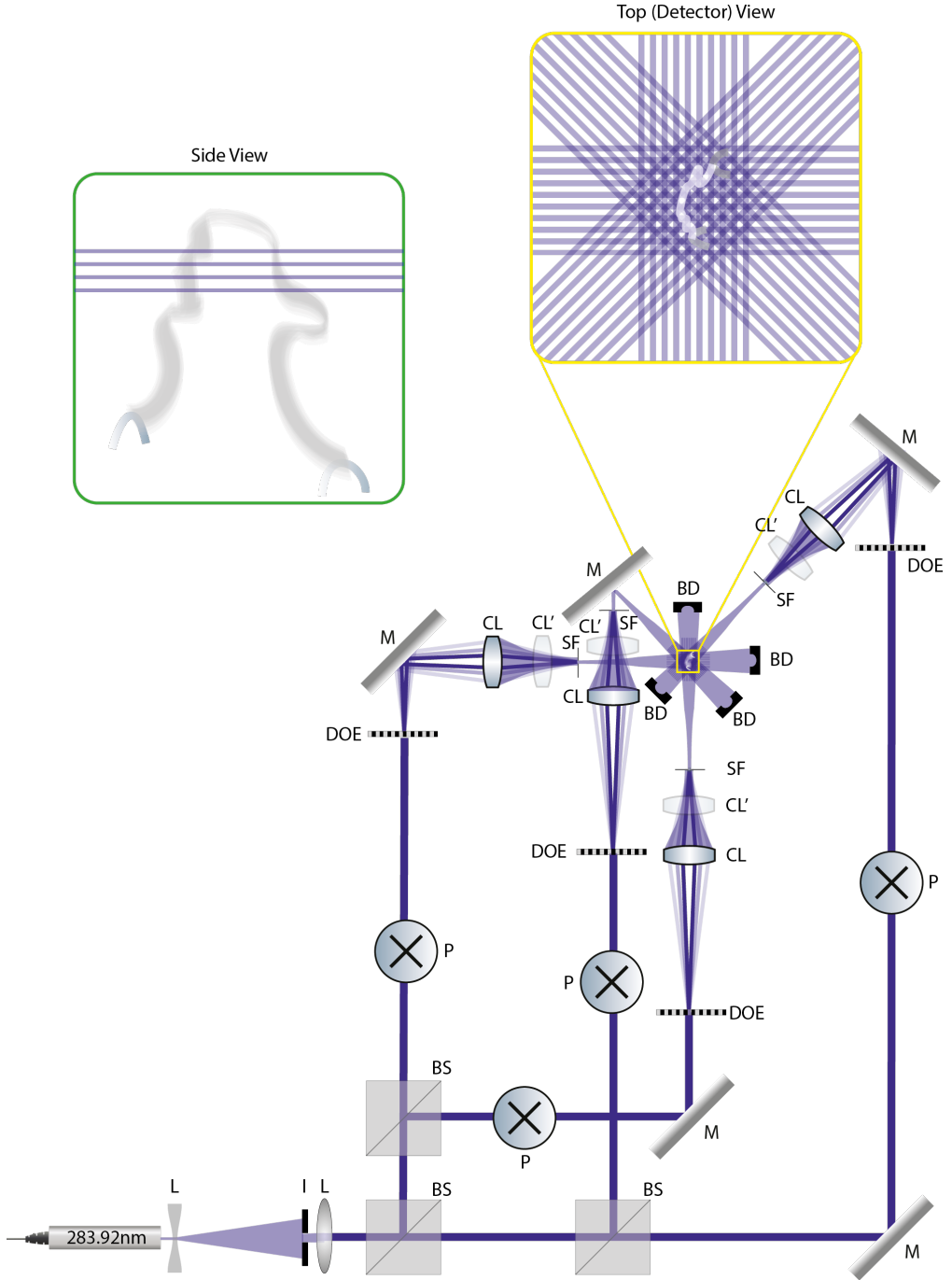
Figure 5.18: A schematic of the volumetric FRAME setup for imaging a gliding arc plasma. BD=beam dumps, BS=beam splitter, CL=vertically oriented cylindrical lens ($f = 750mm$), CL'=horizontally oriented cylindrical lens ($f' = 1500mm$), DOE=diffractive optical element, I=iris, L=lens, M=mirror, P=periscope, SF=spatial filter. Figure adapted from **Paper III**.

The volumetric FRAME setup was designed specifically to investigate the three dimensional distributions of ground state hydroxyl radicals (OH) in the vicinity of a gliding arc plasma (GAP) [95]. Conceptually, of course, it is also transferable for the investigation of other similar samples such as flames, [8]. As a sample, GAP produced species are difficult to volumetrically image due to erratic nature of the GAP. Additionally, there is an unwanted background signal which, if using structured illumination, can be eliminated due to stimulating laser induced fluorescence in the OH only. Since the volumetric FRAME setup uses structured illumination encoding it provides the background light suppression required, as well as being able to capture multiple images in a snapshot. In this implementation structured light sheets were used to "slice" the GAP at different heights. The resulting images could then be "stitched" together in the post processing stage to construct a 3D visualisation of the OH distribution.
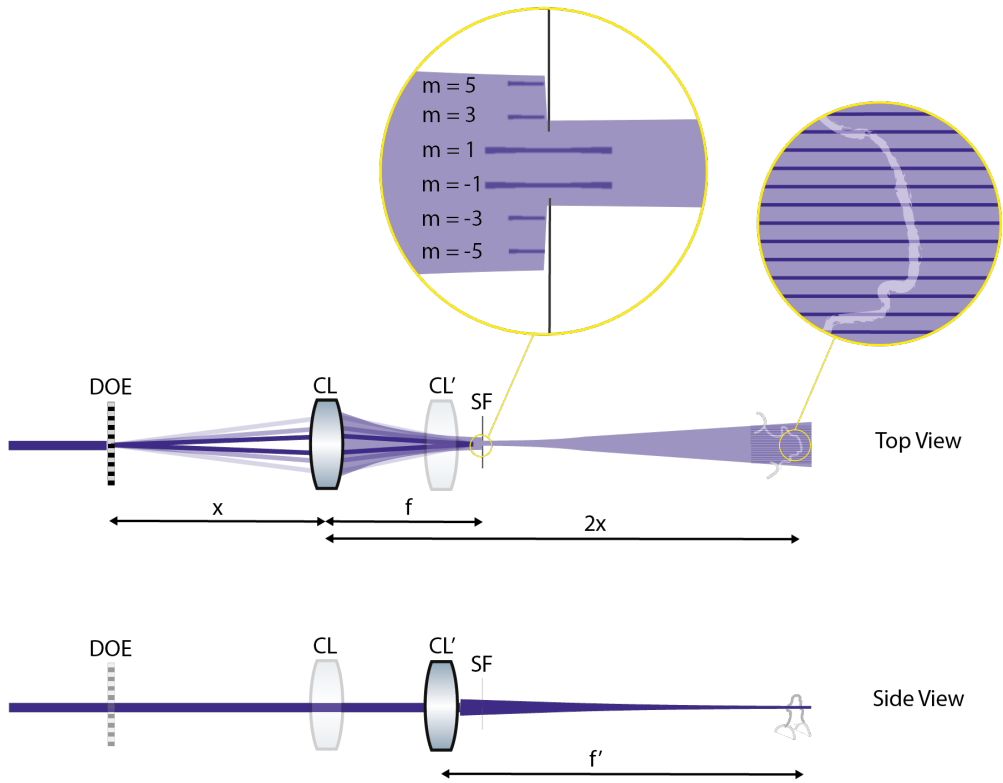

Figure 5.19: **Structured laser sheet formation**: A schematic of the structured laser sheet formation including the cutting of the higher orders to extend the depth of focus and optimise the modulation depth of the encoding pattern. CL=vertically oriented cylindrical lens ($f = 750mm$), CL'=horizontally oriented cylindrical lens ($f' = 1500mm$), DOE=diffractive optical element, SF=spatial filter. Figure adapted from **Paper III**.

A schematic of the experimental setup is shown in fig. 5.18. A Nd:YAG pumped dye laser (pulse energy $40mJ$, pulse duration $6ns$ and repetition rate $10Hz$) is used which gen-

erates 283.92nm UV laser light. The laser beam is expanded and collimated, and an iris is used to cut and improve the beam profile. The beam is then split equally into four optical paths and shaped into laser sheets using two cylindrical lenses. A DOE is used in each optical path to apply spatial modulation to the laser sheets. The DOE is placed before the first cylindrical lens which is the imaging lens, which forms the modulation pattern on the sample. The second lens is placed after the first but before its focal point and is the sheet making lens, i.e. shaped the beam into a thin laser sheet. A beam blocker is used to remove the higher diffractive order in the Fourier plane of the imaging lens allowing only the ± 1 order to propagate. Fig. 5.19 shows a schematic illustrating the structured laser sheet formation. Using periscopes in each optical path the laser sheet heights were adjusted such that they each had a separation of 0.5mm between them. The periscope were also used to ensure that the height of the laser sheets was inline with the GAP probe volume. Since the setup uses modulated laser sheets the encoding is the same in each path when incident on the sample unless the directions of the beams is changed beforehand. To achieve a different encoding for each laser sheet they were directed onto mirrors positioned around the sample such that they were then reflected towards it at different angles. As a result, when viewed from above, the modulation directions across the sample all differ and thus when imaged can be differentiated from each other. To capture the LIF signals from the laser sheets from above a mirror was placed over the sample, high enough not to be damaged by the GAP, which directed the fluorescence horizontally, towards the detector. An ICCD camera (Gen 2 Istar, 1024x1024 pixels, Andor Instruments) was used in combination with UV-transmissive optics (Nikon UV 105mm). Additionally a notch filter (310nm $\pm 20nm$)was placed in-front of the camera to filter out any stray laser light and plasma emission. To additionally decrease the majority of the plasma emission and be able to capture the LIF signals a gate width of 10ns was set on the camera.

The GAP is highly dynamic and its position, as captured by the camera, is constantly moving. Additionally it is not possible to have a constant GAP induced OH image when viewed in "live" mode on the coupled computer software since the laser sheets and the camera are not always synchronised such that an LIF response is obtained. The GAP is also generated between two electrodes and operates at a high voltage such that the entire system is contained within a safety cage (see fig. 5.20). For these reasons, in conjunction with the fact that the laser operates in the UV, it is difficult to check the modulation pattern of the beams in a conventional way, by either checking the modulation by inspection with card in the beam path or interacting with the sample and viewed in a continuous mode on the computer. To overcome this and find a position with a good modulation pattern, a quartz cuvette filled with a fluorescing liquid (tonic water containing quinine) was used as an initial sample (fig. 5.21). In the figure it is possible to resolve a modulation pattern in the LIF from one of the laser sheets. Each of the laser sheets were adjusted such that they had the maximum spatial overlap, as viewed from above (fig. 5.22). Their height were also adjusted to ensuring they were parallel to the liquid surface throughout the sample, i.e. the

modulations patterns were equally in focus throughout the probe volume. The laser sheets need to be parallel to ensure they are have a consistent separation from each other so that the 3D reconstruction is accurate.

Figure 5.20: A photograph of the gliding arc plasma inside the safety cage.

Since each of the structured laser sheets "slice" the GAP probe volume at different heights, when viewed from above, the signals they generate will emanate from different distances from the camera. It was therefore critical to choose the correct aperture size such that the encoding from each laser sheet could be discerned in the same camera exposure. Different aperture sizes were tested in order to determine which gave the most consistent modulation patterns for all the laser sheets. Fig. 5.23 shows the modulation patterns for each of the laser sheets where it is possible to se that it is quite poor for sheet 1 but good for the other three. Both the beam shaping components should therefore be adjusted as well as the aperture size until all the beams have a clear and consistent modulation. Sheet 4 (fig. 5.23) illustrates what a good modulation pattern should look like in this case.

After alignment of the laser sheets was done using the tonic water the sample was exchanged for the GAP. Any additional fine tuning of the modulation pattern was then done iteratively by capturing images of the GAP induced OH distribution, inspecting the modulation pattern on the computer, and adjusting the position of the encoding optics accordingly.
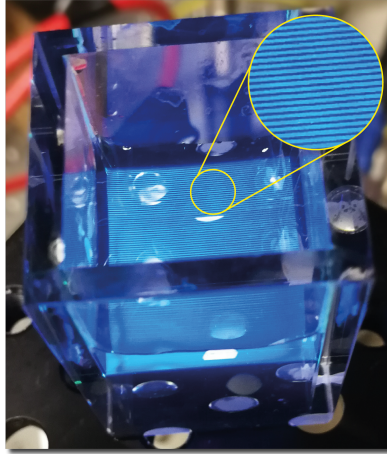
Figure 5.21: A photograph of the fluorescing tonic water in a quartz cuvette with the modulation pattern from one the the modulation laser sheets visible.

Four Structured Sheets in Tonic Water
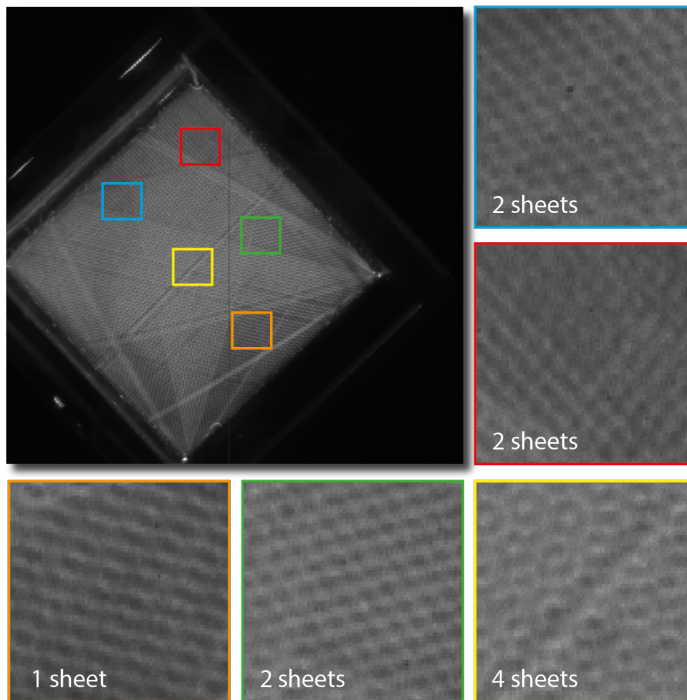
Figure 5.22: Laser sheet spatial overlap: A raw detector image of the fluorescing tonic water with all four laser sheets incident on it. The degree of spatial overlap of the different laser sheets can be seen from the varying modulation patterns across the field of view.
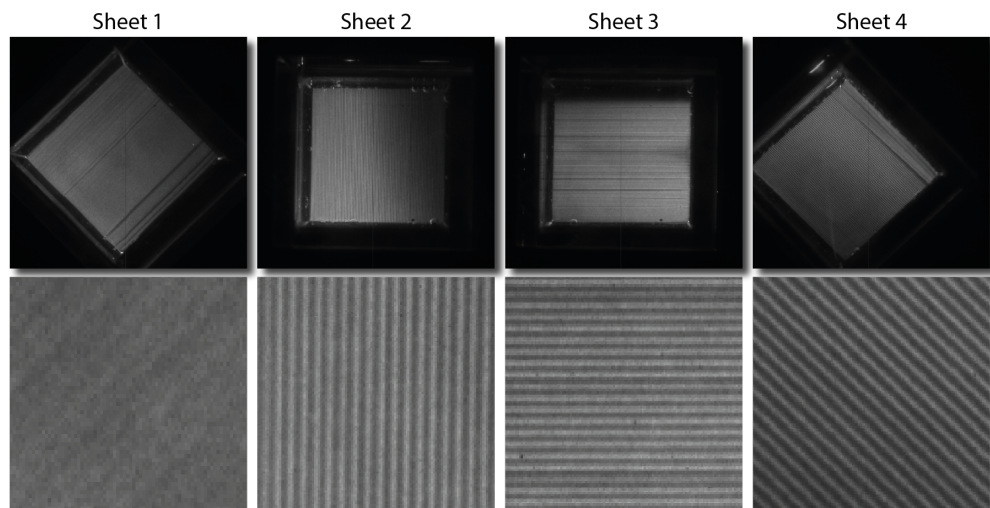
Figure 5.23: **Laser sheet spatial modulation:** Raw detector images showing the modulated fluorescence from tonic water due to each of the laser sheets.

Due to the erratic nature of the GAP as well as the gating of the detector and laser source capturing a good image of the GAP induced OH distribution was challenging. Fig. 5.24 illustrates a what a good image of the GAP induced OH distribution might look like. Here the modulation patterns from all four sheets is present since the GAP is centred in the field of view, where there is a spatial overlap between all four laser sheets. Additionally the region of the GAP which has been "sliced" is of the two column like parts of the arc shape which means the arc has been cut through the middle. If the arc is formed too low then only a portion of the top may be captured and it may even not be sliced by all the sheets in such a case (e.g. image 54 in fig. 5.26). To ensure that there would be a selection of suitable images to reconstruct 3D images of the OH distribution from, over 5000 images were obtained in sets of on average, 100 images at a time. Figs. 5.25 and 5.26 show one such set of 100 images. In this set fewer than 30% of the images have actually captured the GAP induced OH distribution with the remainder capturing background light only. Images 13, 17, 30, 66 and 88, for example, show images where the GAP is not centred enough in the field of view and will therefore not be sliced by all four laser sheets. The most promising images in this set are 59, 68, 80, 83 and 86. This means that only 5% of the images captured in this set could potentially give good 3D OH distribution reconstructions. Despite the challenges volumetric images of the GAP induced OH distribution were successfully captured and reconstructed, where examples of the 3D results can be found in **Paper III**.
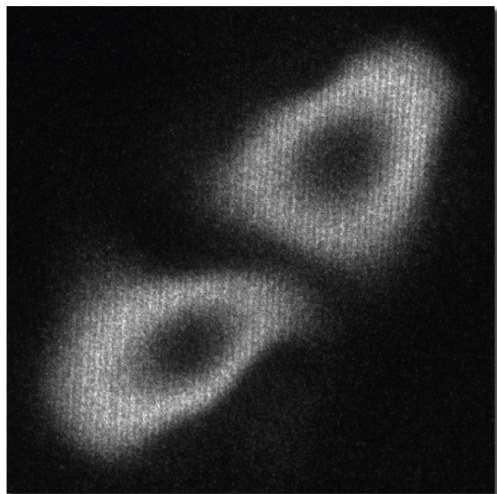
Figure 5.24: A good result: A raw data image illustrating a good image capture of the gliding arc plasma induced OH distribution.
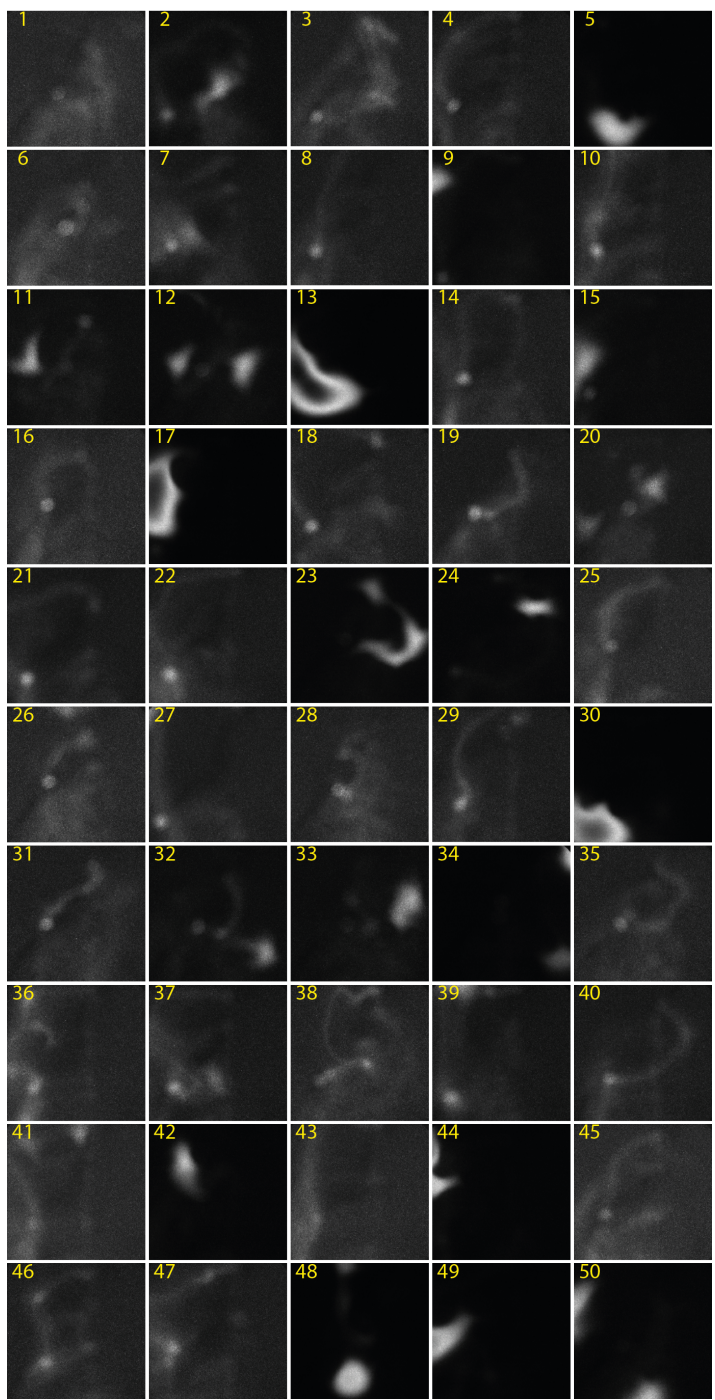
Figure 5.25: The first 50 images captured of the gliding arc plasma induced OH distribution in one of the data collection sets.
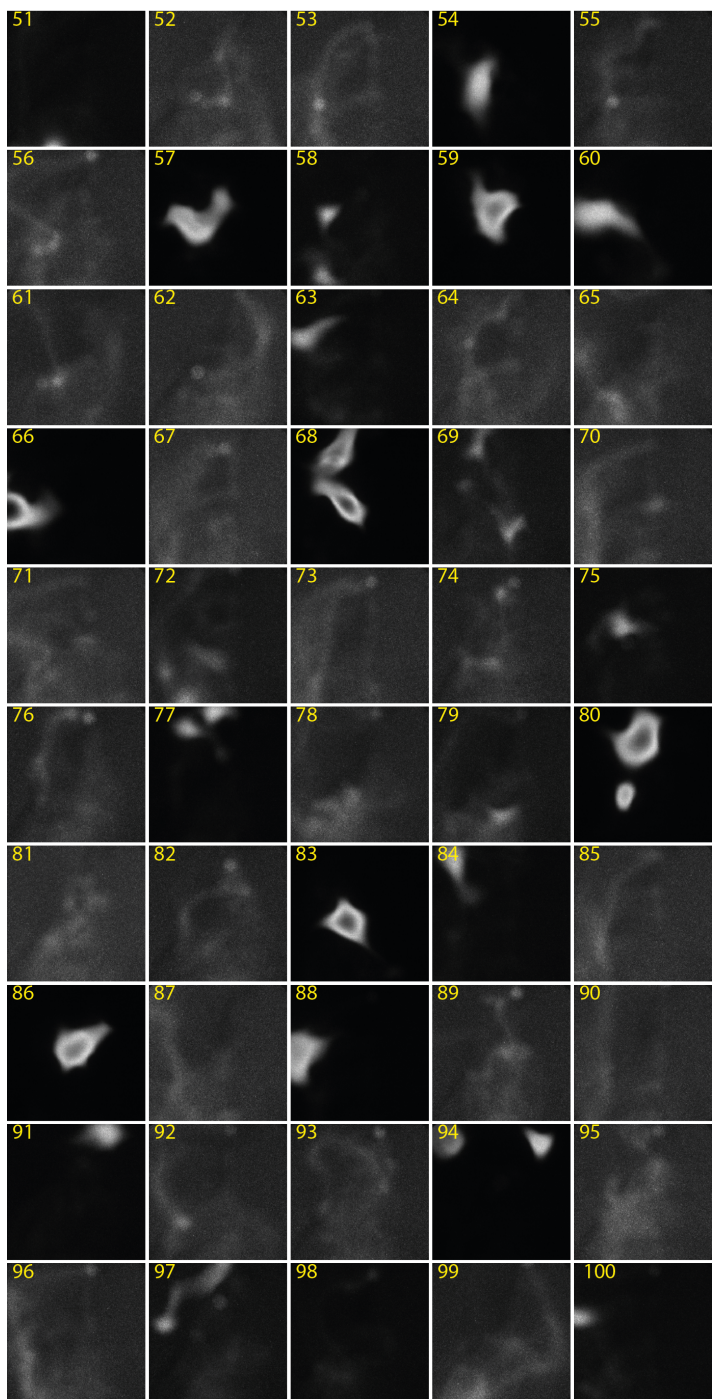
Figure 5.26: The last 50 images captured of the gliding arc plasma induced OH distribution in one of the data collection sets.
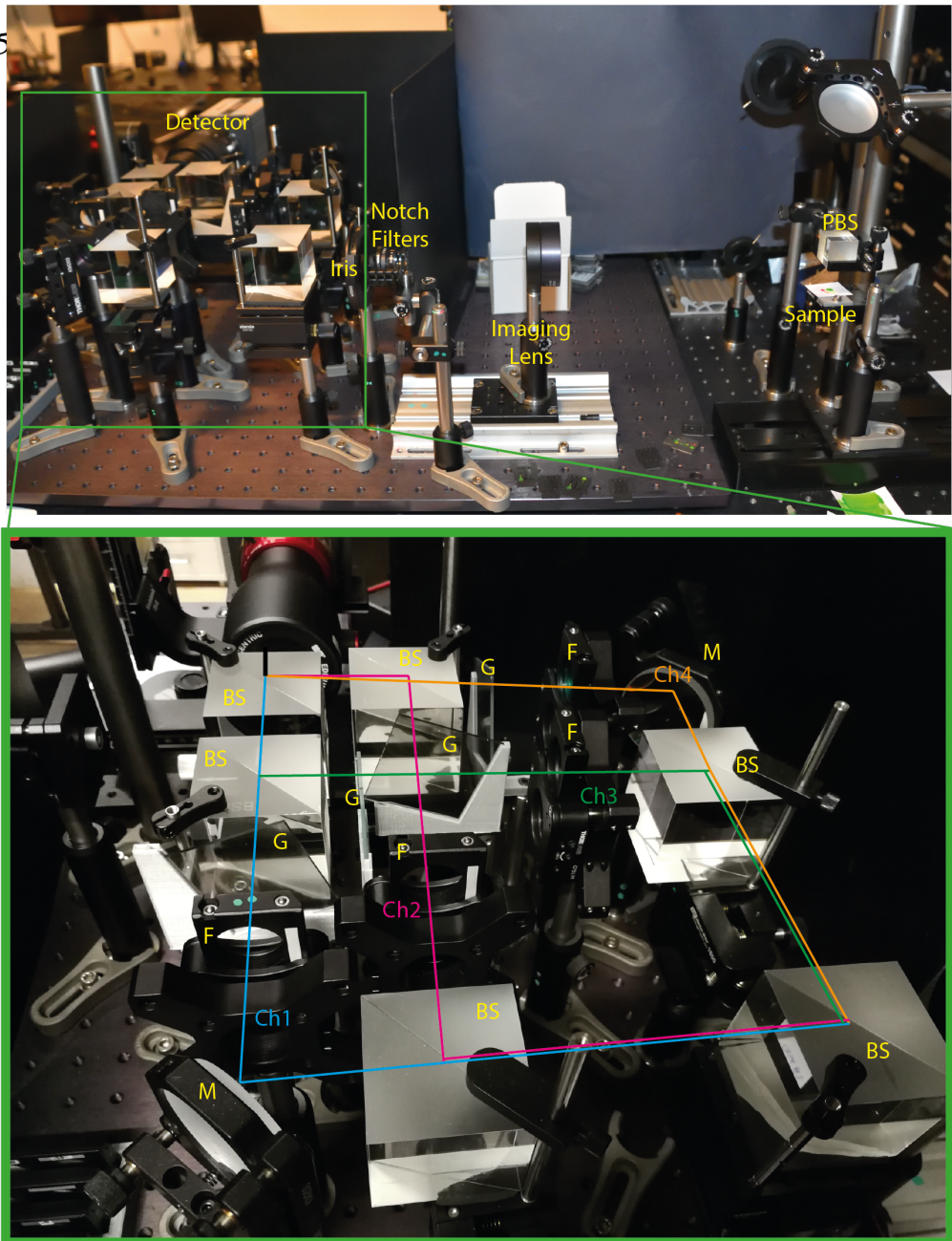
Figure 5.27: *Emission encoding setup:* A photograph of the emission encoding setup with the four channels marked. BS=beam splitter, F=filter, G=line grating, M=mirror, PBS=polarising beam splitter.

The passive FRAME approach applies encoding to the light emitted from the sample which is illuminated with homogenous illumination. Applying encoding in this way is not in

itself novel, [83, 84, 82, 81, 80], although in previous demonstrations each setup has been built for a single purpose and therefore lack versatility. The setup constructed for the passive FRAME approach was designed to be low cost and versatile. It can be considered as an add-on module which could be used with existing optical arrangements which require emission filtering. The setup was demonstrated for spectral, polarisation, temporal and depth of focus imaging where the results of each can be found in **Paper II**.

Fig. 5.27 shows a photograph of the emission encoding experimental setup. Note that only the sample to detector portion is shown since the illumination used for the different imaging schemes was changed but the emission encoding portion remained the same, only the filters were switched depending on the application. To apply the encoding to the emitted light three BS are used to equally split the light into four optical paths, or channels. Filters were placed at the start of each of the separate channels to provide the selectivity of the optical property desired. The filtered light was then spatially modulated using line gratings before using an additional three BS to recombine and spatially overlap the light from each channel onto the detector. Due to a stronger contrast in the modulation pattern, i.e. very good modulation depth, when the encoding was applied to the emitted light when compared with the illumination encoding, in conjunction with the same detector, high spatial frequency gratings ($20 lp/mm$) could be used and well resolved in the detected images.

The setup used different illumination setups and filter combinations to achieve different imaging schemes. By using either glass plates, spectral filters of polarisation filters the setup could be used to obtain depth of focus, multispectral, fluorescence, temporal and polarisation imaging. For details of the different illumination used along with the results obtained the reader is referred to **Paper II**. The remainder of this section will instead cover experimental challenges faced along with additional computational post processing that was performed beyond the FRAME demultiplexing procedure.

Although conceptually the emission encoding setup is simple, successful experimental implementation of it was not straightforward. The use of only one detector and one imaging lens, but for four different optical channels, imposed challenges on the arrangement of optical components and also the multiplexing of the images. Some of the main challenges faced are listed below along with descriptions of how they were tackled.

- Maintaining setup alignment

- Restrictions imposed by using one detector and one imaging lens

- Precisely equal optical path lengths

- Spatial overlapping of images

- Minor misalignments

Maintaining setup alignment

The beam splitters (BS) were susceptible to movement which made aligning and maintaining the alignment of the setup impossible. Sorbothane vibration dampening rubber sheeting was therefore adhered to the surface of the BS holders and more robust metal clamps were added in order to secure the BSs.

Restrictions imposed by using one detector and one imaging lens

The setup design required careful calculation to ensure that it would have equal path lengths, be compatible with using only one detector and one imaging lens and have space for all the required components to split, filter, encode, and recombine the light. The imaging lens imposes a restriction on the space, for the other optical components, available between it and each grating in the setup. The gratings have to be positioned such that an image of the sample is formed on them. The setup design was based around the imaging distances, *2f*, of suitable achromatic lenses, where an $f = 300mm$ lens was determined to be able accommodate the required components in a compact arrangement.

Precisely equal optical path lengths

The setup splits the emitted light from a sample along four different optical paths before recombining the four filtered and encoded images onto the detector. In order for each image to be in focus when captured by the detector, the optical path length of each channel had to be precisely aligned and of the same length. Two steps are involved in ensuring that a focussed and encoded image is captured from each channel. The imaging lens needs to form an image of the sample onto the grating. The grating position needs to be correct such that the detector objective images the focussed grating modulation pattern onto the detector sensor. The distance between the imaging lens and the each grating therefore needs to be the same. These requirements remove the flexibility of being able to optimise one channel independently of another. Instead, channel 1 was aligned first and then used as a reference against which all the other channels were adjusted. The positions of the BSs, mirrors, gratings and filters were all adjusted to achieve the same image on the detector, as channel 1.

Spatial overlapping of images
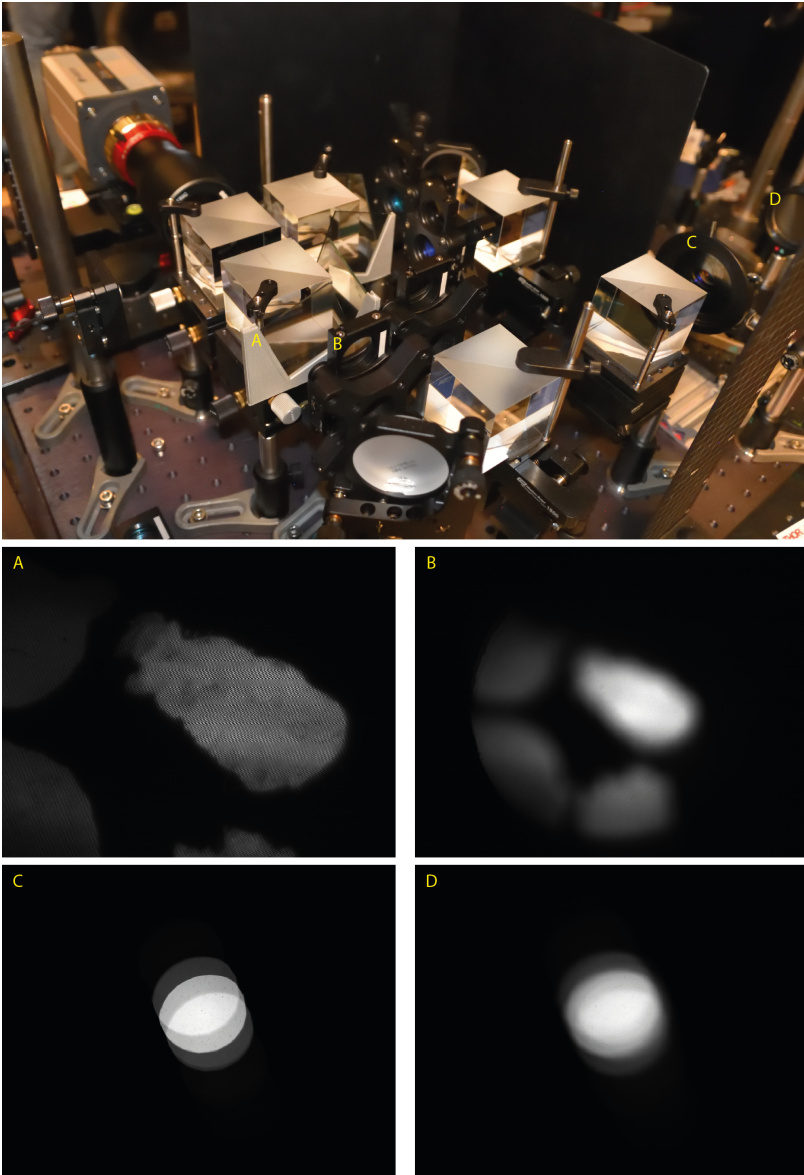
Figure 5.28: **Aligning procedure:** A photograph of the emission encoding FRAME setup with; A=grating, B=filter, C=iris and D=imaging lens, marked. The labelled images at the bottom show the detector views when focussed on the different components.

As part of the alignment, aside from the focusing requirements, the images needed to be spatially overlapped on the detector. To align the setup to achieve this, the detector objective was adjusted (varying its focal length) in order to focus on different components along each

optical path. Fig. 5.28 shows the setup with the positions of a grating, a filter, the iris and the imaging lens marked with A, B, C and D respectively. Images of the detector view when it is focussed on each of these components is shown. By ensuring there is an overlap of the respective components along each channel, again with respect to channel 1, the spatial overlap and the focus of the multiplexed images could be adjusted.

Minor misalignments

An additional measure was taken to compensate for minor misalignments in the image overlap to ensure there was in fact a pixel to pixel overlap in the processed images. An array of dots printed on paper was imaged prior to recording any measurements. Fig. 5.29 shows the detector view of the array when all four channels images are multiplexed as well as individually. Fine adjustments could be made experimentally to ensure the dots were as spatially overlapped as possible and also equally in focus along each channel. Computationally the images could be used as a basis to warp the captured sample images so that they had a pixel to pixel overlap. This was of particular importance for the linear unmixing of the fluorescent samples where the spectral decomposition of each pixel is determined. Errors in the pixel to pixel overlap will lead to errors in the decomposition of the fluorescence signals and inaccurate fluorophore determination.

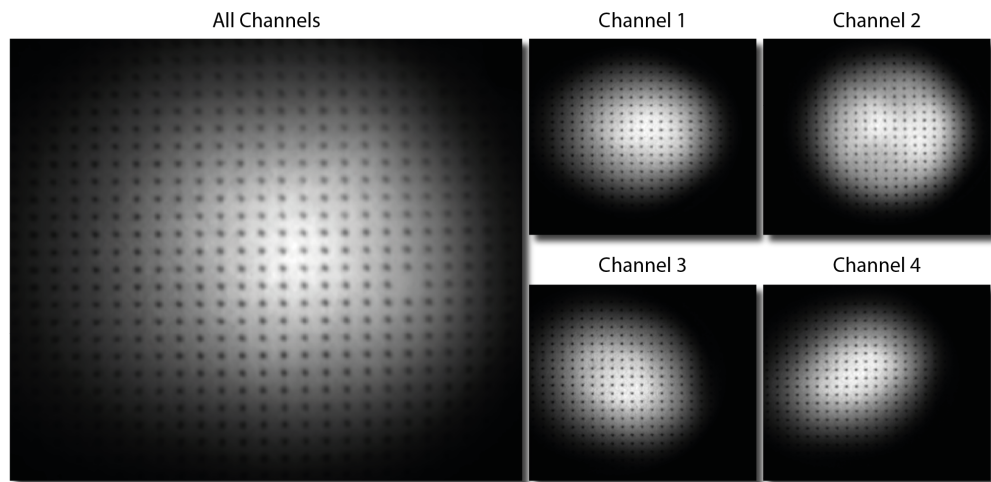**Figure 5.29**: Detector views of a dot array used to fine tune the image overlap and focusing. Further used in the post processing to warp the images to achieve pixel to pixel overlap. A white square can be seen in the centre right, where a dot is missing, is used as a reference point in each of the images for warping them.

Linear Unmixing of Fluorescence
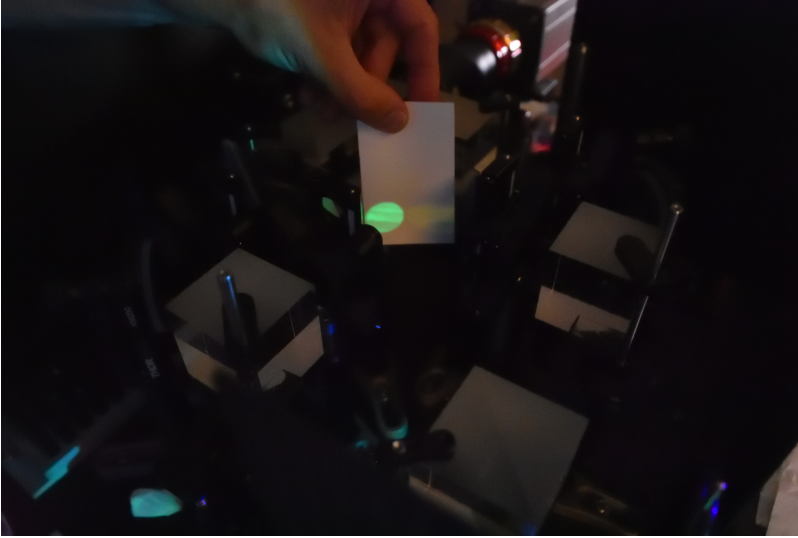
Figure 5.30: A photograph of the setup when capturing spectral images. The different light intensities from channels 2 and 3 can be seen incident on the white card, illustrating the different light transmission through each of the channels due to the different spectral filters in each.

The spectral imaging of the fluorescent samples implemented additional processing of the extracted images to determine the spatial distribution of the different fluorophores present in the sample. Fig. 5.30 shows the different transmitted light intensities along channels 2 and 3, due to the use of different spectral filters in each channel, in the setup arrangement used for spectral fluorescence image capture. When a multiplexed image is captured in this case each image will pertain to the light intensity in a specific spectral emission range. Using the FRAME demultiplexing method it is possible to separate the multiplexed images to obtain the image from each channel. If the spectral filters, however, allow the transmission of light from more than one fluorophore, then it will not be possible to differentiate between them in each of these images. To do so one can apply linear unmixing to the extracted images. Fig. 5.31 shows a sample composed of three different fluorescent dyes, where each has been drawn in a different shape, L, T or H. The leftmost image in the figure show the raw detector image along with inset sub-images which show the four extracted channel images. The different fluorophores have different intensity contributions within each channel image which are indicated with bar plots and correspond to the marked regions of interest. These are the characteristic spectral responses for each of the three fluorophores as determined using this emission encoding setup. By then using linear unmixing to analyse the extracted images it is possible to determine the distribution of the fluorophores in the sample. The leftmost image in fig. 5.31 shows the raw image after demultiplexing and linear unmixing.

The inset sub-images show the individual fluorophore distributions in the sample. The result confirms that the emission encoding setup is linear unmixing compatible and yields the ability to accurately identify multiple fluorophores which are co-localised. This sample is static and with the FRAME emission encoding setup, snapshot multispectral images can be captured. The result shown in fig. 5.31 therefore forms the basis for both testing and establishing a characteristic spectral emission profile calibration set to be able to linearly unmix dynamic samples which contain the same fluorophores. The setup was therefore then also used to capture a sequence of snapshot multispectral images of a dynamic sample composed of the same three fluorescent dyes. Fig. 5.32 shows a droplet of dye exploding across the surface of two other dyes which are slowly mixing. Each of the raw images captured were demodulated into the different channel images and then linearly unmixed using the same parameters and spectral responses obtained from the stationary case.
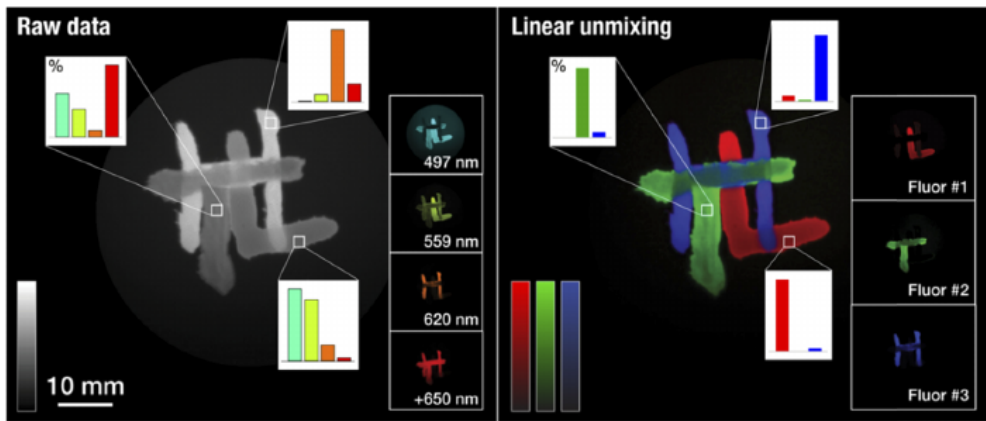
Figure 5.31: Left: A raw detector image showing four multiplexed spectral emission channel images of a fluorescing sample containing three different fluorescent dyes. The relative light intensity values from each spectral channel, for the three dyes, are shown in the bar plots. The inset images show the four extracted images pertaining to each of the spectral channels. Right: The same image but after demultiplexing and linear unmixing. The inset images show the individual linearly unmixed images corresponding to each fluorescent dye. Courtesy of OSA.
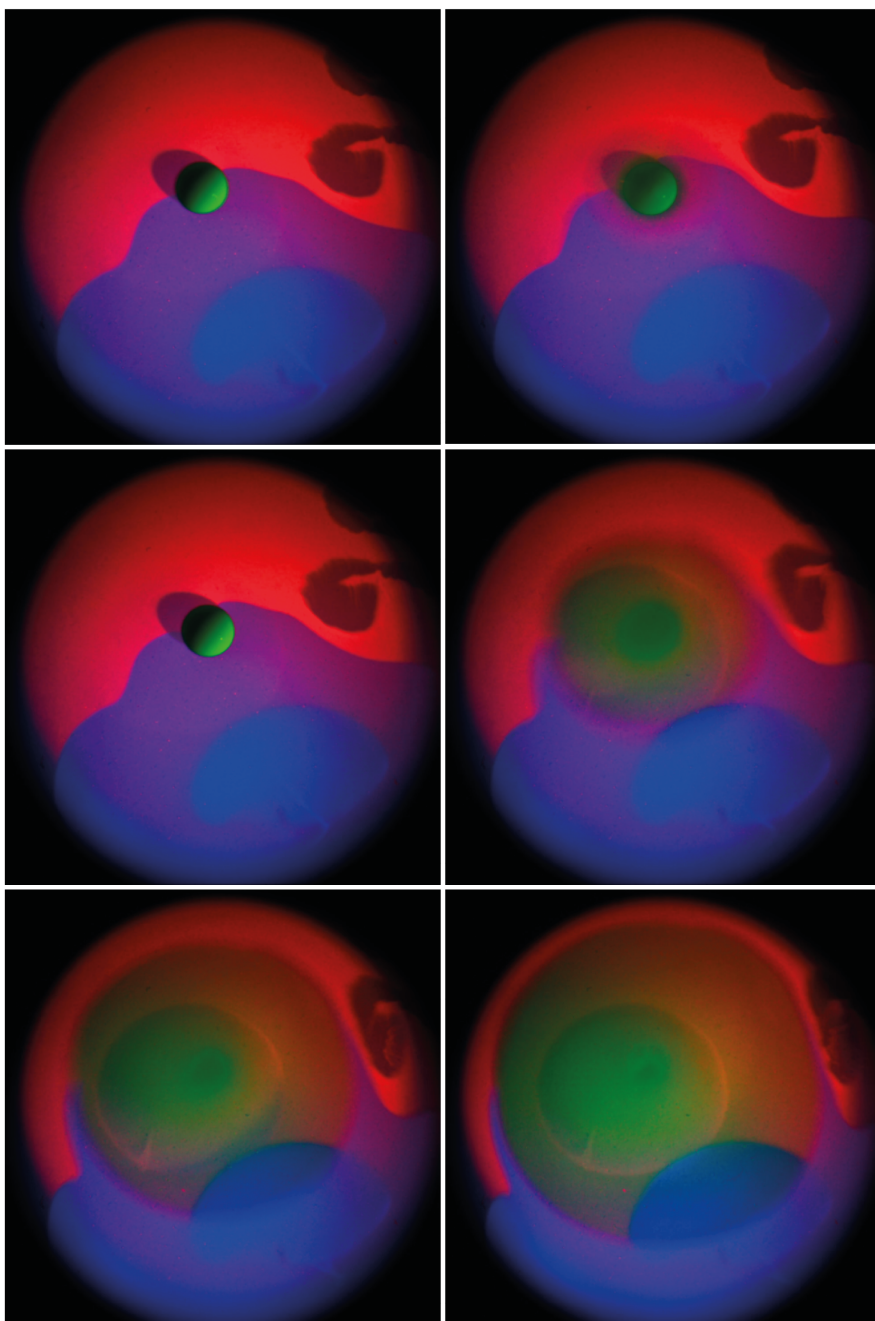
Figure 5.32: A sequence of recombined and false coloured extracted images capturing the bursting of a droplet of fluorescent dye (green) across the surface of two other mixing fluorescent dyes (red and blue).

5.3.5 Multispectral Illumination and Emission Encoding
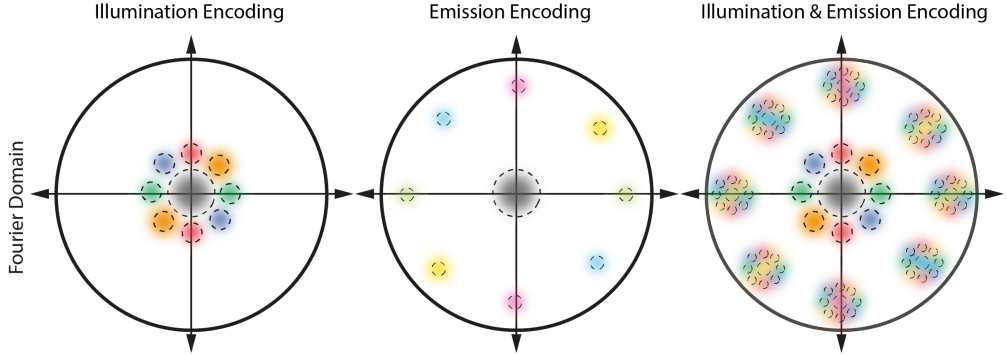
Figure 5.33: Illustration of the Fourier domain for (a) illumination encoding, (b) emission encoding and (c) illumination and emission encoding.

The multispectral illumination and emission encoding FRAME setup combines two of the FRAME imaging approaches, i.e. the research presented in **Papers I** and **II**. By doing so the resulting multiplexed images obtained contain double modulated images which also provide the ability to trace a complete optical path, from illumination to detection. Fig. 5.33 illustrates how the Fourier transform looks for illumination encoding, emission encoding, and both illumination and emission encoding. The Fourier domains for the single encoding setups are the same as previously explained in the introduction to the FRAME principle. The illustrations in fig. 5.33 show a lower encoding frequency for the illumination than for the emission, as this is what was experientially chosen for the double modulated demonstration. When encoding is applied on both the illumination and detection parts of the setup one obtains the same multiplexed images as one would in either of these stand alone cases. This can be seen in the Fourier domain for the combined illumination and emission encoding where one can see that it has the same clusters as if one had superimposed the two individual Fourier domains with each other. What one will notice is that there are actually an additional 16 cluster pairs which are also present in the combined Fourier domain. These correspond to the double modulated images, where each cluster contains an image which corresponds to one laser excitation response and one spectrally filtered channel. Since the setup uses four laser sources and four emission encoding channels there are 16 different combinations possible, hence the 16 additional clusters pairs. As a result, the double modulated approach presented produces 24 different spectral images.

Mathematical Description

A laser modulated image can be expressed by eq.(5.15) where the expression has been simplified to express one modulation encoding and in one dimension. A second encoding,

which can be described by eq.(5.16), is then applied to the emitted light, i.e. to the laser modulated image (eq.(5.15)). The phase is assumed constant for all the encoding patterns and so we will set ρ to zero.

$$I_L = 0.5(A + Asin(2\pi\nu_1 x + \rho)) \tag{5.15}$$

$$S_{Em} = 0.5 + 0.5sin(2\pi\nu_2 x + \rho) \tag{5.16}$$

To obtain the double modulated image one therefore multiplies eq.(5.15) and eq.(5.16), as given by eq.(5.17).

$$I_{DM} = (0.5A + 0.5Asin(2\pi\nu_1 x))(0.5 + 0.5sin(2\pi\nu_2 x)) \tag{5.17}$$

$$I_{DM} = \frac{1}{4}A + \frac{1}{4}Asin(2\pi\nu_1 x) + \frac{1}{4}Asin(2\pi\nu_2 x) + \frac{1}{4}Asin(2\pi\nu_1 x)sin(2\pi\nu_2 x) \tag{5.18}$$

$$I_{DM} = \overbrace{\frac{1}{4}A}^{DC} + \overbrace{\frac{1}{4}Asin(2\pi\nu_1 x)}^{Laser\ Mod} + \overbrace{\frac{1}{4}Asin(2\pi\nu_2 x)}^{Channel\ Mod}$$
$$+ \overbrace{\frac{1}{8}A(cos(2\pi\nu_1 x - 2\pi\nu_2 x) - cos(2\pi\nu_1 x + 2\pi\nu_2 x))}^{Laser\ \&\ Channel\ Mod} \tag{5.19}$$

The expression given by eq.(5.19) shows the mathematical descriptions of the non-modulated, DC, part of the image found at the centre of the Fourier domain. The images pertaining to only the laser encoding and the channel encoding are given by the second and third terms in eq.(5.19), respectively. The double modulated images are expressed by the final term in eq.(5.19). From this expression it can be seen that there is a 50% reduction in the proportion of the encoded information in the double modulated versus the single modulated images. Demultiplexing of the images was performed in the same way as given in **Section 5.2.1**. To extract the double modulated images the demodulation was first performed using the different channel reference matrices, to shift the channel clusters to the centre of the Fourier domain, and then followed by the laser reference matrices, in order to shift the double modulated clusters to the centre of the Fourier domain.

Experimental Setup
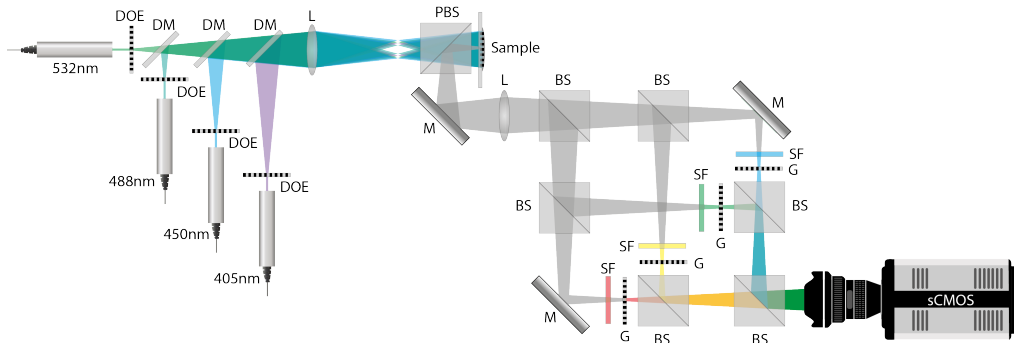
Figure 5.34: A schematic of the double modulated FRAME setup. BS=beam splitter, DM=dichroic mirror, DOE=diffractive optical element, G=grating, L=lens, M=mirror, PBS=polarising beam splitter, SF=spectral filter. Figure with courtesy of Elias Kristensson.
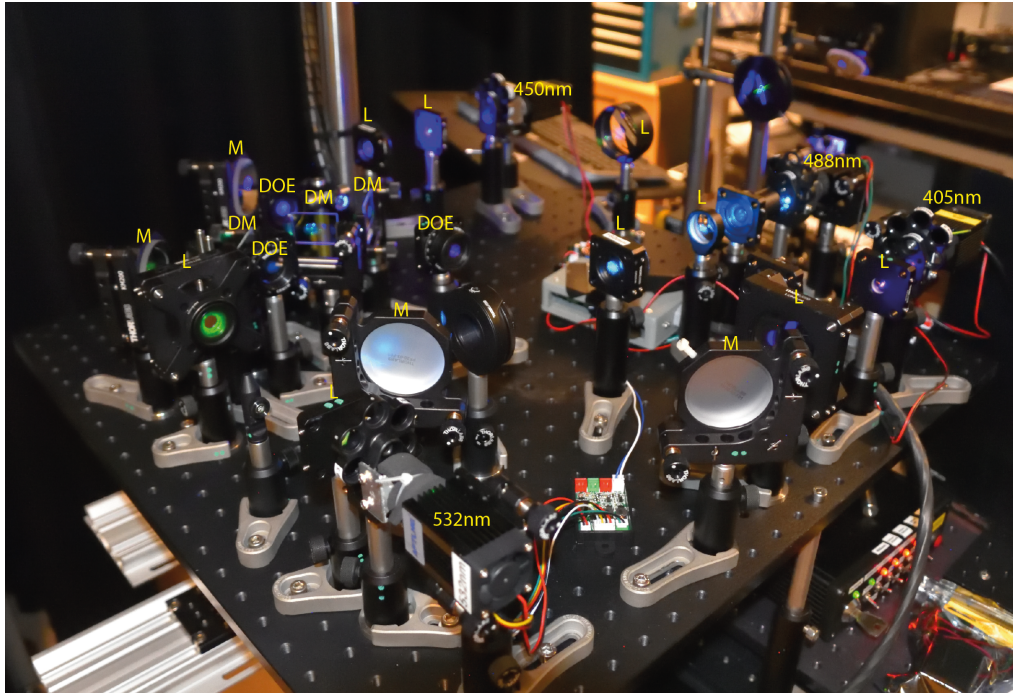
Figure 5.35: A photograph of the illumination part of the double modulated FRAME setup showing how four lasers (405nm, 450nm 488nm and 532nm) are encoded and spatially overlapped. DM=dichroic mirror, DOE=diffractive optical element, L=lens, M=mirror.

Fig. 5.34 shows a schematic of the complete setup. The illumination encoding portion of the setup, shown in fig. 5.35, consists of four different lasers (405nm, 450nm, 488nm,

532nm). As before, each laser is expanded and collimated and then encoded with a spatial modulation pattern, before being spatially overlapped using a recombination arm consisting of a series of dichroic mirrors. Line gratings could have been used for the encoding, as in **Paper I**, however, since the emitted light is split and modulated a second time, DOEs were used in order to preserve as much light as possible within the setup. An achromatic lens was used to image the encoded beams onto the sample, where an iris (fig. 5.36) was placed in the Fourier plane in order to block all higher diffractive orders, allowing only ±1 orders to propagate.
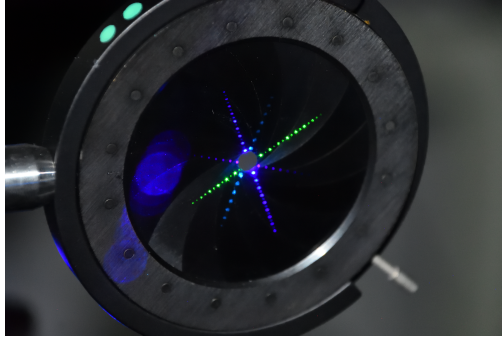
Figure 5.36: A photograph of the diffractive patterns of the four modulated lasers, incident on an iris. Only the ±1 orders propagate through the centre, all other orders are blocked by the iris.

The structured illumination is incident on a fluorescent sample (fig. 5.37) stimulating a fluorescence emission maintaining the same encoding before being directed, using a PBS, towards the emission encoding portion of the setup. An imaging lens projects the encoded sample emission onto line gratings, which provide the secondary modulation encoding in the setup. Each grating is located along a different optical path, where BSs are used to split the emission equally into the different channels. Each encoding channel has a spectral filter with spectral transmission profiles which span portions of the wavelength range of the fluorescence emission of the fluorophores used. As a result, all the fluorescence can be captured within the multiplexed image.

Figure 5.37: A photograph of a fluorescing sample containing seven different fluorophores.

A challenge faced in this setup was imposed by the double modulation of the light. Both modulations needed to be discernable in the detected image. To achieve this the encoding due to the structured illumination needed to be imaged onto the line gratings which provided the emission encoding. The sample also needed to be in focus along with the modulated emission due to the illumination. To provide the required flexibility the entire illumination setup (fig. 5.35) was mounted on rails such that its position could be adjusted accordingly. This way the sample distance could be set such that it was in focus on the line gratings of the emission encoding part and the illumination could be adjusted in line with this.

Demultiplexing and Linear Unmixing
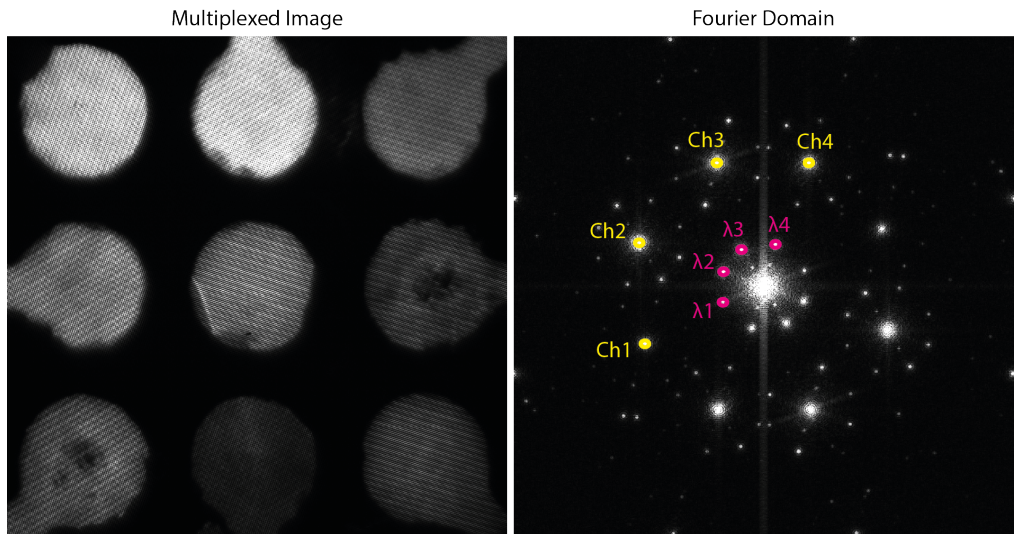
Figure 5.38: A multiplexed image showing the raw data captured by the detector. The corresponding Fourier domain image is shown with the positions of the four laser and four spectral channel clusters marked in pink and yellow respectively.

To demonstrate the ability to determine different fluorophores in the captured images of the samples, linear unmixing was performed. Since linear unmixing requires having a calibration set of all the fluorophores, the first step required demodulating and extracting all 24 encoded images from the multiplexed image. Fig. 5.38 shows a raw, multiplexed image of nine different fluorophores along with its corresponding Fourier domain. The encoded image clusters due to the four lasers are marked, shown in pink, and similarly the those corresponding to the four spectral emission channels are marked, shown in yellow. The computational code is then constructed such that it locates the remaining 16 data clusters which result from the applied double modulation, marked in blue as shown in fig. 5.39. The 24 extracted images are shown in fig. 5.39 and it is these images that are used to

construct the calibration set used for linear unmixing. (Note: due to the reduction in the proportion of information in the single and double encoded images, as shown in eq. (5.19), the extracted images were weighted to compensate for this in the linear unmixing which follows.) The different fluorophore locations are then marked in the raw image, as shown in fig. 5.40. The recorded intensities corresponding to the location of each square in the extracted images it collected which produces a spectral "fingerprint" composed of 24 values. Conventional linear unmixing of the extracted images as a whole is then performed. Fig. 5.40 shows the nine unmixed images corresponding to each of the fluorophores. Although this sample is stationary, the information obtained from it can be applied to linearly unmix dynamic samples containing any of the same fluorophores.

Paper iv, which summarises the findings of this setup, shows how when using only four different illumination sources or four different spectral emission channels, only a maximum of four fluorophores can be unmixed. Even though this is mathematically the case, when the spectral absorption or emission profiles of the fluorophores are very similar it can be difficult to unmix them at all. Since the setup in fact combines four illumination sources and four spectral emission channels one should be able to unmix 16 fluorophores. In reality this setup obtains 24 unique spectral images which means that using linear unmixing, it in fact has the potential to unmix up to 24 different fluorophores. The results, presented in **Paper iv**, show that the setup can successfully unmix four "difficult" fluorophores, i.e. with heavily overlapping spectral absorption and emission profiles, and also as many as nine different fluorophores.
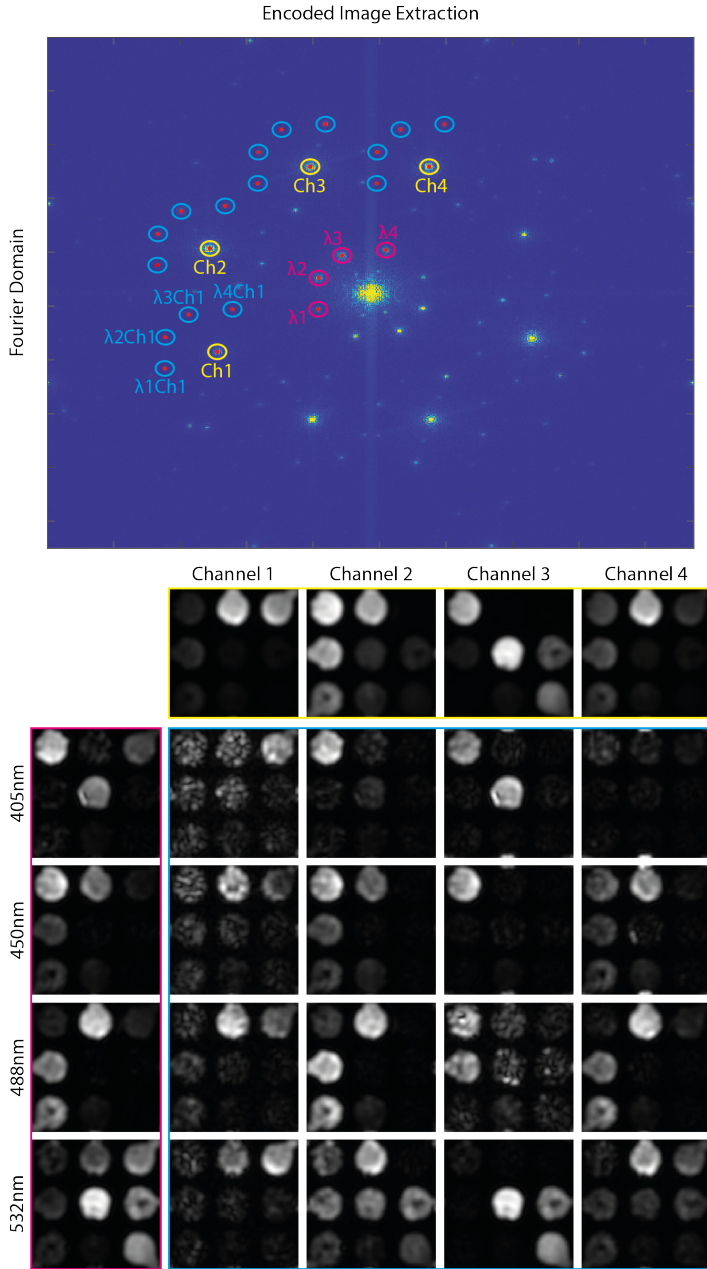
Figure 5.39: The Fourier domain of a double modulated multiplexed image is shown in the top of the figure, with the clusters corresponding to the four lasers, four spectral channels and the 16 double modulated images marked in pink, yellow and blue respectively. The extracted images corresponding to each of the marked clusters are shown in the array in the bottom of the figure.
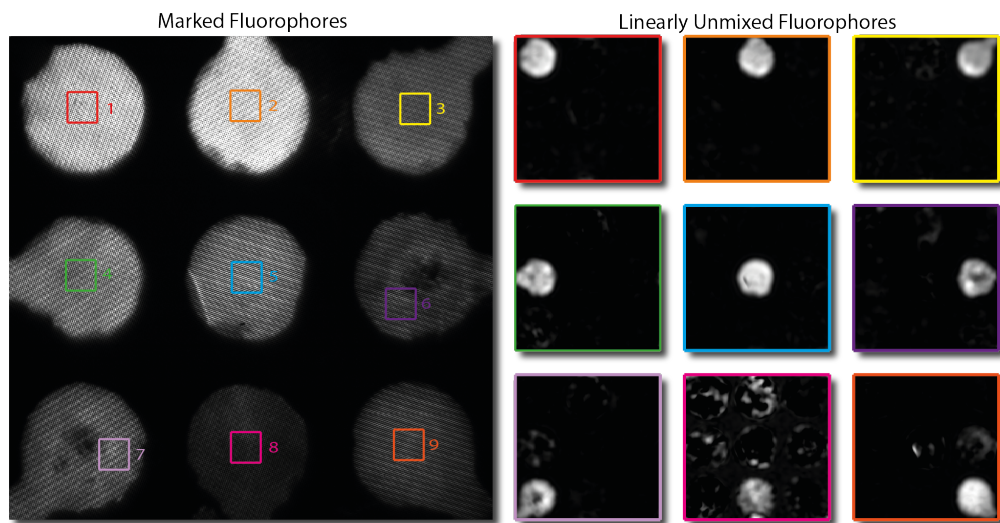
Figure 5.40: Squares selecting regions of each of the nine different fluorophores present in the sample are shown on the raw image to the left. On the right, the nine linearly unmixed images of the fluorophores are shown, where only one fluorophore is present in each image.

Chapter 6

Summary and Outlook

To conclude, several novel experimental snapshot imaging approaches implementing the FRAME technique have been developed. By using structured illumination, detection or both, FRAME has demonstrated snapshot imaging of fluorescence, multispectral, polarisation, depth of focus, temporal and volumetric information through the use of spatially encoded multiplexed images. Moreover the technique has therefore shown that emissions due to spectrally close excitation sources of as little as 3nm in separation, can be successfully isolated from a multiplexed image under simultaneous illumination. A demonstration of a double modulation encoding of both the illumination and the emission also yielded an additional 16 sample images, such that linear unmixing of nine fluorophores, with the potential for up to 24, could be performed using a total of only four unique illumination sources and four unique spectral emission channels. Mathematically such a case would previously have been limited to only 16 fluorophores. The general versatility in the implementation of the FRAME approach has been shown where there is still much remaining, untapped potential.

Throughout the development of FRAME there were numerous moments of discovery, some which were addressed during the research and others which there was either not the time or the opportunity to do so. The latter would therefore be interesting to cover for future work on the development of FRAME.

The setups obtained different qualitative images but lacked quantitative information. In cases of fluorescence imaging, for example, it would be useful to obtain accurate quantitative information about fluorophores, such as their concentration, such that the approach can have broad applicability in "real" applications for cases where obtaining only qualitative information is not sufficient. An example of such a case is where measurements of fluorescence loss due to photobleaching are used for the characterisation of biomolecule

behaviour [96].

As demonstrated by *C.Hu et al.* [94], it is possible to double the image storage capacity of FRAME through the use of $\pi/2$ phase shifted modulation patterns which have the same spatial frequency and rotation as each other. Simulations were performed to gain a basic understanding of the robustness and limitations of this phase related image doubling, however, no experimental implementations were performed. Future work could therefore action this experimentally and explore what information to store in the additional images that can be obtained. Since the extracted images obtained using FRAME have a lower spatial resolution due to the use of modulated encoding, the additional images could be used to generate higher spatial resolution images, or to encode additional parameters in parallel such as spectral and polarisation.

When Fourier filtering the multiplexed images only Gaussian filter shapes were used. When considering an increased density of encoded image capture there is a risk that there will be a high level of cross talk due to the proximity of the image clusters. A bespoke filter shape, such as the non-uniform band-pass filters found in [88], could therefore be designed and used to try to isolate the densely packed cluster information while maintaining a minimal level of cross talk from neighbouring image clusters.

Increasing the number of images stored could also be achieved by using a range of different modulation frequencies in the encoding patterns. In the double modulated demonstration the lasers were encoded with a lower spatial frequency than the spectral detection channels. As a result the modulated image copies due to the lasers were located at a different radial distance from the centre compared with the detection channel image copies. In a similar way one could, instead, use a greater number of illumination sources only, for example, and give them each encodings which had different spatial frequencies and try to utilise as much of the sparsely occupied region of the Fourier domain. The drawback with this approach would be the variable resolution of the extracted images that is achievable, however, perhaps there are suitable applications where the increased image capacity outweighs the need for high resolution images.

Considering **Paper iv** specifically, there are two main areas which would be interesting to address in future work. Firstly, the unmixed multispectral images could benefit from more robust computational analysis to make the most out of the 24 coded images captured. Currently only linear unmixing has been applied to distinguish the different fluorophores, however, other image analysis techniques and machine learning approaches may in fact be more suitable. Additionally, since the setup applies emission encoding by splitting the light into four optical paths there is a risk that the pixel to pixel overlap is not precise enough. For this reason the linear unmixing may suffer from inaccuracies if this is not addressed properly. This links to the second point which is to explore the possibility of achieving the same emission encoding but without the need to split the light into separate optical paths.

Custom optical components which encode the same spectral information in a single optical path, could be manufactured and integrated into the setup to achieve this. The use of such components could also make the setup more light efficient and could open up for greater image storage capacity, including additional dimensional information capture.

Finally, throughout the work in this thesis the development and demonstrations of FRAME have been focussed on the proof of concept. There is therefore a need for the application of, for example, the spectral imaging implementation on biological and medical samples. Collaboration with researchers in these fields in order to demonstrate the results achievable with FRAME, compared to current techniques used, would therefore highlight advantages which have been already been noted in the proof of concept publications.

Summary of Papers

Paper i: Implementation of a multiplexed structured illumination method to achieve snapshot multispectral imaging

This paper presents FRAME for snapshot multispectral imaging using structured illumination. The paper gives an introduction to the FRAME technique both experimentally and computationally. The analytical variables and the outcomes they yield are presented to illustrate how the technique can be customised depending on the users needs. The paper also demonstrates filterless fluorescence imaging whereby the different spectral images are shown to be demultiplexed even when the illumination wavelengths only differ by *3nm*, and in theory less than *3nm* separation is still resolvable.

I designed and built the experimental setup. Myself and EK collected and analysed the data. I was responsible for the preparation of the manuscript and figures.

Paper ii: A versatile, low-cost, snapshot multidimensional imaging approach based on structured light

This paper applies the FRAME encoding to the emitted light from various different samples to collect different optical information, namely; depth of focus, polarisation, temporal, spectral and fluorescence. A single setup was built with the functionality of switching filters in order to be able to use the detection scheme to capture the different optical information. Different illumination arrangements were used in combination with the detection encoding setup to obtain the different imaging schemes. Results demonstrate that the setup was able to obtain images comparable with their ground truths. Additionally, due to the nature of the setup with four distinct optical paths, or channels, it was demonstrated that it was applicable for cases with greatly varying emission intensities. Channel balancing could be experimentally implemented and then computationally rescaled correctly to yield the correct relative intensities but maintain demultiplexing capabilities. The setup was therefore shown to be a versatile and low cost experimental "add on" solution applicable for use in already existing experimental setups with flexible detection requirements.

I designed and built the passive experimental setup. Adjustments to the setup were also made by EK and VK for capture of different dimensional data. Myself, EK and VK all made adjustments to the illumination side of the experimental setup for each of the different measurements we were responsible for. I was responsible for the polarisation, spectral and fluorescence setup and measurements. VK was responsible for the videography by time multiplexing setup and measurements. EK was responsible for the depth of focus setup adjustments and measurements. Data analysis was performed by myself, EK and VK. Figures were created by myself, EK and VK. I was responsible for the preparation of the manuscript, whereby VK was responsible for the videography by time multiplexing portion of the text.

Paper III: Single-shot 3D imaging of hydroxyl radicals in the vicinity of a gliding arc discharge

This paper uses the FRAME encoding approach for snapshot volumetric imaging and a gliding arc plasma. Structured laser sheets were used to obtain images at four different heights within a gliding arc plasma. The structured pattern in the sheets allowed for each different height to be identifiable in the captured multiplexed image. This was decoded and computationally stitched to visualise the three dimensional shape of the gliding arc plasma.

I designed the experimental setup. Myself and YB built the experimental setup with input from EK and AE. CK provided the gliding arc plasma as well as operational assistance and instruction of it. SP and JZ provided the laser system as well as operational instruction of it. Myself, YB, PS, AE and EK collected the experimental data. YB, EK and AE analysed the data. YB was responsible for the preparation of the manuscript. I made small contributions to parts of the analysis, editing and proof reading of the manuscript. CK, TH, JZ, EK and AE also provided contributions to the manuscript as well as editing it. MR, EK and AE conceived and coordinated the project.

Paper IV: Double modulated FRAME: Multiple fluorophore unmixing using a snapshot multiplexed structured illumination and detection setup

This paper combined structured illumination and structured detection with fluorescence imaging. Samples containing multiple fluorophores were probed with four different structured illumination wavelengths, each with a unique spatial frequency and rotation (encoding). The corresponding emissions for each laser source maintained the encoding. The emissions were split equally into four optical paths, or channels, each with a different spectral filter and line grating. Each channel therefore applied a second modulation, or encoding, each of which corresponded to a certain spectral transmission region. The signals were them recombined onto a detector where a multiplexed image was captured. The data was then linearly unmixed. Linear unmixing is conceptually limited to the successful separation of fluorophore numbers equal to or fewer than the number of unique spectral excitation or detection channels and therefore in this case should be only eight (four lasers and four spectral channels). The double modulation approach demonstrated

produces 24 unique images within the multiplexed image and therefore has the potential to unmix up to 24 different fluorophores. The results presented demonstrate the effectiveness of the approach showing successful linear unmixing of; fluorophores with heavily spectrally overlapping excitations and emissions, and a sample with nine fluorophores.

I designed and built the experimental setup. EK and VK also made adjustments to the experimental setup. EK designed the sample holders. VK prepared most of the fluorophores with contributions from AA, EK and I. AA provided some of the fluorophores. Myself, VK and EK recorded the experimental data. SE and EK created the computational code. Myself, SE, EK and VK analysed the data. EK made the figures. I was responsible for the preparation of the manuscript.

Bibliography

[1] G. Lu and B. Fei, "Medical hyperspectral imaging: a review," *Journal of Biomedical Optics*, vol. 19, no. 1, pp. 1 – 24, 2014.

[2] L. V. Wang and H.-i. Wu, *Biomedical optics: principles and imaging*. John Wiley & Sons, 2007.

[3] A. Pliss, A. N. Kuzmin, A. V. Kachynski, and P. N. Prasad, "Nonlinear optical imaging and raman microspectrometry of the cell nucleus throughout the cell cycle," *Biophysical journal*, vol. 99, no. 10, pp. 3483–3491, 2010.

[4] N. Ugryumova, J. Jacobs, M. Bonesi, and S. J. Matcher, "Novel optical imaging technique to determine the 3-d orientation of collagen fibers in cartilage: variable-incidence angle polarization-sensitive optical coherence tomography," *Osteoarthritis and cartilage*, vol. 17, no. 1, pp. 33–42, 2009.

[5] M. C. Pierce, R. L. Sheridan, B. H. Park, B. Cense, and J. F. De Boer, "Collagen denaturation can be quantified in burned human skin using polarization-sensitive optical coherence tomography," *Burns*, vol. 30, no. 6, pp. 511–517, 2004.

[6] P. Andresen, G. Meijer, H. Schlüter, H. Voges, A. Koch, W. Hentschel, W. Oppermann, and E. Rothe, "Fluorescence imaging inside an internal combustion engine using tunable excimer lasers," *Appl. Opt.*, vol. 29, no. 16, pp. 2392–2404, 1990.

[7] L. Gao and L. V. Wang, "A review of snapshot multidimensional optical imaging: measuring photon tags in parallel," *Physics reports*, vol. 616, pp. 1–37, 2016.

[8] E. Kristensson, Z. Li, E. Berrocal, M. Richter, and M. Aldén, "Instantaneous 3d imaging of flame species using coded laser illumination," *Proceedings of the Combustion Institute*, vol. 36, no. 3, pp. 4585 – 4591, 2017.

[9] A. Ehn, J. Bood, Z. Li, E. Berrocal, M. Aldén, and E. Kristensson, "Frame: femtosecond videography for atomic and molecular dynamics," *Light: Science & Applications*, vol. 6, 2017.

[10] Z. Li, J. Borggren, E. Berrocal, A. Ehn, M. Aldén, M. Richter, and E. Kristensson, "Simultaneous multispectral imaging of flame species using frequency recognition algorithm for multiple exposures (frame)," *Combustion and Flame*, vol. 192, pp. 160 – 169, 2018.

[11] S. Taylor, "Optical frame: Investigating the effects of filtering the optical fourier domain to be used as a new approach for frame," 2020. Student Paper.

[12] R. e. a. Lin, "The reuven ramaty high-energy solar spectroscopic imager (rhessi)," *Solar Physics*, vol. 210, pp. 3–32, Nov 2002.

[13] W. L. Smith, D. K. Zhou, F. W. Harrison, H. E. Revercomb, A. M. Larar, H.-L. Huang, and B. Huang, "Hyperspectral remote sensing of atmospheric profiles from satellites and aircraft," in *Hyperspectral Remote Sensing of the Land and Atmosphere* (W. L. Smith and Y. Yasuoka, eds.), vol. 4151, pp. 94 – 102, International Society for Optics and Photonics, SPIE, 2001.

[14] T. H. Pham, F. Bevilacqua, T. Spott, J. S. Dam, B. J. Tromberg, and S. Andersson-Engels, "Quantifying the absorption and reduced scattering coefficients of tissuelike turbid media over a broad spectral range with noncontact fourier-transform hyperspectral imaging," *Appl. Opt.*, vol. 39, pp. 6487–6497, Dec 2000.

[15] D. Wu and D.-W. Sun, "Advanced applications of hyperspectral imaging technology for food quality and safety analysis and assessment: A review — part i: Fundamentals," *Innovative food science and emerging technologies*, vol. 19, p. 1—14, July 2013.

[16] M. Klukkert, J. X. Wu, J. Rantanen, J. M. Carstensen, T. Rades, and C. S. Leopold, "Multispectral uv imaging for fast and non-destructive quality control of chemical and physical tablet attributes," *European journal of pharmaceutical sciences : official journal of the European Federation for Pharmaceutical Sciences*, vol. 90, p. 85—95, July 2016.

[17] H. D. Young, R. A. Freedman, and A. L. Ford, *Sears and Zemansky's university physics*, vol. 12. Pearson Addison-Wesley, 2008.

[18] J. Tennyson, *Astronomical spectroscopy: an introduction to the atomic and molecular physics of astronomical spectra*, vol. 2. World Scientific, 2010.

[19] N. M. Cordina, N. Sayyadi, L. M. Parker, A. Everest-Dass, L. J. Brown, and N. H. Packer, "Reduced background autofluorescence for cell imaging using nanodiamonds and lanthanide chelates," *Scientific Reports*, vol. 8, 2018.

[20] V. I. Martynov, A. A. akhomov, N. V. Popova, I. E. Deyev, A. G. Petrenko, and N. H. Packer, "Synthetic fluorophores for visualizing biomolecules in living systems.," *Acta Naturae*, vol. 8, 2016.

[21] P. Kauranen, S. Andersson-Engels, and S. Svanberg, "Spatial mapping of flame radical emission using a spectroscopic multi-colour imaging system," *Applied Physics B*, vol. 53, pp. 260 – 264, 1991.

[22] J. Hunicz and D. Piernikarski, "Investigation of combustion in a gasoline engine using spectrophotometric methods," in *Optoelectronic and Electronic Sensors IV* (J. Fraczek, ed.), vol. 4516, pp. 307 – 314, International Society for Optics and Photonics, SPIE, 2001.

[23] C. L. Kohnhorst, D. L. Schmitt, A. Sundaram, and S. An, "Subcellular functions of proteins under fluorescence single-cell microscopy," *Biochimica et Biophysica Acta (BBA)-Proteins and Proteomics*, vol. 1864, no. 1, pp. 77–84, 2016.

[24] M. Dickinson, G. Bearman, S. Tille, R. Lansford, and S. Fraser, "Multi-spectral imaging and linear unmixing add a whole new dimension to laser scanning fluorescence microscopy," *Biotechniques*, vol. 31, no. 6, pp. 1272–1278, 2001.

[25] K. S. Park, D. U. Kim, J. Lee, G. H. Kim, and K. S. Chang, "Simultaneous multi-color imaging of wide-field epi-fluorescence microscopy with four-bucket detection," *Biomed. Opt. Express*, vol. 7, pp. 2285–2294, Jun 2016.

[26] S. Schlachter, S. Schwedler, A. Esposito, G. K. Schierle, G. Moggridge, and C. Kaminski, "A method to unmix multiple fluorophores in microscopy images with minimal a priori information," *Opt. Express*, vol. 17, pp. 22747–22760, Dec 2009.

[27] M. Bates, B. Huang, G. T. Dempsey, and X. Zhuang, "Multicolor super-resolution imaging with photo-switchable fluorescent probes," *Science*, vol. 317, no. 5845, pp. 1749–1753, 2007.

[28] M. Bates, G. T. Dempsey, K. H. Chen, and X. Zhuang, "Multicolor super-resolution fluorescence imaging via multi-parameter fluorophore detection," *ChemPhysChem*, vol. 13, no. 1, pp. 99–107, 2012.

[29] T. Zimmermann, J. Rietdorf, and R. Pepperkok, "Spectral imaging and its applications in live cell microscopy," *FEBS Letters*, vol. 546, no. 1, pp. 87 – 92, 2003. Signal Transduction Special Issue.

[30] T. Zimmermann, "Spectral imaging and linear unmixing in light microscopy," in *Microscopy techniques*, pp. 245–265, Springer, 2005.

[31] X. Xu, Y. Qiao, and B. Qiu, "Reconstructing the surface of transparent objects by polarized light measurements," *Opt. Express*, vol. 25, pp. 26296–26309, Oct 2017.

[32] J. Kim and A. Ghosh, "Polarized light field imaging for single-shot reflectance separation," *Sensors*, vol. 18, no. 11, p. 3803, 2018.

[33] S. G. Demos and R. R. Alfano, "Optical polarization imaging," *Appl. Opt.*, vol. 36, pp. 150–155, Jan 1997.

[34] V. V. Tuchin, "Polarized light interaction with tissues," *Journal of Biomedical Optics*, vol. 21, no. 7, pp. 1 – 37, 2016.

[35] D. Karayel, M. Wiesehoff, A. Özmerzi, and J. Müller, "Laboratory measurement of seed drill seed spacing and velocity of fall of seeds using high-speed camera system," *Computers and Electronics in Agriculture*, vol. 50, no. 2, pp. 89–96, 2006.

[36] P. Wang, J. Liang, and L. V. Wang, "Single-shot ultrafast imaging attaining 70 trillion frames per second," *Nature Communications*, vol. 11, no. 1, pp. 1–9, 2020.

[37] M. Nisoli, P. Decleva, F. Calegari, A. Palacios, and F. Martín, "Attosecond electron dynamics in molecules," *Chemical Reviews*, vol. 117, no. 16, pp. 10760–10825, 2017.

[38] K. Sharp and J. J. Skinner, "Pump-probe molecular dynamics as a tool for studying protein motion and long range coupling," *Proteins: Structure, Function, and Bioinformatics*, vol. 65, no. 2, pp. 347–361, 2006.

[39] S. A. Huettel, A. W. Song, G. McCarthy, *et al.*, *Functional magnetic resonance imaging*, vol. 1. Sinauer Associates Sunderland, MA, 2004.

[40] Z.-P. Liang and P. C. Lauterbur, *Principles of magnetic resonance imaging: a signal processing perspective*. SPIE Optical Engineering Press, 2000.

[41] J. Pawley, *Handbook of biological confocal microscopy*, vol. 236. Springer Science & Business Media, 2006.

[42] B. Matsumoto, *Cell biological applications of confocal microscopy*. Elsevier, 2003.

[43] J. Geng, "Structured-light 3d surface imaging: a tutorial," *Adv. Opt. Photon.*, vol. 3, pp. 128–160, Jun ts.

[44] N. A. Hagen and M. W. Kudenov, "Review of snapshot spectral imaging technologies," *Optical Engineering*, vol. 52, no. 9, pp. 1 – 23, 2013.

[45] N. A. Hagen, L. S. Gao, T. S. Tkaczyk, and R. T. Kester, "Snapshot advantage: a review of the light collection improvement for parallel high-dimensional measurement systems," *Optical Engineering*, vol. 51, no. 11, p. 111702, 2012.

[46] M. W. Kudenov and E. L. Dereniak, "Compact real-time birefringent imaging spectrometer," *Opt. Express*, vol. 20, pp. 17973–17986, Jul 2012.

[47] R. Shogenji, Y. Kitamura, K. Yamada, S. Miyatake, and J. Tanida, "Multispectral imaging using compact compound optics," *Opt. Express*, vol. 12, pp. 1643–1655, Apr 2004.

[48] M. Tamamitsu, Y. Kitagawa, K. Nakagawa, R. Horisaki, Y. Oishi, S. ya Morita, Y. Yamagata, K. Motohara, and K. Goda, "Spectrum slicer for snapshot spectral imaging," *Optical Engineering*, vol. 54, no. 12, pp. 1 – 6, 2015.

[49] R. T. Kester, N. Bedard, L. S. Gao, and T. S. Tkaczyk, "Real-time snapshot hyperspectral imaging endoscope," *Journal of biomedical optics*, vol. 16, no. 5, p. 056005, 2011.

[50] Y. Zhao, C. Yi, S. G. Kong, Q. Pan, and Y. Cheng, "Multi-band polarization imaging," in *Multi-band Polarization Imaging and Applications*, pp. 47–71, Springer, 2016.

[51] T. C. George, D. A. Basiji, B. E. Hall, D. H. Lynch, W. E. Ortyn, D. J. Perry, M. J. Seo, C. A. Zimmerman, and P. J. Morrissey, "Distinguishing modes of cell death using the imagestream® multispectral imaging flow cytometer," *Cytometry Part A: The Journal of the International Society for Analytical Cytology*, vol. 59, no. 2, pp. 237–245, 2004.

[52] S. E. Headland, H. R. Jones, A. S. D'sa, M. Perretti, and L. V. Norling, "Cutting-edge analysis of extracellular microparticles using imagestream x imaging flow cytometry," *Scientific reports*, vol. 4, p. 5237, 2014.

[53] A. A. Wagadarikar, N. P. Pitsianis, X. Sun, and D. J. Brady, "Video rate spectral imaging using a coded aperture snapshot spectral imager," *Opt. Express*, vol. 17, pp. 6368–6388, Apr 2009.

[54] A. Wagadarikar, R. John, R. Willett, and D. Brady, "Single disperser design for coded aperture snapshot spectral imaging," *Appl. Opt.*, vol. 47, no. 10, pp. B44–B51, 2008.

[55] M. E. Gehm, R. John, D. J. Brady, R. M. Willett, and T. J. Schulz, "Single-shot compressive spectral imaging with a dual-disperser architecture," *Opt. Express*, vol. 15, no. 21, pp. 14013–14027, 2007.

[56] A. Gorman, D. W. Fletcher-Holmes, and A. R. Harvey, "Generalization of the lyot filter and its application to snapshot spectral imaging," *Opt. Express*, vol. 18, pp. 5602–5608, Mar 2010.

[57] A. R. Harvey and D. W. Fletcher-Holmes, "High-throughput snapshot spectral imaging in two dimensions," in *Spectral Imaging: Instrumentation, Applications, and Analysis II*, vol. 4959, pp. 46–54, International Society for Optics and Photonics, 2003.

[58] G. Wong, R. Pilkington, and A. R. Harvey, "Achromatization of wollaston polarizing beam splitters," *Optics letters*, vol. 36, no. 8, pp. 1332–1334, 2011.

[59] B. Geelen, N. Tack, and A. Lambrechts, "A snapshot multispectral imager with integrated tiled filters and optical duplication," in *Advanced Fabrication Technologies for Micro/Nano Optics and Photonics VI*, vol. 8613, p. 861314, International Society for Optics and Photonics, 2013.

[60] J. G. Dwight and T. S. Tkaczyk, "Lenslet array tunable snapshot imaging spectrometer (latis) for hyperspectral fluorescence microscopy," *Biomed. Opt. Express*, vol. 8, pp. 1950–1964, Mar 2017.

[61] https://www.sony-semicon.co.jp/e/products/IS/industry/technology/polarization.html.

[62] K. Shinoda, Y. Ohtera, and M. Hasegawa, "Snapshot multispectral polarization imaging using a photonic crystal filter array," *Opt. Express*, vol. 26, no. 12, pp. 15948–15961, 2018.

[63] P. M. Blanchard and A. H. Greenaway, "Simultaneous multiplane imaging with a distorted diffraction grating," *Appl. Opt.*, vol. 38, no. 32, pp. 6692–6699, 1999.

[64] K. Nakagawa, A. Iwasaki, Y. Oishi, R. Horisaki, A. Tsukamoto, A. Nakamura, K. Hirosawa, H. Liao, T. Ushida, K. Goda, *et al.*, "Sequentially timed all-optical mapping photography (stamp)," *Nature Photonics*, vol. 8, no. 9, pp. 695–700, 2014.

[65] G. K. Wallace, "The jpeg still picture compression standard," *IEEE Transactions on Consumer Electronics*, vol. 38, no. 1, pp. xviii–xxxiv, 1992.

[66] M. Rabbani and P. W. Jones, *Digital image compression techniques*, vol. 7. SPIE press, 1991.

[67] K. Sayood, *Introduction to data compression*. Morgan Kaufmann, 2017.

[68] R. Heintzmann and T. Huser, "Super-resolution structured illumination microscopy," *Chemical reviews*, vol. 117, no. 23, pp. 13890–13908, 2017.

[69] G. Ball, J. Demmerle, R. Kaufmann, I. Davis, I. M. Dobbie, and L. Schermelleh, "Simcheck: a toolbox for successful super-resolution structured illumination microscopy," *Scientific reports*, vol. 5, p. 15915, 2015.

[70] R. N. Bracewell and R. N. Bracewell, *The Fourier transform and its applications*, vol. 31999. McGraw-Hill New York, 1986.

[71] H. J. Nussbaumer, "The fast fourier transform," in *Fast Fourier Transform and Convolution Algorithms*, pp. 80–111, Springer, 1981.

[72] A. Gersho and R. M. Gray, *Vector quantization and signal compression*, vol. 159. Springer Science & Business Media, 2012.

[73] M. A. A. Neil, R. Juškaitis, and T. Wilson, "Method of obtaining optical sectioning by using structured light in a conventional microscope," *Opt. Lett.*, vol. 22, pp. 1905–1907, Dec 1997.

[74] S. Abrahamsson, H. Blom, A. Agostinho, D. C. Jans, A. Jost, M. Müller, L. Nilsson, K. Bernhem, T. J. Lambert, R. Heintzmann, and H. Brismar, "Multifocus structured illumination microscopy for fast volumetric super-resolution imaging," *Biomed. Opt. Express*, vol. 8, pp. 4135–4140, Sep 2017.

[75] E. Kristensson, E. Berrocal, and M. Aldén, "Quantitative 3d imaging of scattering media using structured illumination and computed tomography," *Opt. Express*, vol. 20, pp. 14437–14450, Jun 2012.

[76] E. Kristensson, *Structured laser illumination planar imaging SLIPI applications for spray diagnostics*. Lund University, 2012.

[77] E. Berrocal, E. Kristensson, M. Richter, M. Linne, and M. Aldén, "Application of structured illumination for multiple scattering suppression in planar laser imaging of dense sprays," *Opt. Express*, vol. 16, pp. 17870–17881, Oct 2008.

[78] E. Kristensson, L. Araneo, E. Berrocal, J. Manin, M. Richter, M. Aldén, and M. Linne, "Analysis of multiple scattering suppression using structured laser illumination planar imaging in scattering and fluorescing media," *Opt. Express*, vol. 19, pp. 13647–13663, Jul 2011.

[79] A. Roth, E. Kristensson, and E. Berrocal, "Snapshot 3d reconstruction of liquid surfaces," *Opt. Express*, vol. 28, no. 12, pp. 17906–17922, 2020.

[80] S. R. Khan, M. Feldman, and B. K. Gunturk, "Extracting sub-exposure images from a single capture through fourier-based optical modulation," *Signal Processing: Image Communication*, vol. 60, pp. 107 – 115, 2018.

[81] B. K. Gunturk and M. Feldman, "Frequency division multiplexed imaging," in *Digital Photography IX* (N. Sampat and S. Battiato, eds.), vol. 8660, pp. 174 – 180, International Society for Optics and Photonics, SPIE, 2013.

[82] M. Gragston, C. D. Smith, and Z. Zhang, "High-speed flame chemiluminescence imaging using time-multiplexed structured detection," *Appl. Opt.*, vol. 57, pp. 2923–2929, Apr 2018.

[83] M. Gragston, C. Smith, D. Kartashov, M. N. Shneider, and Z. Zhang, "Single-shot nanosecond-resolution multiframe passive imaging by multiplexed structured image capture," *Opt. Express*, vol. 26, pp. 28441–28452, Oct 2018.

[84] M. Gragston, C. D. Smith, J. Harrold, and Z. Zhang, "Multiplexed structured image capture to increase the field of view for a single exposure," *OSA Continuum*, vol. 2, pp. 225–235, Jan 2019.

[85] S. Weinstein and P. Ebert, "Data transmission by frequency-division multiplexing using the discrete fourier transform," *IEEE transactions on Communication Technology*, vol. 19, no. 5, pp. 628–634, 1971.

[86] E. Kristensson, J. Bood, M. Alden, E. Nordström, J. Zhu, S. Huldt, P.-E. Bengtsson, H. Nilsson, E. Berrocal, and A. Ehn, "Stray light suppression in spectroscopy using periodic shadowing," *Opt. Express*, vol. 22, no. 7, pp. 7711–7721, 2014.

[87] I. J. Bhagyajyothi, P. Bhaskar, and C. Parvathi, "Design and development of advanced lock-in amplifier and its application," *Sensors & Transducers*, vol. 153, no. 6, pp. 22–28, 2013.

[88] E. Kristensson and E. Berrocal, "Crossed patterned structured illumination for the analysis and velocimetry of transient turbid media," *Scientific Reports*, vol. 8, no. 1, pp. 1–9, 2018.

[89] J. Pospisil, K. Fliegel, and M. Klima, "Phase estimation of illumination pattern in structured illumination microscopy," in *2017 27th International Conference Radioelektronika (RADIOELEKTRONIKA)*, pp. 1–4, IEEE, 2017.

[90] K. Zhang, J. Yao, J. Chen, and H. Miao, "Phase extraction algorithm considering high-order harmonics in fringe image processing," *Appl. Opt.*, vol. 54, pp. 4989–4995, Jun 2015.

[91] L. Huang, Q. Kemao, B. Pan, and A. K. Asundi, "Comparison of fourier transform, windowed fourier transform, and wavelet transform methods for phase extraction from a single fringe pattern in fringe projection profilometry," *Optics and Lasers in Engineering*, vol. 48, no. 2, pp. 141 – 148, 2010. Fringe Projection Techniques.

[92] Z. Wang, P. Stamatoglou, Z. Li, M. Aldén, and M. Richter, "Ultra-high-speed plif imaging for simultaneous visualization of multiple species in turbulent flames," *Opt. Express*, vol. 25, no. 24, pp. 30214–30228, 2017.

[93] J. Zimmerman, "A method for measuring the distortion of photographic objectives," *Appl. Opt.*, vol. 2, no. 7, pp. 759–760, 1963.

[94] C. Hu, S. Yang, M. Chen, and H. Chen, "Quadrature multiplexed structured illumination imaging," *IEEE Photonics Journal*, vol. 12, no. 2, pp. 1–8, 2020.

[95] A. Fridman, S. Nester, L. A. Kennedy, A. Saveliev, and O. Mutaf-Yardimci, "Gliding arc gas discharge," *Progress in Energy and Combustion Science*, vol. 25, no. 2, pp. 211 – 231, 1999.

[96] A. Esposito, S. Schlachter, G. S. K. Schierle, A. D. Elder, A. Diaspro, F. S. Wouters, C. F. Kaminski, and A. I. Iliev, "Quantitative fluorescence microscopy techniques," in *Cytoskeleton Methods and Protocols*, pp. 117–142, Springer, 2009.